3-14-2008

Functional Remodeling of the Cardiac Glycome Throughout the Developing Myocardium

Marty L. Montpetit
University of South Florida

Functional Remodeling of the Cardiac Glycome

Throughout the Developing Myocardium

by

Marty L. Montpetit

A dissertation submitted in partial fulfillment
of the requirements of the degree of
Doctor of Philosophy
Department of Physiology and Biophysics
College of Medicine
University of South Florida

Major Professor: Eric S. Bennett, Ph.D.
Jahanshah Amin, Ph.D.
Craig A. Doupnik, Ph.D.
Bruce G. Lindsey, Ph.D.
Huntington Potter, Ph.D.
E. Truitt Sutton, Ph.D.

Date of Approval:
March 14, 2008

Keywords: glycosylation, cardiac, development, excitability, sodium channel

DEDICATION

In loving memory of my father, Louis Montpetit.

ACKNOWLEDGEMENTS

This dissertation would not have been completed without the love and support of my family. I would like to give special thanks to my wife, Alison, for her support throughout this process and helping me to see the bigger picture of life. I would also like to thank my parents, the late Louis Montpetit and Mary Lou and Joseph Budek, and my sister, Marla, for their love and continued encouragement

I extend the deepest thanks to Eric S. Bennett, Ph.D. for all the effort he has put forth to help me succeed. I could not have asked for a more supportive mentor. I appreciate the time invested and insight provided by my committee members: Jahanshah Amin, Ph.D., Craig Doupnik, Ph.D., Bruce Lindsey, Ph.D., Huntington Potter, Ph.D., and E. Truitt Sutton, Ph.D.

I would like to thank all those who have worked with me in the lab: Jeanie Harper, Patrick Stocker, Ph.D., Daniel Johnson, Ph.D., Sarah Norring, Tara Schwetz and Barrett McCormick as well as those with whom I have collaborated: Steven R. Head, Stuart M. Haslam, Ph.D., Timothy Gilmartin, Lana Schaffer, Simon J. North, Ph.D., Jihye Jang-Lee, Ph.D. and Jamey D. Marth, Ph.D.

Finally, I would like to extend my gratitude to my friends and family: Gerard Gole, Rickamer Hoover, Kari Bruursema, Ph.D., Iwona Misiuta, Ph.D., Kathleen and Tom Kelly, Kyle and Kristin Crawford, Andy and Kathryn Ross, and Ben and Holly Rapin.

TABLE OF CONTENTS

LIST OF FIGURES

LIST OF TABLES

FUNCTIONAL REMODELING OF THE CARDIAC GLYCOME THROUGHOUT THE DEVELOPING MYOCARDIUM

Marty L. Montpetit

ABSTRACT

Cell surfaces are replete with complex, biologically important glycans responsible for multiple cellular functions including cell adhesion and cellular communication. Proper protein glycosylation is essential for normal development and often pathologies are marked by altered glycosylation. Here, data showed that the auxillary subunit, β_1, modified voltage-gated Na^+ channel (Na_v) gating in an isoform-specific, sialic acid dependent, and saturating manner. The regulated activity of the hundreds of glycogenes (glycosylation-associated genes) is responsible for protein glycosylation; this could result in a glycome of thousands of glycan structures. Microarray analyses indicated that glycogene expression was highly regulated throughout the heart during development. Specifically, >59% of glycogenes were significantly differentially expressed among neonatal and adult atrial and ventricular myocytes. Quantitative-PCR of individual genes confirmed the microarray analyses. Such substantial regulation of glycogene expression likely results in changes in glycan structures attached to cell surface proteins. To confirm this, myocyte glycan profiles were determined and compared among neonatal and adult atria and ventricles using mass spectrometry. The data predicted marked differences in glycan structures among myocyte types, indicating that the glycome is remodeled throughout the heart

during development. To address the question of whether the remodeled glycome can impact cardiac function, action potentials and Na_v activity were measured and compared under conditions in which glycogene expression was regulated. That is, atrial and ventricular myocytes were isolated from control mice and from mice in which the polysialyltransferase, STX, was knocked out. STX is expressed in the neonatal atria, and is essentially absent in neonatal ventricle. Action potential waveforms and Na_v activity measured in atrial myocytes were impacted by STX expression. No changes in ventricular action potential waveform or in Na_v activity were observed; as expected since STX is not expressed in the ventricle. The magnitude of the atrial action potential and the rate of depolarization were decreased in the absence of STX. Further, Na_v gating was shifted consistently in the depolarized direction in STX knockout atrial myocytes. Together, these data indicate that the glycome is tightly controlled and regulated in the heart, and proper glycosylation is essential for normal myocyte function.

CHAPTER 1

INTRODUCTION

Heart disease is the leading cause of death among U.S. citizens[1]. Accounting for over 27% of deaths in 2004, heart disease caused 100,000 more deaths than any other cause[1]. The cardiac action potential is formed through the coordinated gating of voltage-gated ion channels. Conduction of the action potential throughout the heart leads to cardiac contraction. Slight alterations in ion channel function (likely through cardiac remodeling) are associated with many cardiac maladies including heart failure, myocardial infarction and hypertension. Although significant work has been devoted to understand variations in cardiac waveform, this is the first to describe how a remodeled glycome could impact cardiac excitability.

Cardiac remodeling impacts cardiac function

Changing the expression of proteins and therefore the cellular processes in which they are involved is termed remodeling. Cellular remodeling is characteristic of normal development[2-20] and pathologies[21-52]. Cardiac remodeling is evident in development as the human prenatal heart rate is commonly over 150 beats per minute which slows to an average of 72 beats per minute in the adult. Sympathetic innervation and ion channel remodeling are considered responsible for the changing heart rate[53-57]. In the adult mouse

Figure 1.1. Ionic basis of the cardiac action potential.

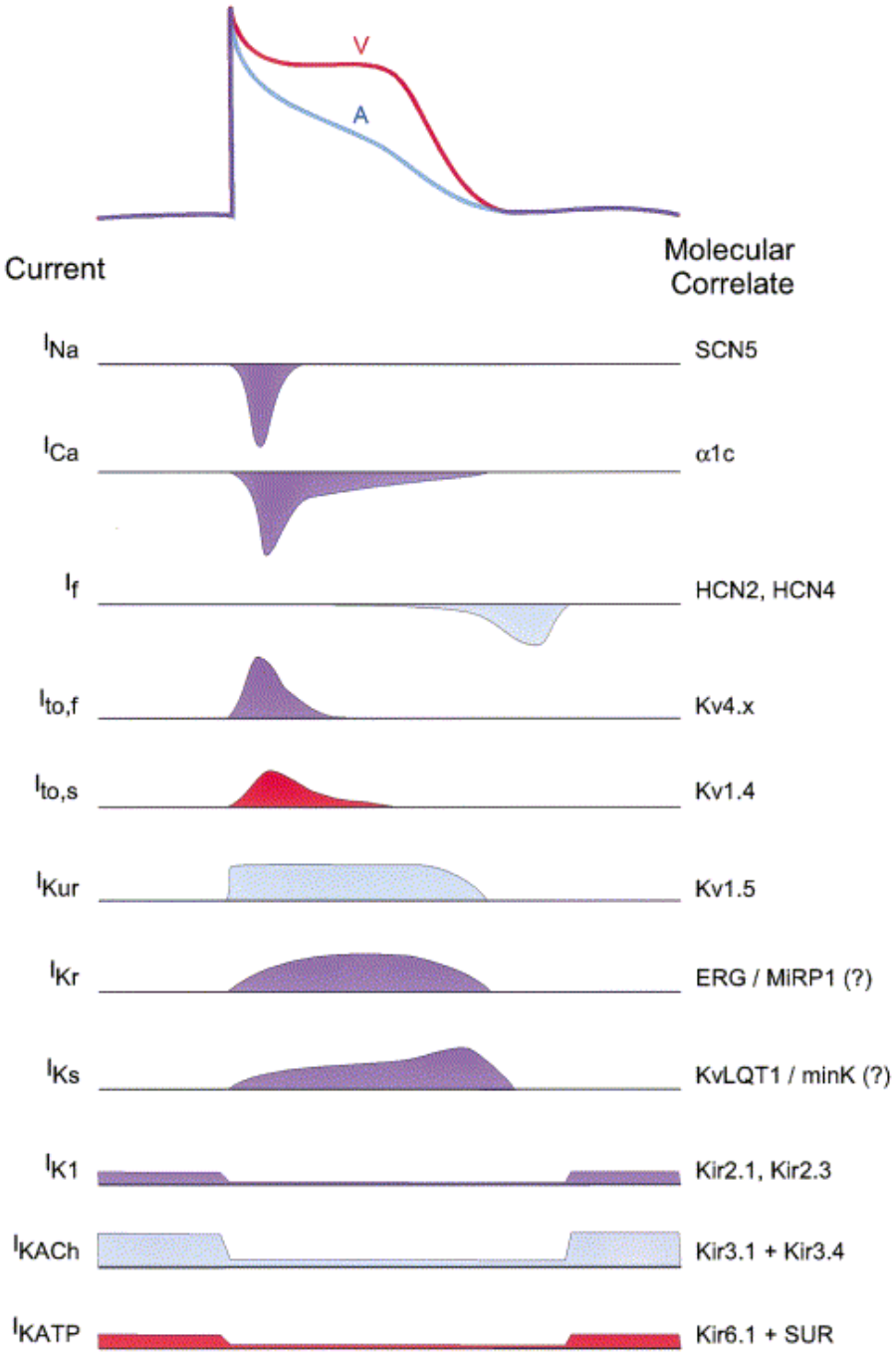

Figure 1.1. Schematic of human action potential waveforms in atria (blue) and ventricle (red) and the major ion currents creating these waveforms. Purple indicates the current is involved in both cell types. Known or presumed channels are noted to the right of each current. Figure from Pond and Nerbonne, 2001[58].

Figure 1.2. Action potential waveforms throughout the heart.

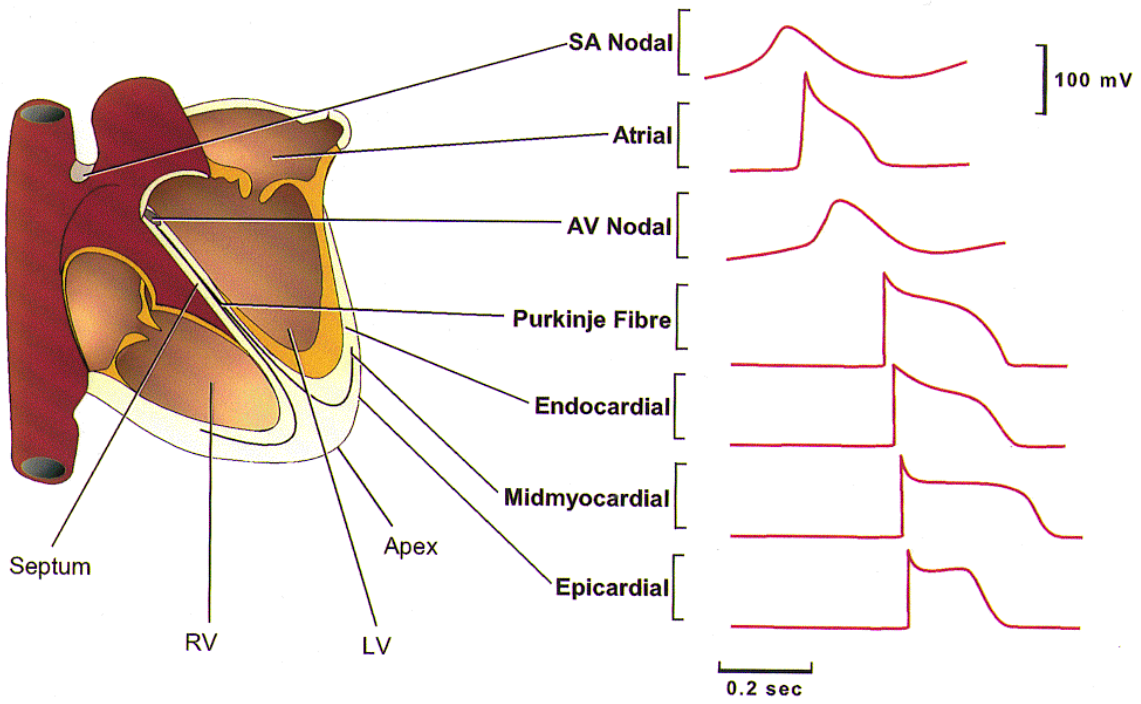

Figure 1.2. Examples of the various action potential waveforms throughout the cardiac conduction and contractile systems. Differential expression of ion channel subunits is assumed to be responsible for these changes in action potential waveform. Action potentials are displaced in time to reflect the temporal sequence of propagation through the heart. SA, sino-atrial; AV, atrio-ventricular; RV, right ventricle; LV, left ventricle. Figure from Nerbonne, 2000[59].

myocardium, ion channel expression changes between the atria and ventricle (Figures 1.1 and 1.2) and within various locations throughout the heart (Figure 1.2) leading to different action potential (AP) waveforms[58,59]. Figure 1.1 shows the difference between the typical atrial and ventricular AP, the currents that constitute the AP, and the expression of the ion channels believed responsible for those currents. Figure 1.2 shows the various action potential waveforms present throughout the heart which are different due to a change in ion currents.

In addition to physiological changes in heart function, cardiac pathologies may result from both electrical and structural remodeling. In atrial fibrillation, sodium currents (I_{Na}), calcium current (I_{Ca}), and the transient outward potassium current (I_{to}) are reduced due to a decrease in the mRNA levels of channels responsible for these currents[50,60]. The decrease in I_{Ca} is likely responsible for shortening of the atrial action potential and the decrease of I_{to} results in loss of the ability of the heart rate to adapt to physiological changes. Atrial fibrillation is also accompanied by atrial enlargement, loss of myofibrils, accumulation of glycogen, alteration of mitochondrial size and shape, fragmentation of sarcoplasmic reticulum and dispersion of nuclear chromatin[61,62]. It is unclear whether atria are enlarged as a cause or as a result of atrial fibrillation[63].

Arrhythmias are the leading cause of death in patients with heart failure (HF)[64]. Recent studies indicate that AP prolongation is a contributing factor to arrhythmias associated with HF[65-69]. Although the exact mechanism for AP

prolongation is not agreed upon, modulated K^+, Na^+, and Ca^{2+} currents have been identified[65-73]. Ionic currents are typically remodeled in HF through changes in the density and/or the expression of various isoforms of ion channels[65-73]. Furthermore, glycosylation is reduced in both hamster[74] and mouse[73,74] models of cardiac heart failure suggesting that glycosylation machinery is altered.

Regulation of glycan biosynthesis is essential for normal physiology

Cell surfaces are replete with glycan structures essential for proper development and normal function of living organisms with roles in protein trafficking, immunity, cell adhesion, receptor activation and endocytosis[75] (Figure 1.3). Protein function may be modulated by glycans through at least two mechanisms: 1) By altering the function of the protein's conjugate and, 2) By conferring biological activity to its conjugate. Glycans act as antigens on a variety of cells and activate the immune response as evidenced by the 1996 cholera pandemic of Bengal, India which was caused by Bengal 139 Vibrio cholerae[76]. This was the 139th identified strain of vibrio cholerae each of which had unique glycan structures. Exposure to and subsequent antibody formation of a single strain does not protect the host from any of the 138 other strains. Furthermore the A, B, O and AB blood types are dictated by the glycans attached with the O blood type lacking glycan structures and A and B each with unique structures. As discussed with Vibro cholerae, glycans act as antigens; therefore, type B blood can not be administered to those with O or A types. Recent studies have

Figure 1.3. Roles of glycans in cellular functions.

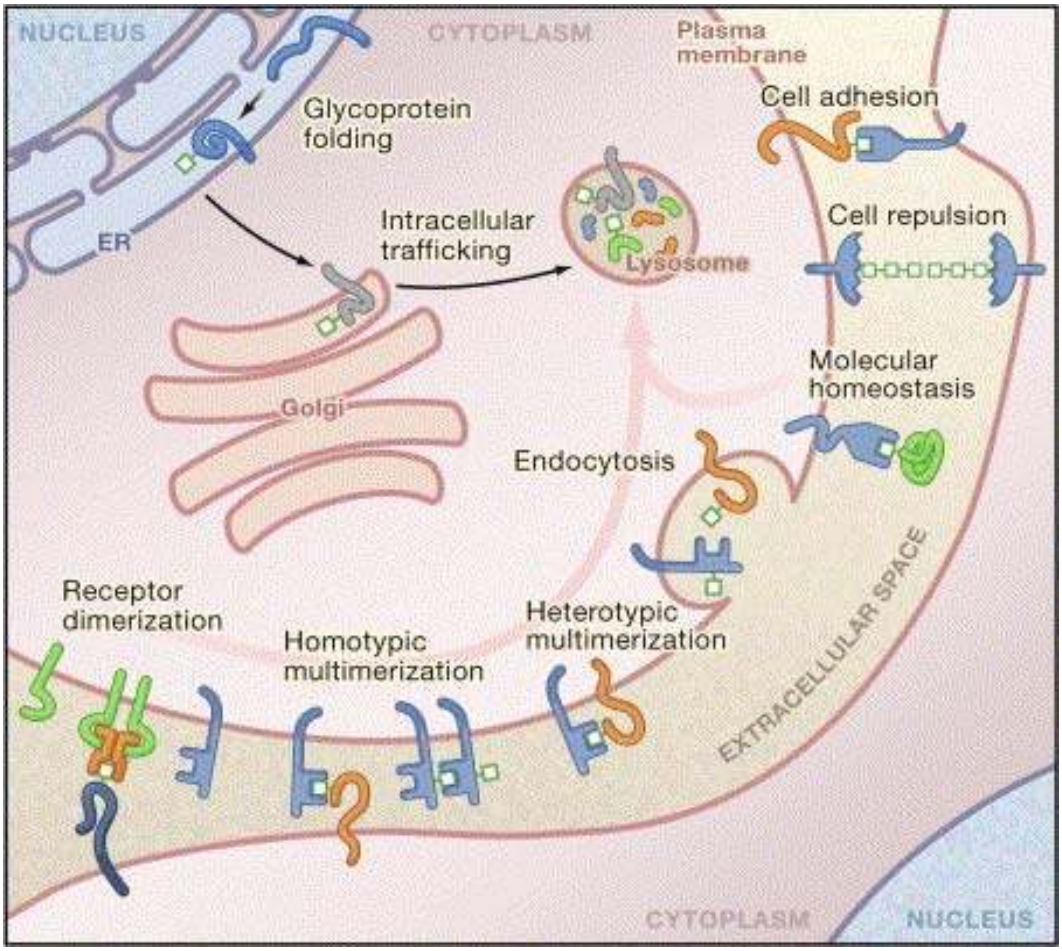

Figure 1.3. Cellular function is regulated by glycans through various mechanisms. The influence of glycans on cellular function ranges from protein folding to cellular communication. Figure from Ohtsubo and Marth, 2006[75].

reported the ability to change blood type B to O by simply altering the glycan; thus circumventing the immune response when, for example, type B blood is transfused into one with blood type A[77]. In these examples, the cell is not inherently immunoreactive, the glycans confer these attributes.

In mammals, proteins and lipids are glycosylated in the endoplasmic reticulum and golgi apparatus where enzymes catalyze oligosaccaride formation from nine monosaccarides[78,79]. Glycosylation is non-template driven, unlike the DNA template necessary for protein synthesis, and requires expression of glycogenes that comprise 1-2% of the human genome[78-82]. Protein glycosylation refers to both N-glycans and O-glycans. N-linked glycosylation is attached to an asparagine residue; hence, the “N-linked” nomenclature. N-linked glycosylation requires the specific sequence of Asn-Xaa-Ser/Thr and sometimes Asn-Xaa-Cys where Xaa is any amino acid except proline. O-glycosylation lacks a specific conserved sequence; instead several enzymes may catalyze the first sugar residue attached to serine or threonine. Glycosylation is a highly ordered process where the product of one enzyme is the substrate for the next and where catabolic glycosidase enzymes are as important as anabolic glycosyltransferase enzymes.

N-glycan synthesis (summarized in figure 1.4) is initiated in the cytoplasm where the first sugars are added to a lipid dolichol. This dolichol-glycan structure then translocates into the lumen of the endoplasmic reticulum where further branching

Figure 1.4. Overview of N-glycan biosynthesis.

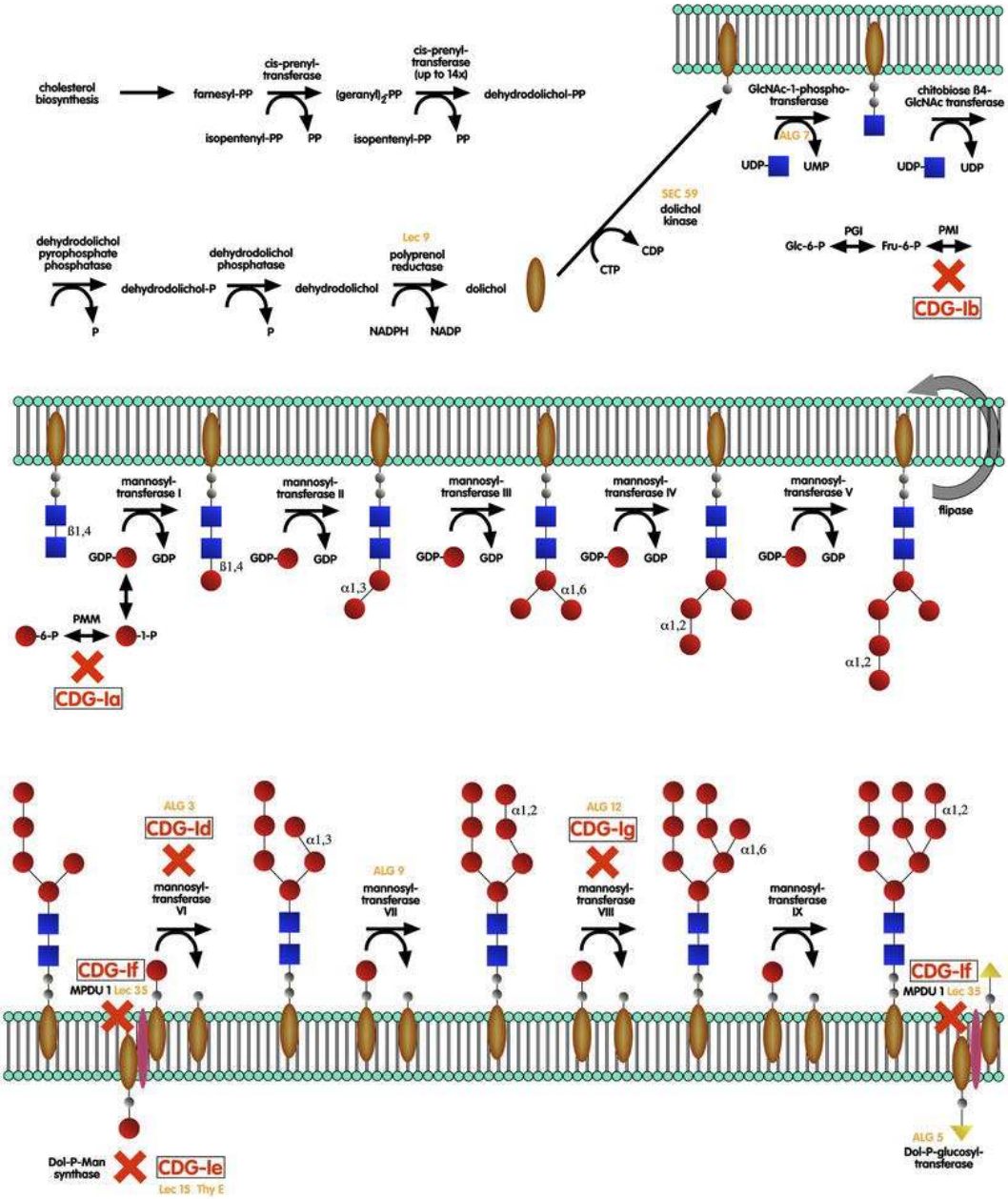

Figure 1.4. Synthesis of N-glycans from initial attachment to dolichol through assembly and processing of N-linked glycans. Molecular defects of known CDG types are indicated where known etiologies occur. N-glycan assembly is initiated in the ER lumen by transferring two GlcNAc residues (blue squares) to Dol-P and completed in the lumen of the golgi. Mannose (red circles), glucose (yellow triangles), fucose (grey triangle), galactose (green rhombus), sialic acid (pink diamonds). The mouse symbol designates a knock-out mouse of that enzyme, in red are yeast or CHO cells expressing specific enzymatic defects. Adapted from Marquardt and Denecke, 2003[82].

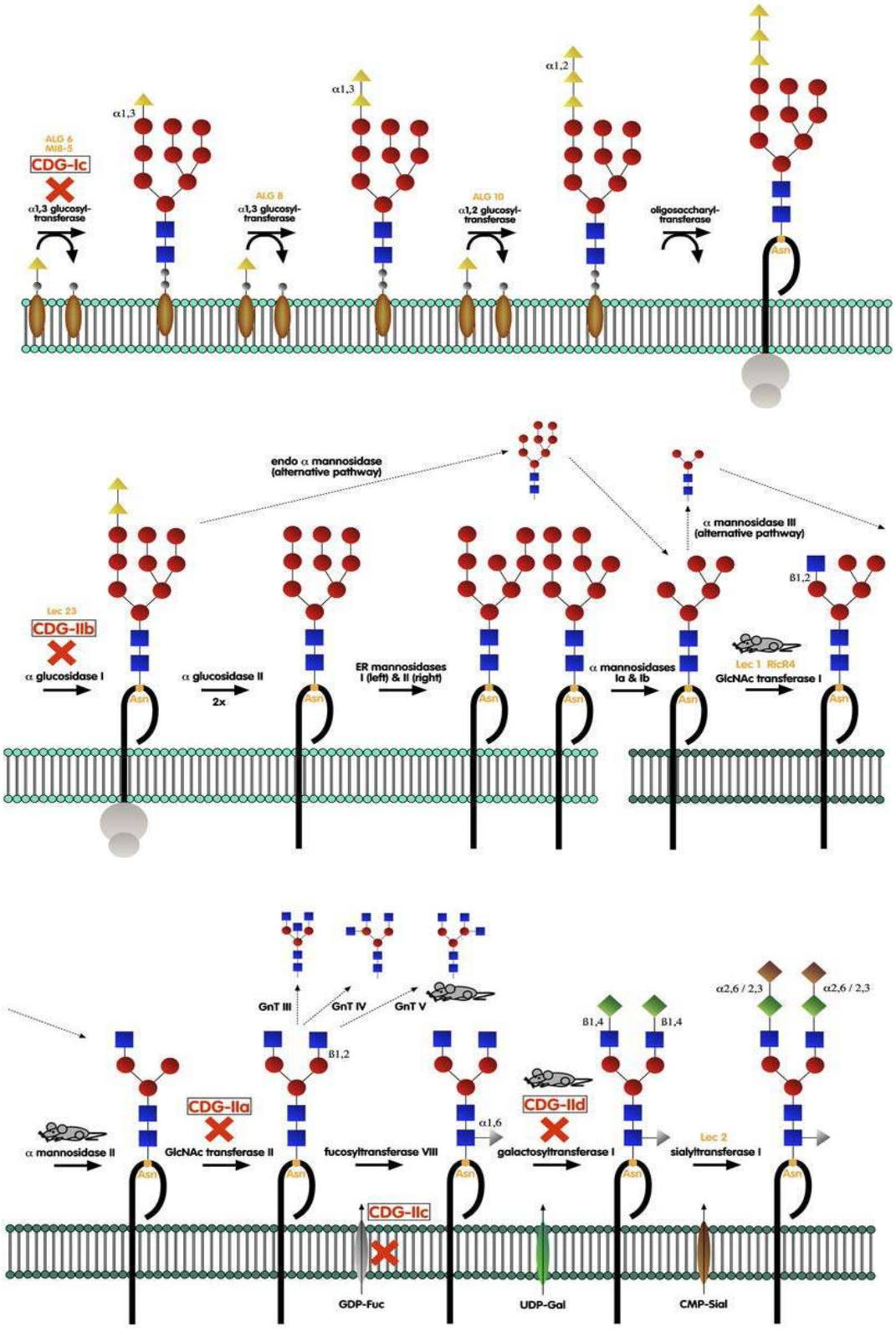
ALG 6
MI8-5
CDG-Ic
α1,3 glucosyl-transferase
α1,3
ALG 8
α1,3 glucosyl-transferase
α1,3
ALG 10
α1,2 glucosyl-transferase
α1,2
oligosaccharyl-transferase
Asn
endo α mannosidase (alternative pathway)
α mannosidase III (alternative pathway)
Lec 23
CDG-IIb
α glucosidase I
α glucosidase II
2x
ER mannosidases I (left) & II (right)
α mannosidases Ia & Ib
Lec 1 RicR4
GlcNAc transferase I
ß1,2
GnT III
GnT IV
GnT V
ß1,2
CDG-IIa
α mannosidase II
GlcNAc transferase II
fucosyltransferase VIII
α1,6
CDG-IId
galactosyltransferase I
ß1,4
ß1,4
Lec 2
sialyltransferase I
α2,6 / 2,3
α2,6 / 2,3
CDG-IIc
GDP-Fuc
UDP-Gal
CMP-Sial

and sugar addition occurs. Eventually the glycan structure is transferred *en bloc* from dolichol to the asparagine residue of a newly synthesized protein. Within the endoplasmic reticulum, the glycan structures are extended and trimmed several times until the glycoprotein is transferred to the golgi. Final processing of the glycan takes place in the golgi. The process includes addition of negatively charged sialic acid residues and when polysialyltransferase enzymes are expressed, sialic acids attach to other sialic acids (termed poly sialic acid) adding substantially more negative charges to a single structure [83].

The glycome is defined as the full set of glycan structures produced in the body[84,85], and is composed of thousands of glycan structures that perhaps is larger than the proteome[75]. Glycan diversity is accentuated by several factors which can be divided into two types: protein determined and cellular factors (Figure 1.5). The protein itself can only be N-glycosylated where specific N-linked sequences are present and accessible according to tertiary protein structure (including protein phosphorylation), and is commonly located extracellularly[78,79]. Sites located within the membrane, intracellularly or where the extracellular 3-dimensional structure prohibits access to those sites, will not be N-glycosylated. Also, the rate at which the protein traverses through the glycosylation pathway may alter the final glycan structure. The second factor is cellular in nature. The repertoire of glycogenes expressed varies from cell type to cell type and, as this study indicates, throughout development. Furthermore, glycosidase and glycosyltransferase enzymes are considered to be constitutively

Figure 1.5. Regulation of glycan expression.

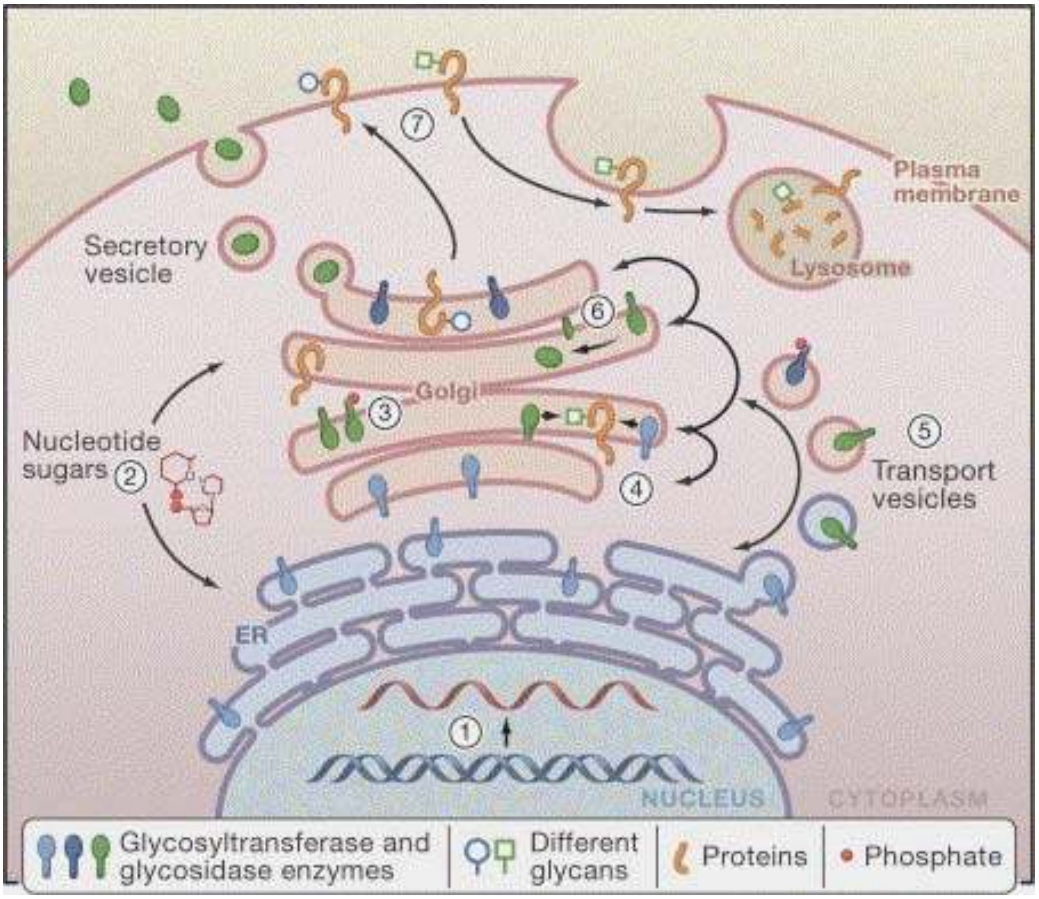

Figure 1.5. Glycan structure expression is regulated through various cellular mechanisms. These include (1) glycosyltransferase and glycosidase gene transcription, (2) nucleotide sugar synthesis and transport to the ER and golgi (sugar transporters not depicted), (3) enzymatic structure modification through phosphorylation, (4) enzyme competition for identical substrates, (5) enzyme trafficking and access to substrates, (6) secretion of catalytic domains resulting from proteolysis within the lumen of the golgi (7) glycan turnover at the cell surface by endocytosis. Figure from Ohtsubo and Marth, 2006[75].

active when expressed, yet competition between enzymes requiring a specific substrate further contributes to glycan diversity.

Glycogene expression and glycan structure are tightly regulated in different tissues, through development and in disease states. Comelli et al. reported that bone marrow, thymus, lymph nodes, spleen, lung, testes, kidney, liver and brain all had unique glycogene expression and glycan populations[86]. Further, glycogene and glycan profiles of immune tissues (bone marrow, thymus, lymphnodes, and spleen) were more similar to each other than non-immune tissues (lung, testes, kidney, liver and brain) as non-immune tissues were more similar than immune.

Glycogene expression and glycan structure are also tightly regulated through development of various tissues. As shown here and in Ishii et al., glycogene expression is altered throughout the developing myocardium and in the developing cerebral cortex, respectively[4]. Glycan profiles are distinct in each developmental stage of each tissue.

Various disease states including Down syndrome, Huntington's disease, glaucoma, and heart failure reveal a change in glycogene expression and possibly glycan structure profiles compared to healthy tissues[28,39,74,75]. Although altered glycan arrays may be present in these disease states, they may or may not cause, contribute to or exacerbate conditions.

Minor changes in glycogene expression may have a major impact on glycan structure and organism physiology[75,82,85,87]. The role of glycosylation is vast, spans every tissue, and is involved in numerous physiological processes. Ongoing research in glycobiology focuses on immune responses, neuron tracking, ligand binding, and cancer indicating the wide range of functions of glycans in normal and pathophysiology[75,86,88,89].

Improper glycosylation results in pathologies that range from mild disease to lethal [85]. Common effects seem to target neuronal, cardiovascular and muscular systems. Congenital disorders of glycosylation (CDG) are autosomal recessive disorders in which a single glycogene is mutated or missing or there is no known cause (as shown in figure 1.4). To date, 28 unique forms of CDG have been identified, 16 N-glycosylation associated, 6 O-glycosylation associated, 4 N- and O-associated and 2 involving glycolipids[90]. Recently, a new category has been identified and classified as CDGs of hyperglycosylation defects. CDG tends to affect individuals differently; for example, one patient of CDG-Ih was effectively treated with a low fat diet and essential oil supplements while four others suffered fatal maladies[90]. With such a vast range of symptoms presented, diagnosis is difficult and with many unknown causes of death in infants, it is likely that many CDG patients are never identified. One common thread through the many CDGs is symptoms consistent with decreased excitability such as hypotonia and decreased metabolic activity. Also, all types of CDG have glycans with

reduced sialylation despite different enzymes ablated. In fact, isoelectric focusing of serum transferrin is the most common assay to diagnose CDG, testing for a decrease in tetra-, penta- and hexa- sialylated transferrins replaced by mono-, di- and tri-sialylated transferrins.

Chagas disease is an ailment affecting over 18 million with thousands of new cases reported each year[91]. Chagas disease is characterized by progressive chronic fibrotic myocarditis and degeneration of tissues innervated by the autonomic nervous system, most commonly marked with cardiac abnormalities such as arrhythmias and cardiac insufficiency[92]. *Trypanosoma cruzi*, the agent of Chagas disease, is a protozoan most commonly transmitted through insect bites, but can be transmitted through blood transfusions as well[93]. *T. cruzi* releases a sialidase to cleave negatively charged sialic acid residues from host cells to incorporate with itself. It is believed that this is the etiology of the major symptoms of Chagas. Changing the level of sialylation may contribute to cardiac arrhythmias and insufficiency possibly through modification of ion channel function.

Ion transport is the basis for cellular communication

Ion transport across the membrane of excitable tissues is essential for proper cellular and tissue function. Cellular membranes are essentially impermeable to ions; thus, ion transport requires assistance in the form of membrane proteins. These proteins can be divided into several groups, transporters, pumps and ion

channels. Transporters allow ions to move across the membrane with other solutes e.g. the sodium/glucose transporter. Pumps require the use of energy to move ions across the membrane. Ion channels are water filled pores that allow ions to flow through the membrane down their electrochemical gradient when open. There are four types of ion channels, leak, ligand gated, stretch activated, and voltage gated channels. Leak channels are considered constitutively active (open) and contribute to maintenance of the resting membrane potential of a cell. Stretch activated ion channels require the membrane to physically stretch the channel to an open state while ligand gated channels open in response to a ligand (i.e., a neurotransmitter) binding to its' extracellular surface. Voltage gated ion channels gate in response to the depolarization and repolarization of the cell membrane.

Cardiac contraction is the result of orchestrated ion channel function

The cardiac action potential is the concerted opening, inactivation, and closing of many types of voltage gated ion channels, the Na^+/K^+ ATPase pump, and possibly some ligand gated ion channels (summarized in Figure 1.1 and 1.6). The result of the cardiac action potential is cardiac systole. The cardiac action potential of contractile myocytes is divided into 5 distinct phases. Phase 0 is the depolarization of the cellular membrane by opening of voltage gated sodium channels (Na_v) which allows sodium ions to move down their electrochemical gradient and into the cell. Phase 1 begins at the height of cellular depolarization and is marked by a sudden repolarization of the cell. This occurs when voltage

Figure 1.6. Schematic of a typical cardiac action potential.

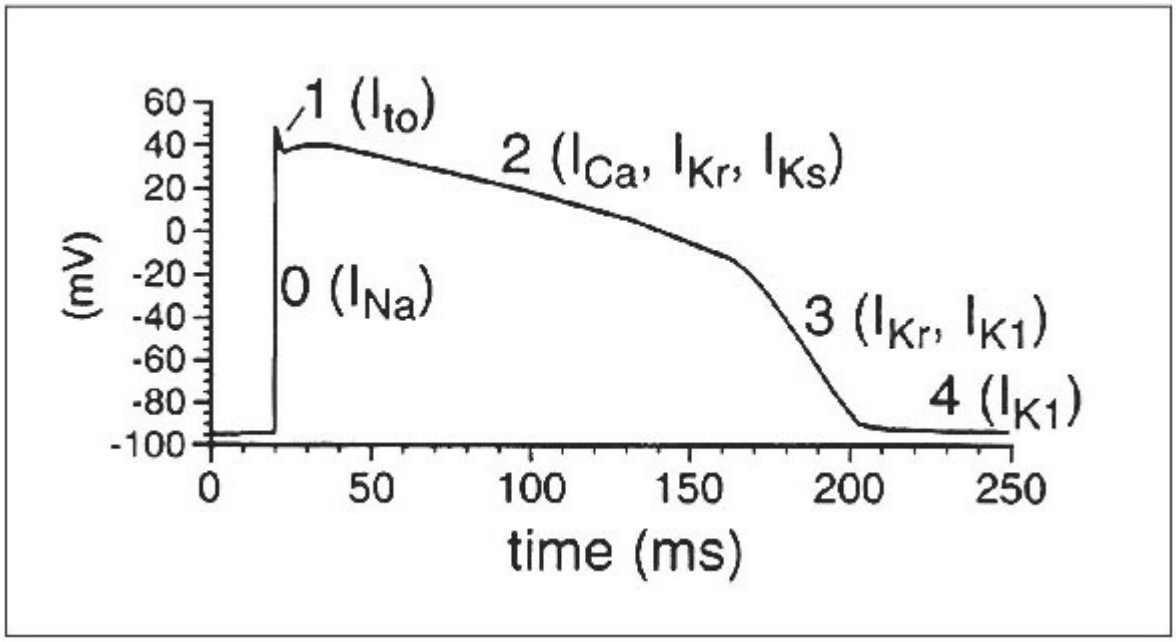

Figure 1.6. The cardiac action potential is shown, with ionic currents responsible for each phase listed. Figure from Keating and Sanguinetti, 2001[94].

gated sodium channels inactivate and sodium can no longer traverse the membrane and around the same time, voltage gated potassium channels open to allow potassium ions to exit the cell (I_{to}); thus, causing a short, rapid repolarization. As I_{to} diminishes, voltage gated calcium channels open to initiate phase 2. Influx of calcium ions is approximately the electrical equivalent to the efflux of potassium ions leading to a flat segment in the cardiac action potential termed the "plateau." In phase 3, calcium channels inactivate and another population of slowly activating potassium channels open which causes the final repolarization and hyperpolarization of the membrane. This hyperpolarization of the membrane is essential for the voltage-gated ion channels to recover from inactivation. In phase 4, mostly leak and ligand gated ion channels are open to maintain the resting membrane potential and allow more channels to return to a closed position so the cell is prepared for the next action potential and resulting systole.

The structure of Na_v dictates channel function

Voltage gated sodium channels (Na_v) are transmembrane proteins which open in response to membrane depolarization to selectively allow sodium ions to pass though[95]. Na_v are composed of a single polypeptide chain approximately 220kD and is composed of 24 transmembrane segments subdivided into 4 homologous domains composed of 6 transmembrane segments each (Figure 1.7). Each of the 6 transmembrane segments are unique, yet have homologous segments in the other 3 domains. The S5 and S6 domains line the pore with an extracellular

Figure 7. Schematic of the voltage-gated sodium channel structure.

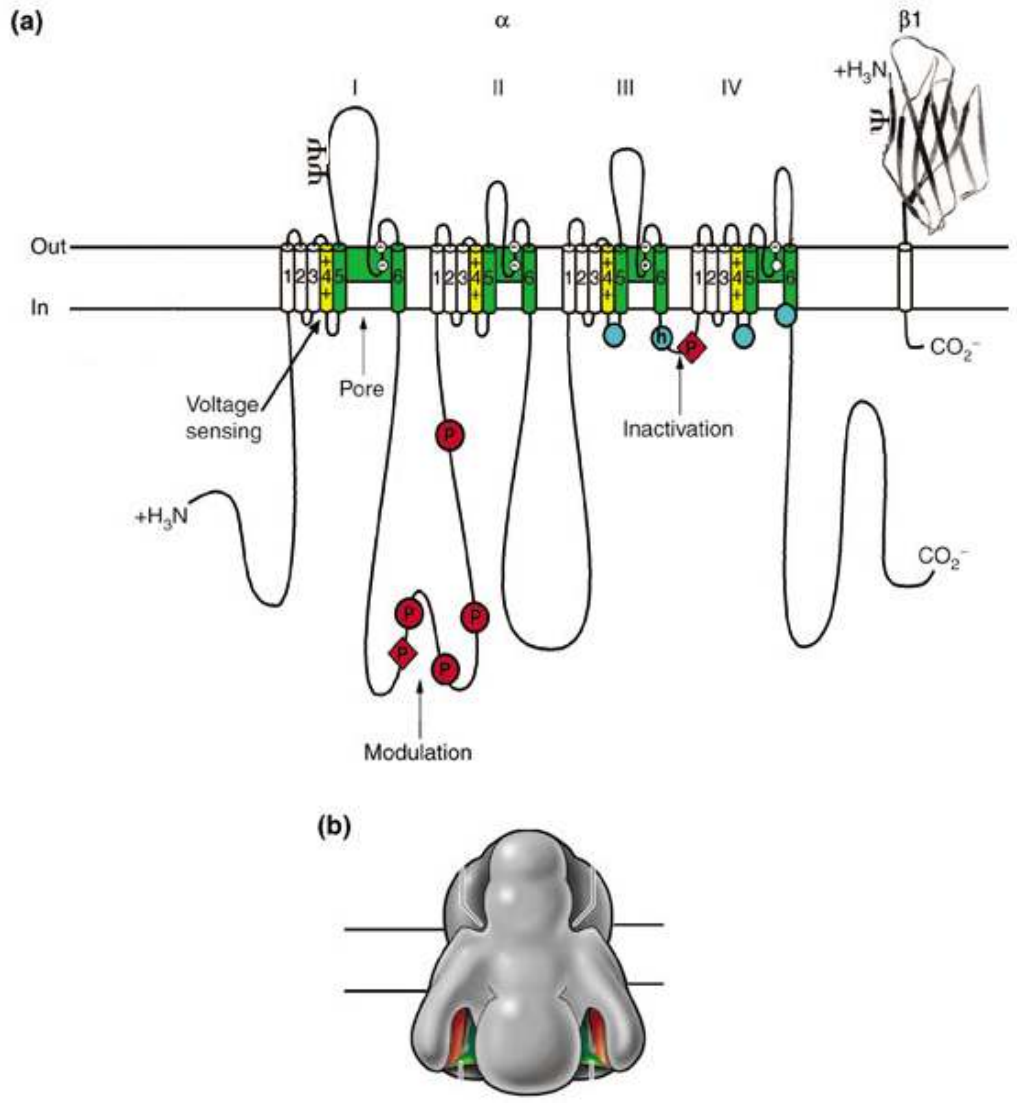

Figure 7. Schematic of voltage-gated sodium channel alpha and beta subunits. (a) A characteristic alpha subunit with four homologous domains, each consisting of six alpha helical transmembrane segments is illustrated with the β_1 subunit. The S5 and S6 (shown in green) of each domain are considered the pore forming segments. The loop connecting the S5 and S6 dips into the pore and forms the selectivity filter (designated by white circles). Note that both proteins are glycosylated (represented by ψ). Blue circles in the intracellular loops of domains III and IV mark the inactivation gate IFM motif and its receptor (h, inactivation gate); P, phosphorylation sites. (b) A hypothetical three-dimensional structure of the Na_v channel α-subunit compiled from electron micrograph reconstructions. Figures adapted from Yu *et al.* 2003[96].

S5-S6 linker that dips into the pore. This pore forming loop is essential to proper channel selectivity, where the specific amino acid sequence of DEKA (aspartate, glutamate, lysine and alanine) defines the channel as sodium specific. When this sequence is changed to the calcium channel sequence of EEEE, the channel allows calcium to pass while preventing sodium entry. Although the remaining structure is currently under debate, there is consensus that the remaining transmembrane segments are located peripherally to the pore. The S4 segment is considered to be the voltage sensor since every third amino acid is a positively charged arginine or lysine and the whole segment moves in response to membrane depolarization. Movement of the S4 segment causes a conformational change and the channel to gate allowing sodium to enter into the cell. Also of note is the intracellular linker of domains III and IV which contains the hydrophobic amino acid sequence; IFM (isoleucine, phenylalanine and methionine) which has been implicated in fast inactivation.

The tertiary and quaternary structure of voltage gated ion channels has been the topic of recent debate within the scientific community as an alternative hypothesis has arisen from crystallography work on the voltage gated potassium channel which shares significant homology with Na_v^{97-100}. Cartoons of both models are shown in figure 1.8. The conventional theory, as proposed through studies from the past 25 years, has the S4 segment located within a water filled column formed by the other segments of the same domain. The S5 and S6 segments form the pore while S1-S3 surround the S4. The S4 segment moves

Figure 1.8. Two competing theories for voltage-gated ion channel gating.

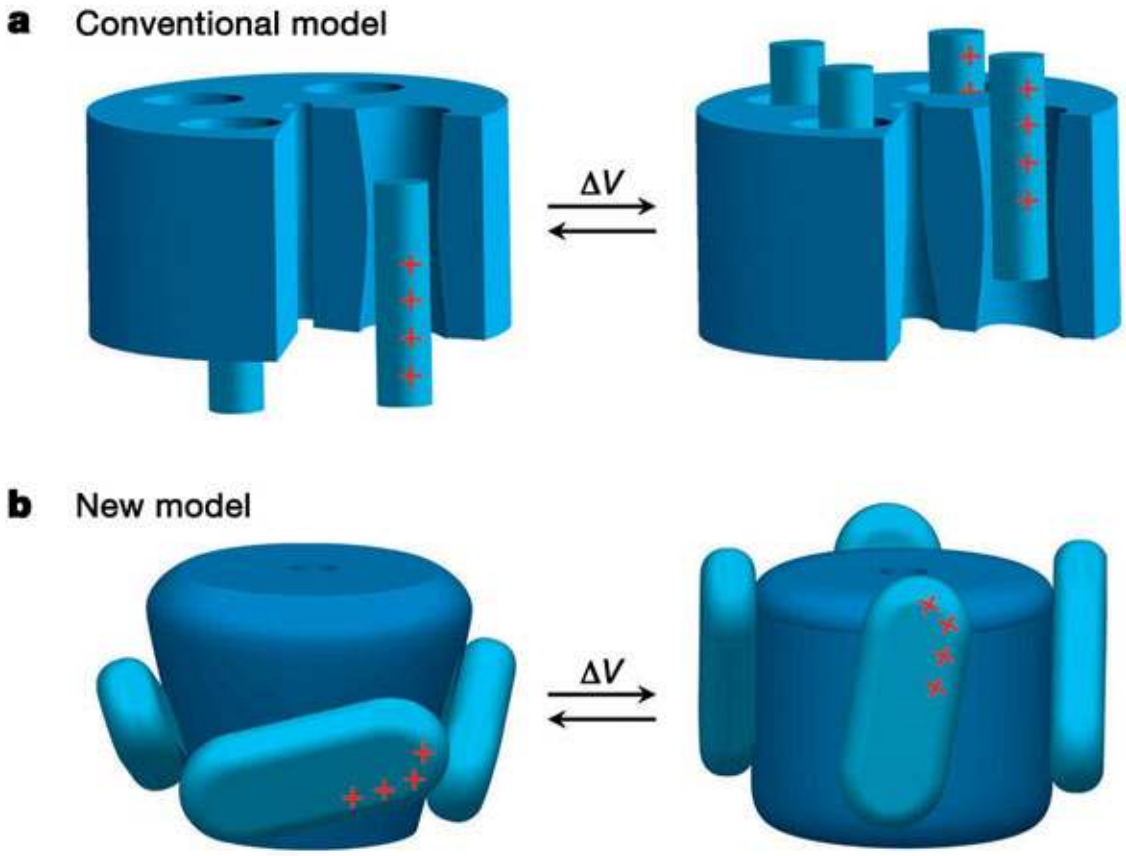

Figure 1.8. Cartoon depicting two models of S4 segment movement in response to a change in membrane potential (ΔV). (+) signs represent positively charged amino acids within the protein structure. Figure from Jiang et al. 2004.[97]

towards the extracellular surface in a perpendicular manner to the cellular membrane in response to membrane depolarization. In the model proposed by Jiang et.al., the S4 segment forms a paddle-like structure with the S3 segment peripheral to the pore which rotates through the lipid bilayer towards the extracellular surface and again causes a conformational change in the pore-forming segments to open the channel[97]. Both theories have two important similarities. First, the positively charged amino acids, composing the S4 segment, move towards the extracellular surface and second, this movement results in channel gating. Since the introduction of the paddle theory in 2003, the scientific community has been vigorously debating these theories with evidence supporting the traditional theory[101-108] and other data supporting the paddle theory[97-100,109-113].

Post-translational modifications may alter ion channel function

The surface potential theory predicts that charges closely associated with the membrane adjacent to voltage gated ion channels contributes to channel gating[95]. The idea is based upon electrostatic attraction of the voltage sensor by negative charges closely localized to the channel. The source of these charges include charged lipids of the cell membrane, charged amino acids of the protein itself or a closely associated protein, ions present in the extracellular fluid and negatively charged sialic acid residues capping glycan structures.

Voltage gated ion channels are heavily post-translationally modified through fatty acylation, phosphorylation, nitrosylation, sulfonation, and glycosylation. Of these posttranslational modifications, glycosylation is the highest proportion with upwards of 30% of the final channel mass being glycans[114-116]. A fully glycosylated and sialylated channel could have as many as 100 sialic acid residues attached to a single channel[114-116]. Each ion channel is differently glycosylated based upon number and location of potential N-linked sites and the other factors involved in N-glycosylation described above.

The impact of glycosylation, particularly sialic acids, on ion channel gating has been the focus of numerous studies[73,117-128]. These studies report that glycosylation can directly alter gating of voltage-gated sodium and potassium channels in an isoform specific manner. For example, in CHO cells, $Na_v1.4$ gating is sialic acid sensitive whereas the gating of $Na_v1.5$ does not change in response to the altering level of sialic acids[117,118]. $Na_v1.4$ is more heavily glycosylated than $Na_v1.5$ likely due to the number of glycosylation sites with mature glycans attached.

$Na_v1.5$ is the predominate sodium channel isoform expressed in mouse cardiac tissue and commonly is considered the cardiac isoform[3]. Studies have concluded that $Na_v1.5$ is the isoform responsible for phase 0 of the cardiac action potential indicating that $Na_v1.5$ gating initiates and propagates the cardiac action potential[129]. $Na_v1.5$ has the same basic structure as other voltage gated sodium

channels and is putatively heavily glycosylated with 13 potential glycosylation sites[117].

A recent study of Na_v function in neonatal and adult cardiomyocytes showed that neonatal ventricular Na_v required a ~10mV greater depolarization to gate than does neonatal and adult atrial and adult ventricular Na_v[123]. Following desialylation through neuraminidase treatment, neonatal atrial and adult atrial and ventricular Na_v gated similarly to untreated (and neuraminidase-treated) neonatal ventricular Na_v. Furthermore, investigators determined that $Na_v1.5$ was similarly expressed throughout the developing myocardium and β_1 did not contribute to the changes. Western blot analysis revealed that neonatal and adult atrial and adult ventricular Na_v had higher levels of sialylation than did neonatal ventricular Na_v. Regulated glycogene expression is likely responsible for the various levels of Na_v glycosylation observed, and the resulting changes in Na_v gating. This suggests that the cardiac glycome may be regulated throughout the heart during development.

This study was designed to determine whether the glycome is remodeled throughout the developing myocardium and whether the remodeled glycome can affect excitability. Glycans, more specifically the negatively charged sialic acid residues commonly capping glycan structures, modulate gating of voltage gated ion channels in both a *cis* (glycans attached to the alpha subunit) and *trans* (glycans attached to an auxiliary subunit) manner as reported in chapter 3. The

level of glycosylation of Na_v changes throughout the developing myocardium and in cardiac failure[74,123]. The change in glycogene expression throughout the developing myocardium is described in chapter 4 and chapter 5 illustrates the correspondingly diverse N-glycan profiles. Finally, chapter 6 suggests that cardiac excitability can be altered through the regulation of a single glycogene.

CHAPTER 2

MATERIALS AND METHODS

Chinese Hamster Ovary (CHO) Cell Culture and Transfection

Pro5 and Lec2 cells were grown as described previously[130]. Briefly, cells were plated onto 35 mm culture dishes at 25-50 % confluence. Following a 24 h incubation, cells were then exposed to a 1 ml Opti-MEM (Invitrogen) medium containing 8 µl lipofectamine (Invitrogen) and 1-2 µg DNA. Following a 5-24 h incubation at 37°C in a 5% CO_2 humidified incubator, the medium was replaced with CHO medium consisting of Dulbecco's modified Eagle's medium (DMEM; Mediatech) supplemented with 25 mM Hepes, 15% fetal bovine serum (FBS; Mediatech), and 100 U ml^{-1} penicillin and 100 µg ml^{-1} streptomycin. Growing medium included the same antibiotics, 10% FBS, and alpha Minimum Essential Medium (αMEM) with (Pro5) or without (Lec2) ribo- and deoxyribonucleosides (Invitrogen). Electrophysiological recordings began 68-76 h post-transfection, selecting cells expressing GFP.

Vector Construction and Mutagenesis

The $rNa_v1.2$ open reading frame (ORF) inserted into pRC-CMV (Invitrogen) was a gift of Dr. Alan Goldin. The $hNa_v1.7$ cDNA ORF was inserted into pcDNA3.1. Expression vectors containing $hNa_v1.4$ and $hNa_v1.5$ were as previously described[118]. $h\beta_1$ was subcloned into the bicistronic vector, pIRES2-EGFP

(Clontech), to ensure expression of β_1 through visual inspection. The $h\beta_1$ mutant ($h\beta_{1\text{-}\Delta N}$) was created using the GeneEditor (Promega) site-directed mutagenesis kit. $h\beta_1$ was cloned into pBluescript vector (Stratagene) as a template. Each asparagine residue initiating an external *N*-linked consensus sequence, N*X*(S/T), was mutated to a serine residue through sequential mutagenesis. The constructs were sequenced to confirm successful mutagenesis. $h\beta_{1\text{-}\Delta N}$ was then subcloned into pIRES2-EGFP for co-expression experiments. $h\beta_1$ and $h\beta_{1\text{-}\Delta N}$ were amplified using PCR with the following oligonucleotides 5'-TCCGGCCACCTGGACGCCCG-3' and 5'-GCGCAGCACGCGCCGCGCAG-3'. PCR products were subcloned into pcDNA3.1/V5-His TOPO TA expression vector (Invitrogen). Both ORFs were subsequently subcloned into pEGFP-N1 (Clontech) to generate C-terminal, GFP-tagged $h\beta_1$ and $h\beta_{1\text{-}\Delta N}$ constructs.

Electrophysiology and Data Analysis

Sodium Current Recordings

Sodium currents were recorded using the whole cell patch clamp technique described previously[117,118]. The combination of an Axon Instruments 200B patch clamp amplifier with a CV203BU headstage (Axon Instruments, Foster City, CA). Pulse acquisition software (HEKA) running on an 800 MHz Pentium III PC computer (Dell Computers) was used to generate pulse protocols. The resultant analog signals were digitized using the ITC-16 analog to digital converter (Intsrutech, Great Neck, NY).

Whole cell patches were formed using techniques previously described [131]. Electrodes were back-filled with electrode solution and manipulated to close proximity to the target cell. Slight negative pressure was applied to the electrode and giga-seals formed between the cell and electrode tip and a short, rapid increase in negative pressure provided electrical access to the interior of the target cell. Pulse protocols are explained explained later. All data were recorded at least 5 minutes after attaining whole cell access to ensure dialysis of electrode solution.

External recording solutions consisted of (in mM): 224 Sucrose, 22.5 NaCl, 4 KCl, 2.0 $CaCl_2$, 5 glucose, and 5 Hepes. Intracellular recording (electrode) solutions contain (in mM): 120 sucrose, 60 CsF, 32.5 NaCl, and 5 Hepes. Both solutions were titrated with 1 N NaOH to pH 7.4 at room temperature. All solutions were filtered using 0.2 μm filters (Invitrogen) immediately prior to use. For the Ca^{2+} perfusion studies, the Ca^{2+} calcium concentration was reduced in the external solution to 0.2 mM. Seals were formed in the bath solution containing 2.0 mM Ca^{2+}. The cells were first perfused with 2.0 mM Ca^{2+} bath solution and followed by perfusion the 0.2 mM Ca^{2+} bath solution to determine directly the shift in V_a with a 10-fold change in external Ca^{2+} concentration. All of the data shown were recorded at least 5 min after attaining whole cell configuration to assure complete dialysis of the intracellular solution. All of the solutions were filtered using Gelman 0.2-μm filters immediately prior to use.

Pulse Protocols

Conductance-Voltage (G-V) Relationship

Pulse protocols were used as previously described [117]. A holding potential of -120 mV was applied to the cell and stepped from -100 to +70 mV in 10 mV increments for 10 ms. Consecutive pulses were initiated every 1.5 s and leak subtracted using the P/4 method which steps negatively from the holding potential to eliminate any leak current. At each potential, steady-state whole-cell conductance was determined by measuring the peak current and dividing by the driving force (difference between the membrane potential and the observed reversal potential). Single Boltzmann fits of the data determined maximum conductance and the average V_a ± SEM were determined from this fit. Normalized data from the Boltzmann fits were averaged with remaining cells of the same type and an averaged conductance-voltage curve was determined using the following Boltzmann relation fit to the data:

Fraction of maximal conductance= $[1+(\exp-(V-V_a/K_a))]^{-1}$,

where V is the membrane potential, V_a is the voltage of half activation, and K_a is the slope.

Steady-State Inactivation Curves (h_{inf})

Cells were prepulsed for 500 ms from the holding potential (-120 mV) to potentials ranging from -130 to -20 mV in 10 mV increments, followed by a +60 mV pulse for 5ms and returning to the -120 mV holding potential. Currents from

each cell were normalized to the maximal current (determined through a single Boltzmann fit), averaged with other cells of the same type and again fit to a single Boltzmann relationship (eq. 2) from which V_i (voltage of half inactivation) and the slope were calculated.

Fraction of maximum current = $[1+(\exp-(V-V_i/K_i))]^{-1}$,

Recovery from Inactivation

Cells were held at -120 mV membrane potential, pulsed to +60 mV for 10 s, and stepped to the recovery potential for 1-20 ms in 1 ms increments. The potential was then stepped again to +60 mV for 10 ms. Peak currents from the two +60 mV pulses were compared to determine the fraction of current measured during the second pulse which represents the fraction of channels that recovered from inactivation during the recovery pulse. Fractional current was plotted as a function of the recovery time between the two test pulses of 60 mV. Single exponential functions were fit to the data to determine the time constants for recovery from inactivation, t_{rec}.

Measurement of Inactivation gating kinetics

Inactivation gating kinetics were determined from attenuating currents (90-10%) of traces used for G-V relationships which were fit to a single exponential function.

Neonatal and Adult Cardiac Tissue Isolation

Neonatal and adult atria and ventricle tissue were isolated for microarray, quantitative PCR, western blot analysis and mass spectrometry. Neonatal mice and adult mice were euthanatized and whole hearts removed and placed in Dulbecco's phosphate buffered saline. Atria were gently removed from the remaining heart and ventricles were dissected away from the base of the heart with great care taken to ensure only atria and ventricles were removed. The remaining portions were discarded. Tissue intended for microarray and quantitative PCR studies was transferred to RNase Later (Sigma, St. Louis, MO) and incubated for minimum one hour. Tissue intended for western blot and mass spectrometry studies was snap frozen in liquid nitrogen to prevent protein degradation and stored at -80^{o}C.

mRNA Isolation

Heterogeneous populations of litter-mate animals were isolated for microarray testing. Neonatal samples were each composed of 7-9 animals (14-18 atria or ventricles) yielding approximately 25-28 mg of tissue. Adult samples were each composed of 4 animals (2 male and 2 female) aged 10-12 weeks yielding approximately 25-28 mg of tissue. Tissue was homogenized by dounce and isolated following RNeasy manufacturer protocols (Qiagen). Beckman Spectrometer was used to determine final RNA concentration.

Microarray

Three RNA samples each of neonatal and adult atria and ventricle were sent to the Consortium for Functional Glycomics Gene Microarray Core E for microarray analysis. Samples were amplified and biotin labeled using the Bioarray High Yield RNA transcript labeling kit (ENzo Life Sciences, Farmingdale, NY). Hybridization and scanning of the glycogene-chip, GLYCOv2, were performed according to Affymetrix's recommended protocols (Affymetrix, Santa Clara, CA).

Microarray Analysis

The GLYCOv2 chip was created by the Consortium for Functional Glycomics and produced by Affymetrix (Affymetrix, Santa Clara, CA). This chip was designed that each probeset consists of 11 perfect match and 11 single base mismatch probe pairs (Table 2.1).

The intensities from each perfect match were compared to corresponding mismatch pair. Invariant set normalization of the data was performed using the DNA-Chip (dChip) Analyzer (www.dchip.org) software package for probe-level and high level analysis of gene expression microarrays. Hierachical clustering and class comparison was accomplished using Biometric Research Branch (BRB) Array Tools v3.2.2. Heatmaps were generated using the dChip program. Class comparison used a p-value cutoff of 0.05 and a multivariate permutation based false discovery rate calculation preset at 10% with 80% confidence level.

Table 2.1 Breakdown of probesets on GLYCOv2

	Probesets In Triplicate	Probesets In Duplicate	Single Probesets	Total genes transcript targets	Total Probesets
Total Human	503	426	101	1030	2462
Total Mouse	443	363	119	925	2174
Total Other (control)	0	0	46	46	46
				2001	4682

Quantitative PCR

Three RNA samples each of neonatal and adult atria and ventricle were reverse-transcribed to cDNA using Superscript II Reverse Transcriptase (Invitrogen) following manufacturer's protocols. Briefly, 1ug of total RNA, 100μM dNTPs and 100ng of random hexameric primers (Invitrogen) were incubated at 65^{o}C for 5 minutes then placed on ice. First strand buffer and 10 mM dithiothreitol (DTT) were added and incubated at room temperature (25^{o}C) for 2 minutes. Finally, 200 μM Superscript II reverse transcriptase was added to the mixture and incubated for 10 minutes at room temperaturefollowed by 42^{o}C for 50 minutes and 70^{o}C for 15 minutes. cDNA is ready for use in real time reactions.

Primer sets were designed using PrimerQuest (IDT) and are shown below. Primer sets were tested for efficiency and precise amplification using dilution curves. Quantitative PCR was performed on 12 gene products including HPRT and β-actin as controls. Each primer set was run in triplicate for each sample. SYBR Green PCR master mix (Superarray), primers and cDNA were combined in one well of a 96 well PCR plate (Rio-Rad) and covered using RT-PCR optical tape (Bio-Rad). PCR products were detected in real time using the iCycler iQ detection system (Bio-Rad) with PCR conditions of 5 minutes at 95^{o}C followed by 40 cycles of 30 sec at 95^{o}C, 30 sec at 60^{o}C and 30 sec at 72^{o}C. Relative expression levels were reported using the $\Delta\Delta^{CT}$ method of analysis where triplicate threshold values of a single gene are averaged and compared to the

control (either HPRT or β-actin) then this Δ^{CT} value is compared to the Δ^{CT} of another sample.

Quantitative PCR primer sequences

ST3Gal3	CTG TGA TGA AGT GGC AGT CG	CTC GCT GGA TGT TGT CTG TC
ST3Gal5	AAA GTC CCA CTC CAG CCA AAG C	GTG TAG CCA AGA CAA CGG CA
STX	AGC CAG CCT CAT CCA AAT G	TAT CCT TCT CCG CAT CCA AG
ST6Gal1	GAC CAG GAG TCA AGT TCA GCG T	AGA AGA CAC GAC GGC ACA CT
ST8Sia6	TGC TGC TCC TCC TGC GTA T	TAT GTG CTG TTC CTG GTG CGT G
ST6GalNAc6	AAC AAA GAG CAG CGG TCA GC	GTT GCC GAG GAT AGG GAA GTA GG
Versican	TGG CTG TGG ATG GTG TTG TG	TGC TCT GGG CTT GCT ATG AC
HPRT	GCA GTA CAG CCC CAA AAT GG	GGT CCT TTT CAC CAG CAA GCT
B-actin	CCA ACC GTG AAA AGA TGA CC	CCA GAG GCA TAC AGG GAC AG

Glycan Screening

Glycan Isolation

N-glycans were isolated as previously described[132]. Cardiac tissue was homogenized in 0.5% SDS tris buffer and dialyzed in 12-14 kDa cut-off dialysis tubing in an ammonium hydrogen carbonate solution (50 mM, pH 7.4) for 48 hours. Once dialyzed, samples were lyophilized. Reduction and carboxymethylation of samples were carried out by incubation in 0.5ml of 2 mg/mL DTT in deoxygenated tris buffer (0.6M, pH 7.4) for 45 minutes at 37^{o}C followed by addition of 0.5 ml of 12mg/mL iodoacetic acid in tris buffer (0.6M, pH 7.4) and incubation for 90 minutes at room temperature in the dark. Reaction was terminated by dialysis for 48 hours and the sample was lyophilized. Samples were then digested in 1 mL of a 50mM ammonium hydrogen carbonate solution (pH 8.4) with approximately 2 mg of TPCK treated bovine pancreas trypsin at

37^{o}C for 16 hours. The sample was purified through a Sep-Pak C18 conditioned with 5mL methanol, 5mL 5% (v/v) acetic acid in water 5mL propan-1-ol and 30 mL of 5% (v/v) acetic acid followed by collection of 3mL of 20% (v/v) and 40% (v/v) propanol in 5% (v/v) acetic acid. These fractions are pooled and lyophilized followed by digestion with 3 units of N-glycosidase F (PNGase F) in 200 uL of 50mM ammonium hydrogen carbonate (pH 8.4) at 37^{o}C for 20 hours. The digested sample was purified through a pre-conditioned Sep-Pak C18 (5mL methanol, 5mL 5% acetic acid, 5mL propan-1-ol and 15 mL of 5% acetic acid), eluted with 5mL of 5% acetic acid.

Glycan derivatization

N-glycans were prepared for mass spectrometry by chemical derivatization using the sodium hydroxide procedure[133]. 5 pellets of sodium hydroxide and 3mL of dry DMSO were crushed together in a glass mortar. 1mL of the resulting slurry was added to the dry sample in a glass tube followed by 0.5mL of methyl iodide. The mixture was vigorously mixed on an automatic shaker for 15 minutes at room temperature. The reaction was quenched by addition of water, Permethylated N-glycans were extracted with 1mL of chloroform and washed with 3mL of water several times. The organic phase was dried under a stream of nitrogen. Derivatized and dried glycans were then purified through a pre-conditioned Sep-Pak C18 (5mL methanol, 5mL water, 5mL acetonitrile, 15 mL water) and eluted with 15%, 35%, 50% and 75% (v/v) acetonitrile in water.

Mass Spectrometry

Mass spectrometry was performed through the Consortium for Functional Glycomics and the methods were described previously[132]. The permethylated sample was dissolved in 10 µl of methanol, and 1 µl of dissolved sample was mixed with 1 µl of 2,5-dihydroxybenzoic acid (20mg/mL in 70:30 (v/v) water:methanol), spotted onto a metal plate and dried under vacuum. MALDI-MS and MALDI-MS/MS data were acquired using a Perseptive Biosystems Voyager-DE^{TM} STR mass spectrometer in the reflectron mode with delayed extraction and a 4800 MALDI-TOF/TOF (Applied Biosystems, Damstadt, Germany) mass spectrometer respectively. The collision energy for MALDI-MS/MS experiments was set to 1kV and argon was used as collision gas.

Cardiomyocyte Isolation for Electrophysiology

The cardiomyocyte isolation protocol was adapter from a method described previously[134]. Neonatal (postnatal day 2-3) mice we rapidly euthanized and hearts excised and placed in 0 Ca^{2+} Tyrode's Solution. Atria and ventricles were carefully separated and digested in 260 units Type I collagenase (Sigma, St. Louis, MO)/ mL 0 Ca^{2+} Tyrode's Solution at 37^{o}C for 40 minutes. Cells were centrifuged at 160 g for 5 minutes and the supernatant replaced with fresh collagenase solution. Cells were gently triturated and incubated at 37^{o}C for 30 minutes followed by centrifugation at 160 g for 5 minutes. The supernatant was replaced by CHO media (DMEM supplemented with 10% Fetal Bovine Serum (Gibco) and 100 U/ml penicillin and 100mg/ml streptomycin (Gibco), triturated,

and incubated at 37^{o}C for 20-40 minutes to stop digestion. Again the cells were centrifuged for 5 minutes at 160 g and plated on laminin-coated 35mm dishes in fresh CHO media.

Cardiomyocyte Electrophysiology

Sodium Current Recordings

Recording techniques were described above. External recording solutions consisted of (in mM): 20 NaCl, 10 TES, 5 KCl, 1 $CaCl_2$, 5 CsCl, 10 glucose, and 100 choline chloride adjusted to pH 7.35 with CsOH. Intracellular recording (electrode) solutions contain (in mM): 20 NaCl, 10 TES, 2 MgCl2, 2 $CaCl_2$, 20 EGTA, and 105 CsF adjusted to pH 7.35 with CsOH. All solutions were filtered using 0.2 μm filters (Invitrogen) immediately prior to use.

Action Potential Recordings

Myocytes were patched and recorded in external solution (in mM): 135 NaCl 5 KCl, 2 $CaCl_2$, 1 $MgCl_2$, 10 HEPES, 10 glucose, pH 7.4. Patch pipettes were filled with a solution with the following constituents (in mM): 110 K-Asp; 20 KCl, 10 NaCl, 4 ATP-Mg, 10 HEPES, pH 7.3. APs were recorded at room temperature (22-25 °C) using an Axopatch 200B amplifier (Axon Instruments) and pCLAMP 9 software (Axon Instruments). APs were triggered by a 2-ms injection of a depolarizing current at a frequency of 1 Hz. Analysis of APs was performed using Clampfit 9 software (Axon Instruments, Foster City, CA).

Transgenic mouse

The STX knockout mouse was provided through collaboration with Dr. Jamey Marth, University of California San Diego. Neonatal mice were 2-3 days post-natal and adult mice were 10-12 weeks post-natal.

Data Analysis

Sodium current electrophysiological data were analyzed using Pulse/PulseFit (HEKA) and Sigmaplot 2001 (SSPS Inc.) software. Action potential data were analyzed using Clampfit (Axon) and Sigmaplot 2001 (SPSS Inc). Figures were produced using Sigmaplot 2001 (SPSS Inc), Microsoft Excel (Microsoft), or Corel Draw (Corel).

CHAPTER 3

THE β_1 SUBUNIT MODULATES Na_v GATING IN AN ISOFORM-SPECIFIC, SIALIC ACID-DEPENDENT MANNER

Cardiac remodeling often involves modulating ion channel expression and/or function. One mechanism of this remodeling likely involves regulated expression and function of Na_v alpha and beta subunits. With ten identified Na_v alpha isoforms, changing expression of these isoforms would modify ion currents[135]. The role of β_1 was not conclusively established with theories of the role of β including nodal stabilization, cellular localization, functional expression, kinetics and voltage-dependence of channel gating[136]. Previous studies report that N-glycans alter function of some Na_v alpha isoforms. Here we report β_1 subunit sialic acids alter the voltage dependence of Na_v gating.

The β_1 subunit external domain is essential for correct modulation of sodium channel gating and is the site of four potential N-glycosylation sites[137]. At least three of these four sites are thought to be glycosylated in the mature protein. Published reports agree that β_1 causes a hyperpolarizing shift in the voltage dependence of inactivation and in several studies, activation gating was also shifted in the hyperpolarized direction by β_1[138-145].

Voltage gated sodium channel α and β subunit isoforms each have a unique glycosylation signature determined through their differing number and location of N-glycosylation sites. In an attempt to determine how N-glycans alter Na_v function, four isoforms, the adult skeletal muscle isoform ($Na_v1.4$), the cardiac isoform ($Na_v1.5$), a peripheral nerve isoform ($Na_v1.7$), and a brain isoform ($Na_v1.2$), were expressed in the fully glycosylating Pro5 and reduced sialylating Lec2 cell lines. $Na_v1.4$ and $Na_v1.5$ were previously reported [117,118] and $Na_v1.2$ and $Na_v1.7$ were studied here for the first time. Table 3.1 and figures 3.1-3.4 indicate that $Na_v1.5$ and 1.7 are not sensitive to α sialic acids; whereas, $Na_v1.2$ shows a small, insignificant depolarizing shift in gating when sialylation is reduced. $Na_v1.4$ shows a significant ~14.6mV depolarizing shift in the absence of sialic acids.

In an attempt to determine the role of the β_1 subunit in voltage gated sodium channel gating, we co-expressed β_1 with each of the four Na_v isoforms. When co-expressed in the fully sialylating Pro5 cell line, β_1 induced a hyperpolarizing shift in all measured gating parameters of three of four α subunits. β_1 did not have an effect on $Na_v1.4$ gating. These data generally agree with previously published work with most studies indicating that β_1 induces a hyperpolarizing shift in the gating of various α subunits[137,143,146-150].

Table 3.1. The measured gating parameters for α±β_1±sialic acid

Channel construct	n	V_a (mV)	V_i (mV)	τ_h (ms)	t_{rec} (-120 mV) (ms)
$Na_v1.4$ + SA	9	-31.3 ± 2.0	-71.5 ± 3.3	2.4 ± 0.4	1.8 ± 0.05
$Na_v1.4$ - SA	9	-16.7 ± 1.7[a]	-60.8 ± 1.5[a]	7.9 ± 1.1[a]	1.3 ± 0.03[a]
$Na_v1.4$ + β_1 + SA	11	-29.2 ± 1.6	-70.0 ± 2.3	2.9 ± 0.5	1.7 ± 0.02
$Na_v1.4$ + β_1 - SA	9	-16.3 ± 1.1[a]	-63.1 ± 1.8[b]	8.1 ± 0.2[a]	1.4 ± 0.03[a]
$Na_v1.5$ + SA	13	-29.0 ± 2.2	-78.7 ± 2.5	2.8 ± 0.4	4.0 ± 0.1
$Na_v1.5$ - SA	10	-29.5 ± 1.6	-79.5 ± 1.9	2.4 ± 0.2	4.1 ± 0.1
$Na_v1.5$ + β_1 + SA	11	-37.4 ± 1.6[a]	-86.1 ± 3.2[b]	2.0 ± 0.1[b]	5.6 ± 0.3[a]
$Na_v1.5$ + β_1 - SA	9	28.6 ± 0.9	-78.8 ± 1.6	2.9 ± 0.2	4.1 ± 0.1
$Na_v1.7$ + SA	10	-15.1 ± 1.2	-70.0 ± 2.4	4.8 ± 0.8	5.5 ± 0.09
$Na_v1.7$ - SA	9	-14.4 ± 1.7	-70.0 ± 3.7	5.2 ± 1.2	5.5 ± 0.06
$Na_v1.7$ + β_1 + SA	12	-23.8 ± 1.8[a]	-76.2 ± 2.0[b]	3.0 ± 0.4[b]	7.8 ± 0.2[a]
$Na_v1.7$ + β_1 - SA	9	-13.4 ± 1.3	-68.3 ± 1.5	5.1 ± 0.8	5.5 ± 0.2
$Na_v1.2$ + SA	9	-14.6 ± 1.6	-60.5 ± 3.1	3.3 ± 0.7	2.5 ± 0.08
$Na_v1.2$ - SA	10	-11.7 ± 1.8	-62.7 ± 3.1	3.1 ± 0.5	2.2 ± 0.04[b]
$Na_v1.2$ + β_1 + SA	12	-20.8 ± 0.7[a]	-68.1 ± 2.7[b]	2.3 ± 0.3[b]	3.1 ± 0.07[a]
$Na_v1.2$ + β_1 - SA	9	-11.9 ± 1.0	-62.2 ± 2.8	3.2 ± 0.6	2.2 ± 0.06[b]
hSkM1P1 + SA	10	-23.5 ± 2.3	-70.4 ± 2.5	3.4 ± 0.5	1.8 ± 0.07
hSkM1P1 - SA	8	-26.7 ± 1.2	-68.8 ± 2.5	3.4 ± 0.8	1.8 ± 0.05
hSkM1P1 + β_1 + SA	9	-32.7 ± 2.0[a]	-75.9 ± 1.6[b]	2.3 ± 0.4[b]	2.4 ± 0.06[a]
hSkM1P1 + β_1 - SA	11	-24.0 ± 1.5	-69.2 ± 1.5	3.7 ± 0.6	1.9 ± 0.04

Table 1. The measured gating parameters for α±β_1±sialic acid. The data are the mean parameter values ± S.E. τ_h data were measured for $Na_v1.4$, $Na_v1.5$, and hSkM1P1 at -40mV and for $Na_v1.2$ and $Na_v1.7$ at -30mV. Two-tailed Student's t test was used to determine the significance of β_1 sialic acids comparing each condition with the parameter measured for the fully sialylating α subunit alone. Significance ($p<0.1$) demarcated with an (a) and highly significant ($p < 0.005$) demarcated with a (b). Table from Johnson *et al.* 2004[120].

Figure 3.1. Alpha and β_1 subunit sialic acids modify channel activation in an α subunit dependent manner.

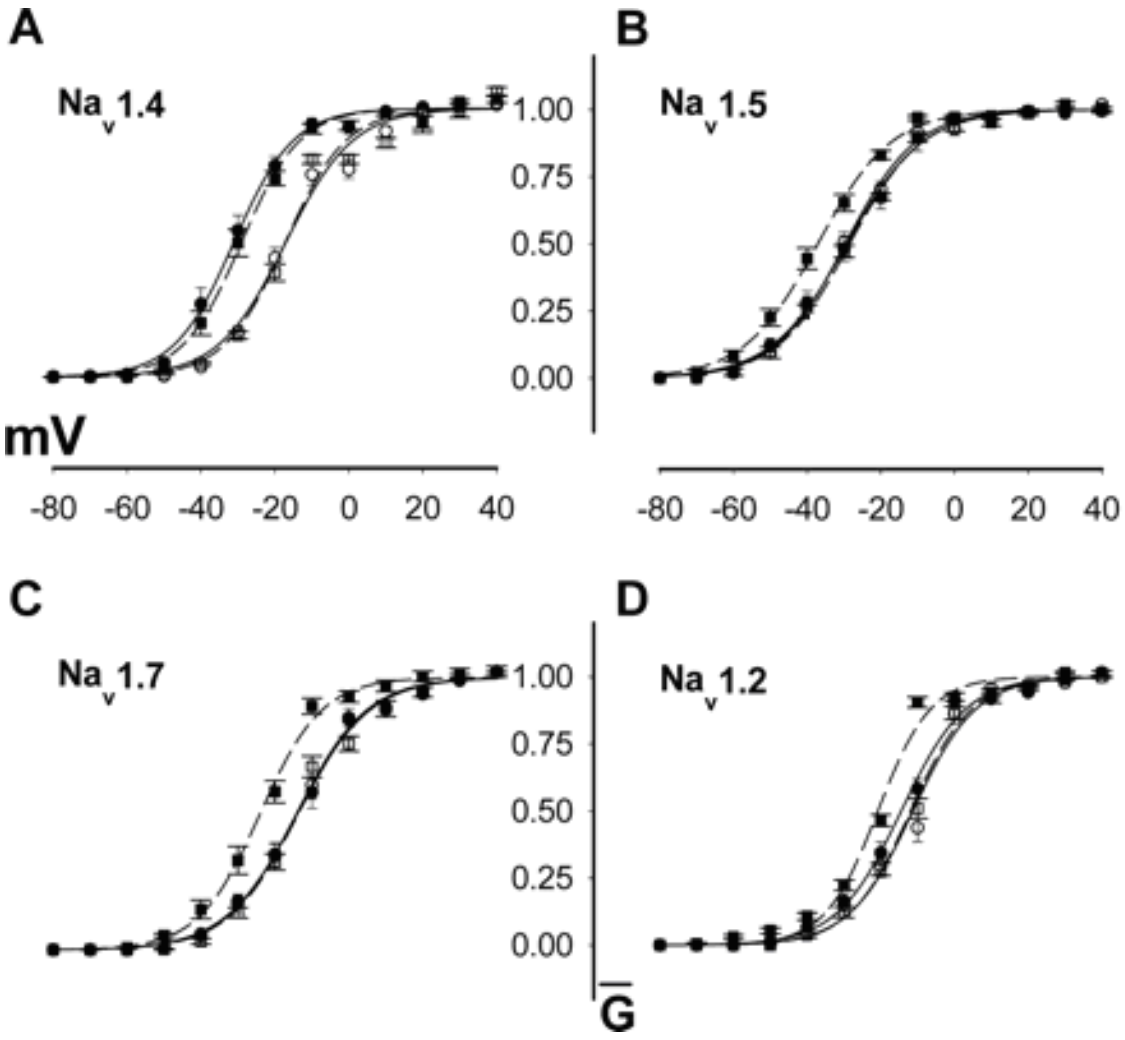

Figure 3.1. Conductance-voltage (*G-V*) relationships for four voltage-gated sodium channel α subunits ± β_1 as expressed in the fully sialylating, Pro5, and reduced sialylating, Lec2, cell lines. The data are the mean normalized peak conductance (G) ± S.E. at a given membrane potential and are shown as curves that are fits of the data to single Boltzmann relationships. Data are summarized in Table 1. *Circles* with *solid lines*, α subunit alone; *squares* with *dashed lines*, α+ β_1. *Filled symbols*, in Pro5 cells; *open symbols*, in Lec2 cells. *A*, $Na_v1.4$. *B*, Na_v 1.5. *C*, $Na_v1.7$. *D*, $Na_v1.2$. Figure adapted from Johnson *et al*. 2004[120].

Figure 3.2. Alpha and β_1 subunit sialic acids modify channel inactivation in an α subunit dependent manner.

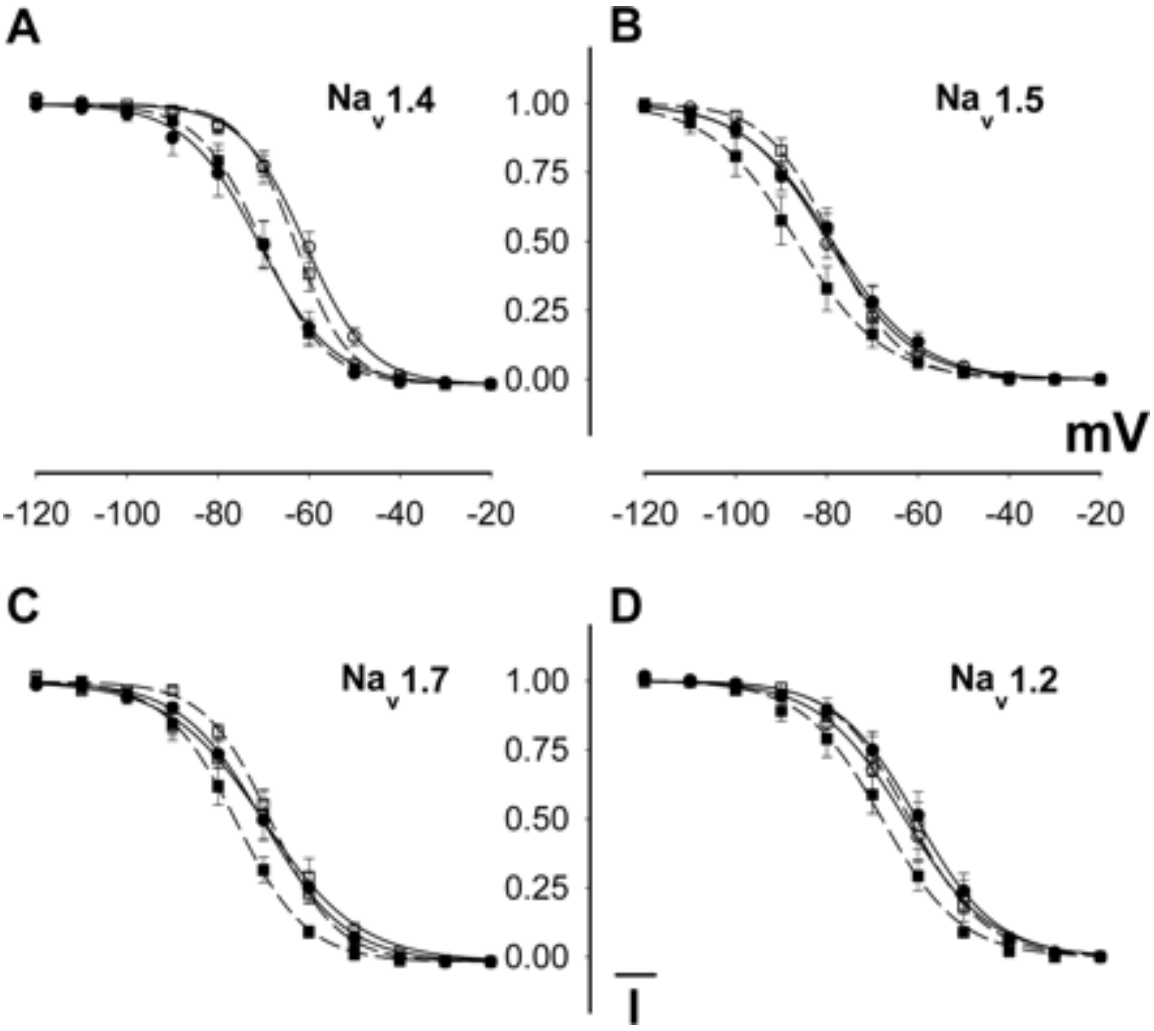

Figure 3.2. Steady state channel availability (h_{inf}) curves for the four α subunits ± β_1 ± sialic acid. The data are the mean normalized peak current (Ī) ± S.E. measured during a maximally depolarizing test pulse following a 500-ms prepulse to the plotted potentials. Lines and symbols are identical to those described in figure 3.1. Figure from Johnson *et al*. 2004[120].

Figure 3.3. Alpha and β_1 subunit sialic acids alter channel fast inactivation rates in an α subunit dependent manner.

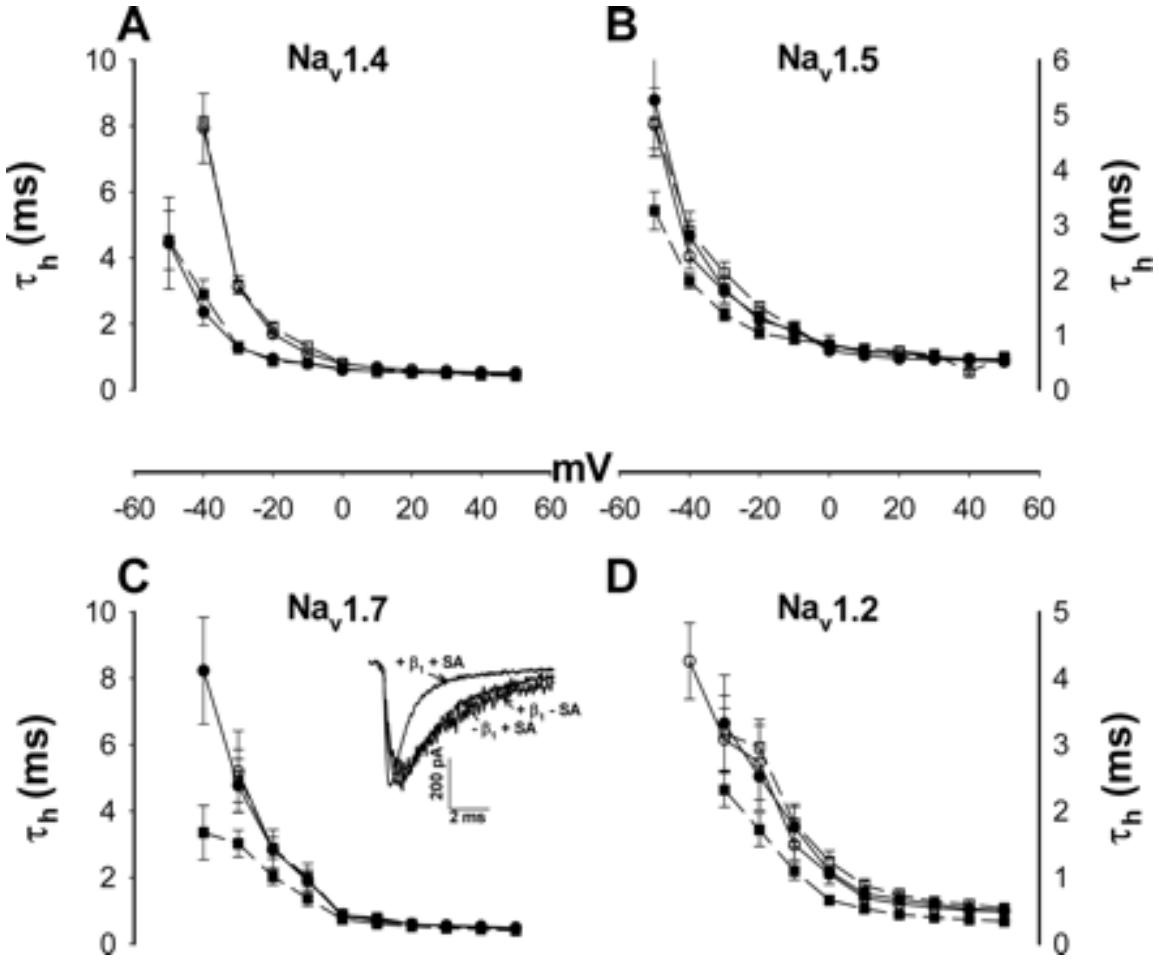

Figure 3.3. The rate of fast inactivation for the four α subunits ± β_1 ± sialic acid. The data are the means ± S.E. time constants for fast inactivation (τ_h) as a function of membrane potential. *Inset* to *C*, representative normalized whole cell Na^+ current traces measured at –20 mV for Na$_v$1.7. Note that the rate at which the current attenuates (inactivates) is much faster in the presence of β_1 sialic acids, consistent with the observed shift in τ_h along the voltage axis. The *scale* shown is for Na 1.7 + β_1 + SA current traces, to which the other current traces were normalized. Lines and symbols are identical to those described in figure 3.1. Figure from Johnson *et al.* 2004[120].

Figure 3.4. Alpha and β_1 subunit sialic acids modify channel recovery from inactivation in an α subunit dependent manner.

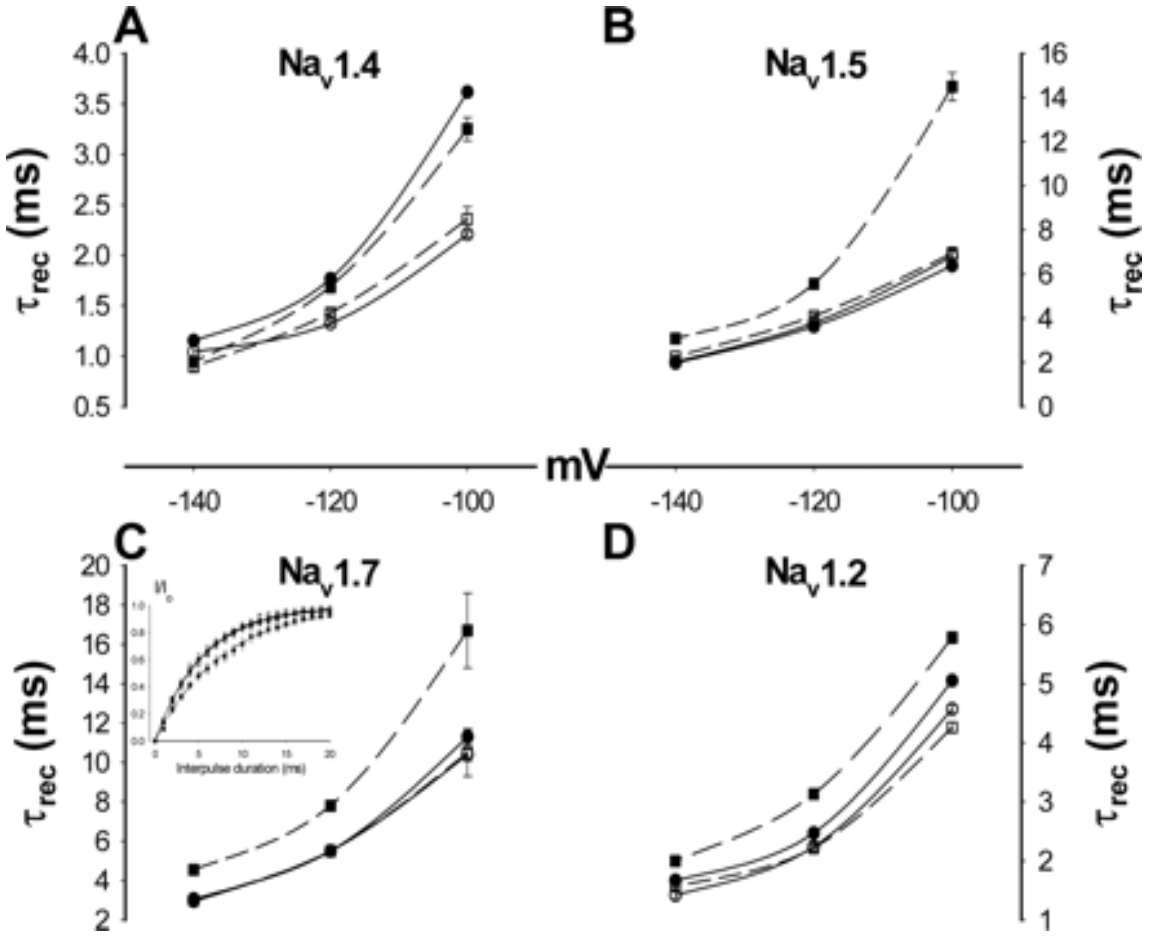

Figure 3.4. Time constants for recovery from fast inactivation (τ_{rec}) ± S.E. measured for the four α subunits ± β_1 ± sialic acid at three recovery potentials. *Inset* to *C*, typical plot of the fractional recovery measured following a –120mV recovery potential for Na$_v$1.7 ± β_1 ± SA. The data are the means ± S.E. fractional current measured during a second depolarizing test pulse following the plotted interval at –120 mV recovery pulses of various durations. The *lines* are exponential fits of the data from which the τ_{rec} were determined. Lines and symbols are identical to those described in figure 3.1. Figure from Johnson *et al*. 2004[120].

Due to the fact that β_1 is heavily glycosylated, we tested the hypothesis that β_1 sialic acids modulate Na_v gating. β_1 induced a hyperpolarizing shift in the gating of three of the four α subunits studied when expressed in Pro5. This effect was eliminated when expressed in the essentially non-sialylating Lec2 cell line as all four α subunits gated the same as α expressed alone. β_1 did not alter any gating parameter of $Na_v1.4$ under either sialylating or non-sialylating conditions. As shown in figures 3.1-3.4, all effects of β_1 on gating can be attributed to the sialic acids attached to β_1, since in the absence of β_1 sialic acids, Na_v gating is not modulated.

In addition to N-linked glycosylation, sugars can be attached to serine or threonine residues of membrane proteins termed, O-linked glycosylation. Mutagenesis of the four N-linked glycosylation sites provides a method to determine that N-linked sialic acids are responsible for modulating Na_v gating. The mutant β_1 lacks all N-linked glycosylation, yet all other post-translational modifications remain. As exhibited in figure 3.5, $\beta_{1\text{-}\Delta N}$ (β_1 with all N-glycosylation sites mutated resulting in no N-glycosylation) had no effect on gating of any of the Na_v α subunits previously modulated by β_1. Thus, we confirm that β_1 N-linked sialic acids are fully responsible for the observed shifts in Na_v α gating.

Figures 3.1-3.4 showed that the heavily glycosylated $Na_v1.4$ was sensitive to α subunit sialic acids (cis effect), but not sensitive to β_1 sialic acids (trans effect). Conversely, the putatively lesser glycosylated $Na_v1.2$, 1.5 and 1.7 were not

Figure 3.5. β_1 subunit sialic acids modify channel gating parameters in a saturating manner.

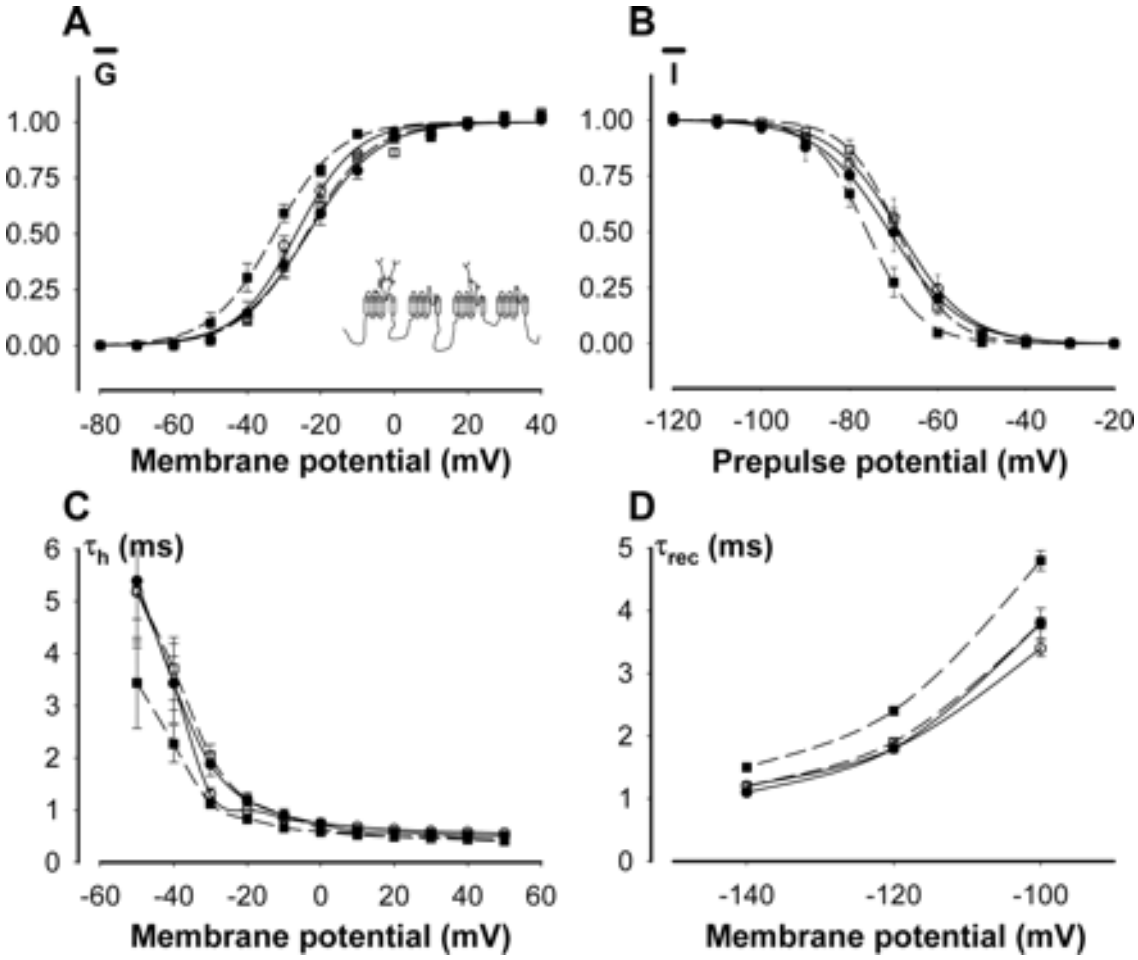

Figure 3.5. Voltage-dependent steady state and kinetic gating for hSkM1P1 ± β_1± SA is shown. *Circles*, hSkM1P1 expressed alone; *squares*, hSkM1P1 + β_1. *Filled symbols*, in Pro5 cells; *open symbols*, in Lec2 cells. A schematic of hSkM1P1 structure illustrates that the chimera consists of $Na_v1.4$ with the less glycosylated $Na_v1.5$ DIS5-S6 loop replacing the $Na_v1.4$ DIS5-S6. *A, G-V* relationship. *B*, steady state channel availability. *C*, fast inactivation time constants. *D*, time constants for recovery from fast inactivation. Figure from Johnson *et al.* 2004[120].

Figure 3.6. The impact β_1 has on Na_v gating is likely through electrostatic interaction.

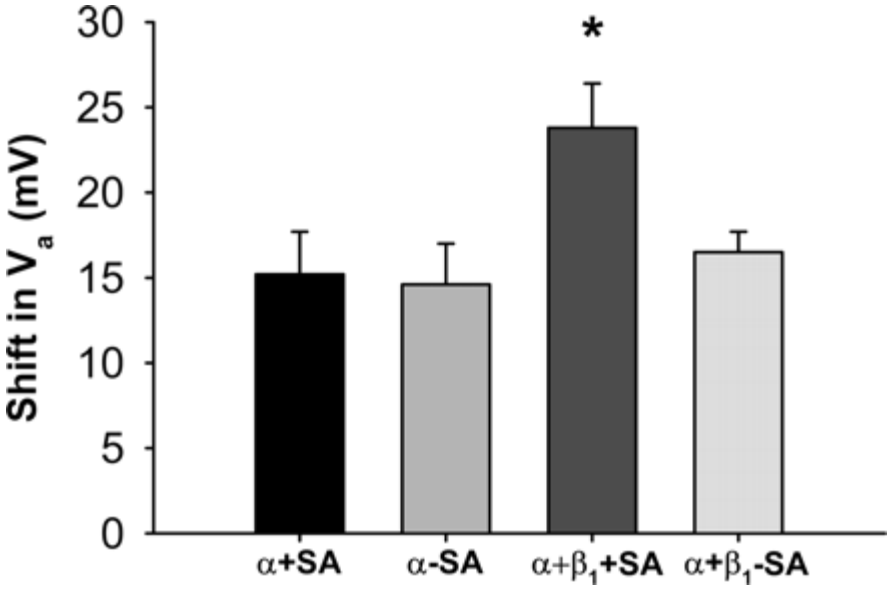

Figure 3.6. A *bar graph* of the observed hyperpolarizing shifts in V_a for hSkM1P1 ± β_1± SA with a 10-fold decrease in external Ca^{2+} concentration used to differentially screen external negative surface charges. Figure from Johnson *et al.* 2004[120].

dependent on α subunit sialic acids, but β_1 sialic acids modified their gating. These data suggest that in this cellular system there may be a saturating limit to the contribution of sialic acids to channel gating, with $Na_v1.4$ sialic acids possibly achieving saturation. Figure 3.6 further supports this theory by showing that gating of a less glycosylated $Na_v1.4$ chimera, hSkM1P1 (a generous gift from Dr. A.L. George Jr.), is no longer dependent on α subunit sialic acids but is sensitive to β_1 sialic acids. These data suggest that by decreasing $Na_v1.4$ sialylation below saturating levels, β_1 can impact channel gating. Thus, it appears that the combined effects of *cis* α subunit DIS5-S6 and *trans* β_1 subunit functional sialic acids on channel gating are saturating.

The surface potential theory of voltage-gated channel gating is often assigned to the phenomenon of negative external surface charges changing channel gating. It has been established that increasing external Ca^{2+} concentrations tends to shift Na_v gating to depolarized potentials. Ca^{2+} tends to screen the negative charges that contribute to the negative surface potential; thus, minimizing the external negative charge sensed by the channel gating mechanism. The voltage sensed by the channel gating mechanism becomes more negative, moving away from the voltage of half activation and requiring a larger depolarization to activate the channel. If sialic acids contribute to this negative surface potential, channel gating will be more sensitive to external Ca^{2+} concentrations as the level of sialylation is increased. If β_1 sialic acids contribute to the surface potential, co-expression of β_1 with hSkM1P1 (a reduced

Figure 3.7. N-glycans are completely responsible for β_1 effects on Na_v gating.

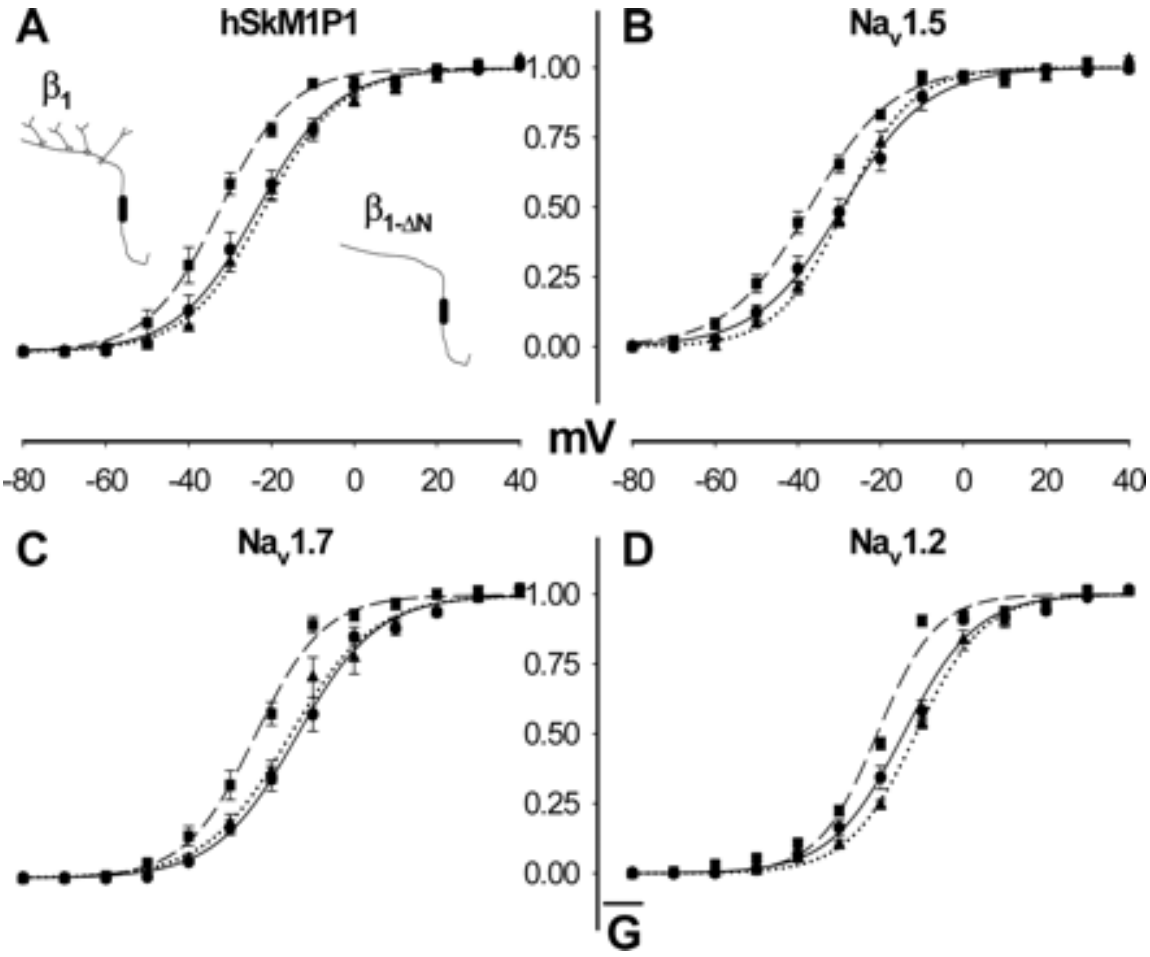

Figure 3.7. G-V relationships for hSkM1P1 (A), $Na_v1.5$ (B), $Na_v1.7$ (C), and $Na_v1.2$ (D) under fully sialylated conditions alone or co-expressed with β_1 or with $\beta_{1\text{-}\Delta N}$. Filled circles with solid lines, α subunit alone (n = 9–13 for each); filled squares with dashed lines, (n = 9–12 for each); filled triangles with dotted lines, α co-expressed with $\beta_{1\text{-}\Delta N}$ (n = 4–6 for each). Figure from Johnson *et al*. 2004[120].

glycosylated form of $Na_v1.4$) in Pro5 cells should show the greatest sensitivity to Ca^{2+}. Figure 3.7 clearly indicates that the presence of β_1 increases sensitivity to external Ca^{2+} concentrations; thus, β_1 sialic acids likely contribute to the negative surface potential.

Discussion

To date, there have been many α and β subunit isoforms identified for the voltage-gated sodium channel, each with unique glycosylation patterns that may modulate sodium current[118,128]. Expression of α subunits and β subunits are regulated over time and in disease states and can be processed differently among cell types possibly as a mechanism to ensure proper cellular function[151-155]. The model in figure 3.8 suggests a scenario where Na_v α and β_1 subunit combinations function differently and sialylation could change the location on the curve as sialylation is changed.

As proposed by this model, various α subunit isoforms may function differently as a result of their level of glycosylation as ten α isoforms have been identified each with a unique putative glycosylation signature. β_1 expression, as previously described and in this study, alters some Na_v channel α isoforms; hence, control of β_1 expression causes acute changes in functional sialic acids associated with an α subunit possibly altering the gating of the α subunit.

Figure 3.8. Model proposing the saturating effects of sialic acids on Na_v gating.

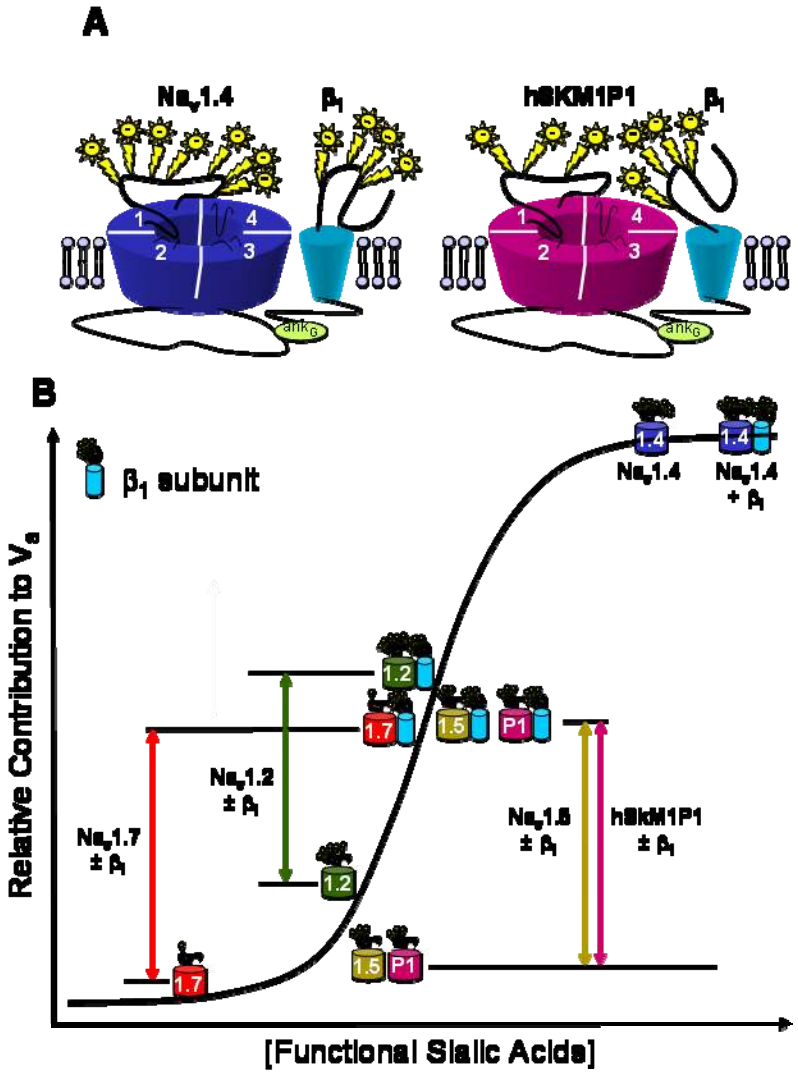

Figure 3.8. Model predicting the possible saturating effects of α and β1 sialic acids on Na_v gating. (A) Possible interactions between $Na_v1.4$ (highly glycosylated) and hSkM1P1 (lesser glycosylated) α subunit and β_1 sialic acids. The data suggest that β_1 sialic acids cannot contribute further to the gating of $Na_v1.4$ but do contribute to the gating of the other α subunits through an apparent electrostatic mechanism. Thus, $Na_v1.4$ shows ineffectual β_1 sialic acids as distant, whereas the hSkM1P1 illustrates that fewer α subunit functional DIS5-S6 sialic acids may allow β_1 sialic acids to interact more intimately with the α subunit and contribute to channel gating. (B) a theoretical G-V curve comparing contributions to V_a associated with various α and β1 combinations. The location of each combination is not precise but is consistent with the data shown here. Figure from Johnson *et al*. 2004[120].

β_1 expression is regulated through development, commonly expressed at the highest levels after 4 weeks of age[156-159]. β_1 is a heavily glycosylated protein; although, this level is different among the tissues in which it is expressed. If β_1 glycosylation alters Na_v α gating, then Na_v would likely be modified differently in each tissue in relation to the level of glycosylation. Here, we report the effect of β_1 on Na_v gating can be entirely attributed to sialic acid residues.

A recent study of Na_v function revealed a sialic acid dependent change in Na_v activity throughout cardiac development[123]. These changes were independent of altered Na_v protein expression as the same Na_v α isoform was expressed in all tissues studied and upregulation of β_1 did not impact Na_v function. Different levels of glycosylation, through glycogene regulation, likely is responsible for these changes and is the focus of the following two chapters.

CHAPTER 4

GLYCOGENE EXPRESSION IS REGULATED THROUGHOUT THE DEVELOPING MYOCARDIUM

Slight changes in ion channel function may lead to devastating maladies such as myotonia, paralysis, epilepsy, long QT syndrome (LQTS) and arrhythmias associated with heart failure[129,148,160-180]. One possible mechanism to modulate Na_v function is through alteration of the glycan structure. A previous report indicated that cardiac Na_v gating is altered in a cell-specific, glycosylation dependent manner[123]. Furthermore, others report that glycosylation is altered in disease states, some of which present with altered excitability[28,29,73-75,87,88,92]. Thus, we determined that glycogene expression is regulated, and that the glycome is remodeled. Then, we questioned whether and how these changes in glycosylation might alter cardiac excitability.

Glycosylation abnormalities have been reported to occur in many disease states including heart failure. Until recently, in depth studies of glycogene expression in cardiac disease and non-disease states have been lacking. Here we present and compare the glycogene expression profiles for four healthy cardiac tissues; neonatal atria (NA), neonatal ventricle (NV), adult atria (AA) and adult ventricle (AV). This investigation utilized the GLYCOv2 gene chip, a customized array

designed by the Consortium for Functional Glycomics, containing 2174 probesets targeting 942 mouse transcripts encoding proteins responsible for glycan biosynthesis and glycan recognition, including glycan transferases, glycan degradation proteins, proteins involved in nucleotide sugar biosynthesis, glycan-binding proteins, and transporters.

To determine the relationship among the four tissue types, we performed hierarchical clustering from all probesets, glycosyltransferases, glycan degradation proteins and nucleotide biosynthesis (Figure 4.1). High correlation within each of the tissue types reveals minimal variability between replicates of each tissue type. Independent clustering of each tissue type indicates the glycogene profile is unique among the four tissue types.

Hierarchical clustering showed that glycogene expression profiles are unique for each of the four tissue types and these differences are evident when displayed as heat maps (Figure 4.2). Due to the lack of a control tissue studied, signals from each gene target are averaged and all relationships are compared to this average with red blocks indicating expression above the mean, blue blocks below the mean, and white as the mean. Despite the differences of overall glycogene expression, there are some important similarities to explore further. The patterns observed provide insight into the changing expression of glycogenes and their role in development, chamber specific expression or high expression in only one tissue type (lower in the three other tissue types).

Figure 4.1 Comparison of glycogene expression among samples.

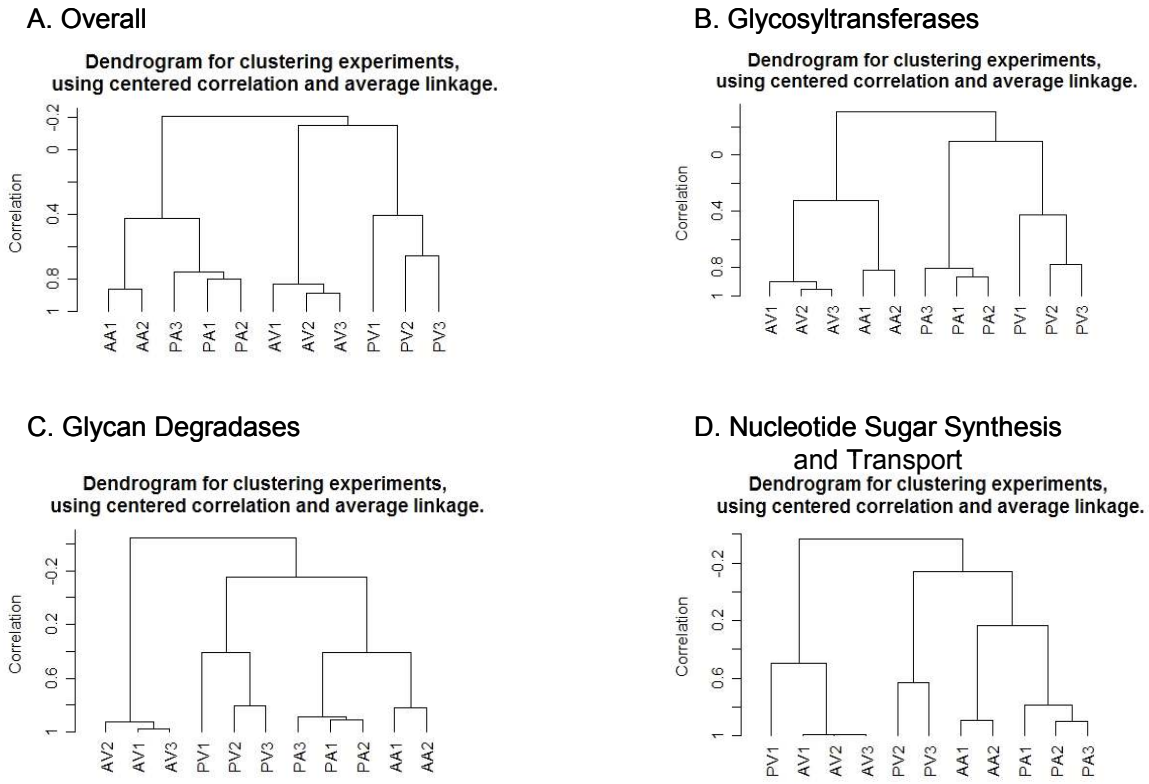

Figure 4.1. Unsupervised hierarchical clustering analysis of glycogenes in the developing murine myocardium. The dendrograms have been constructed using center correlation and average linkage. Three biological replicates are shown for neonatal atria (PA), neonatal ventricle (PV), and adult ventricle (AV) and two biological replicates for adult atria (AA). (A) Overall glycogene expression. (B) Glycosyltransferases. (C) Glycan degradases. (D) Nucleotide sugar synthesis and transporters.

Figure 4.2A. Glycosyltransferase expression throughout the developing myocardium.

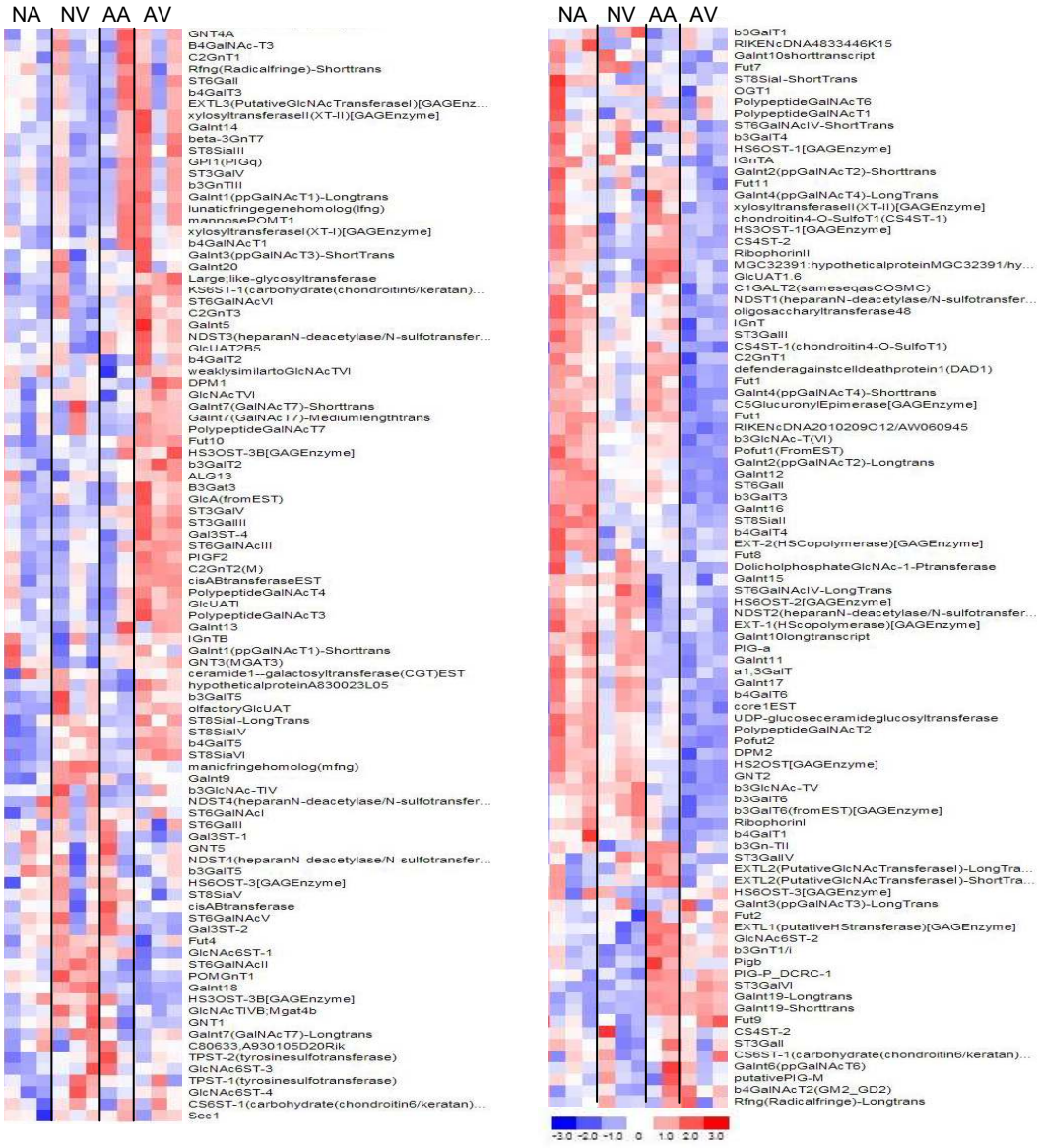

Figure 4.2. Heat maps displaying the relative gene expression levels among each sample and cell type as measured from microarray data. Red indicates upregulation compared to the mean of all samples for a given glycogene whereas blue indicates downregulation and the individual glycogene mean is white. (A) Glycosyltransferases. (B) Glycan degradases. (C) Nucleotide sugar synthesis and transporter genes.

Figure 4.2B. Glycan degradase expression throughout the developing myocardium.

Figure 4.2C. Nucleotide sugar synthesis and transporter gene expression throughout the developing myocardium.

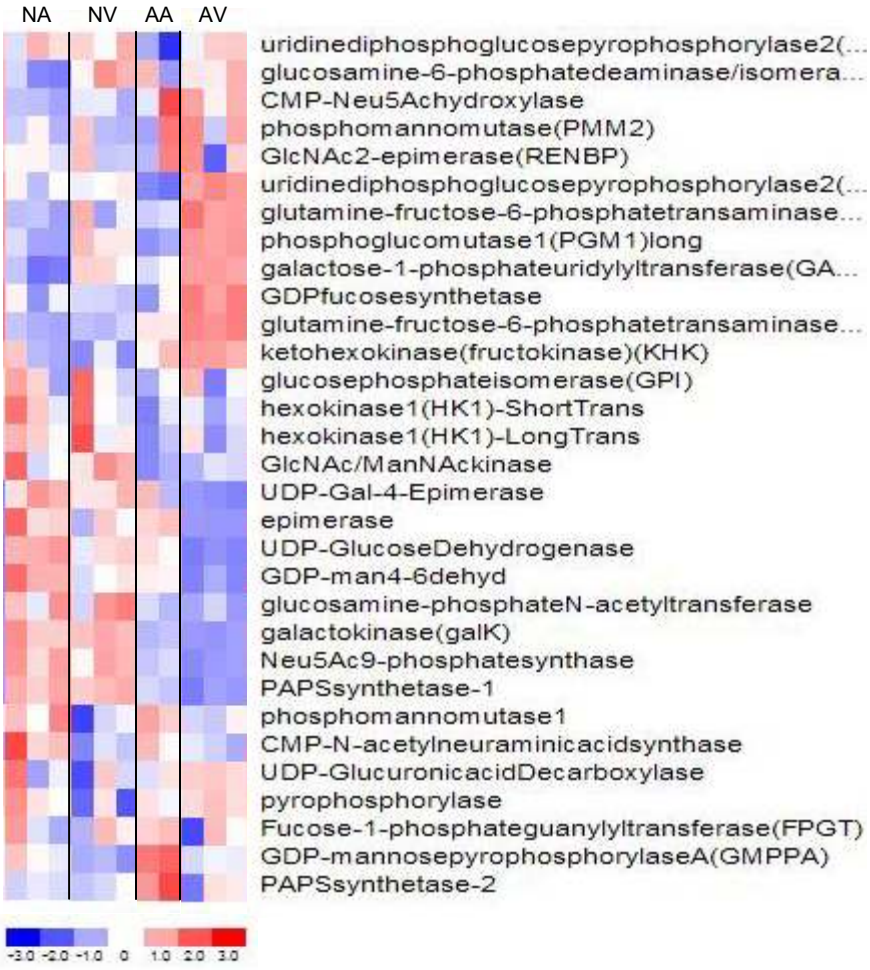

Three distinct expression patterns were identified in the data presented here. First, glycogene expression can be regulated developmentally. This is observed in figure 4.2 where the neonatal tissues are blue or red and adult tissues are the opposite color. Versican is developmentally regulated and is highly expressed in the neonate and essentially absent in the adult. This is likely due to the importance of versican in the development of the heart and its diminished role in adults. On the contrary, ST3GalVI is also developmentally regulated, but present in the adult and absent in the neonate.

Secondly, glycogene expression is also regulated in a chamber-specific manner where genes are expressed above the mean in neonatal and adult atria and below the mean in the neonatal and adult ventricle or vice versa. These changes indicate that the genes involved are essential to normal atrial or ventricular function but not both. Mannosidase-II is categorized with a chamber specific expression pattern since it is expressed at much higher levels in the atria than the ventricles.

The third expression pattern identified is the high (or low) expression of a glycogene in one of the four tissue types compared to the other three. This effect is likely a combination of the two patterns discussed previously where the gene is developmentally expressed (i.e. only present in neonatal tissues) and in a chamber specific manner (i.e. expressed only in the atria). The polysialyltransferase, ST8SiaII (STX), has been shown to be expressed in

various tissues in early developmental stages[181,182], yet ST8SiaII is found to be expressed only in the neonatal atria and is absent in the neonatal ventricle as well as both adult tissues.

Glycogene expression is quite different among the four tissue types and is regulated developmentally, in a chamber specific manner, or as a combination of the two. Furthermore, changing the expression patterns of different enzymes will alter glycosylation biosynthesis at various points throughout the process.

Each glycoprotein and glycolipid has a common core structure which is elongated, possibly branched and eventually terminated. Figure 4.3 illustrates these core structures for N- and O- glycans and glycolipids. For further insight into the impact of a change in glycogene expression, four groups have been created: core structure synthesis, termination, glycan degradation and nucleotide sugar synthesis of which some genes are represented twice; once in core structure synthesis and once in one of the other three groups.

Core Structures

As summarized in table 4.1A, most genes with roles in core glycan synthesis are regulated in a chamber-specific or developmental manner, yet several have no significant change in expression. Most of those genes involved which have some change in expression are involved in the translocation of N-glycan structures from the cytoplasm to the lumen of the endoplasmic reticulum. On the contrary,

Figure 4.3. The three basic glycosylation structures.

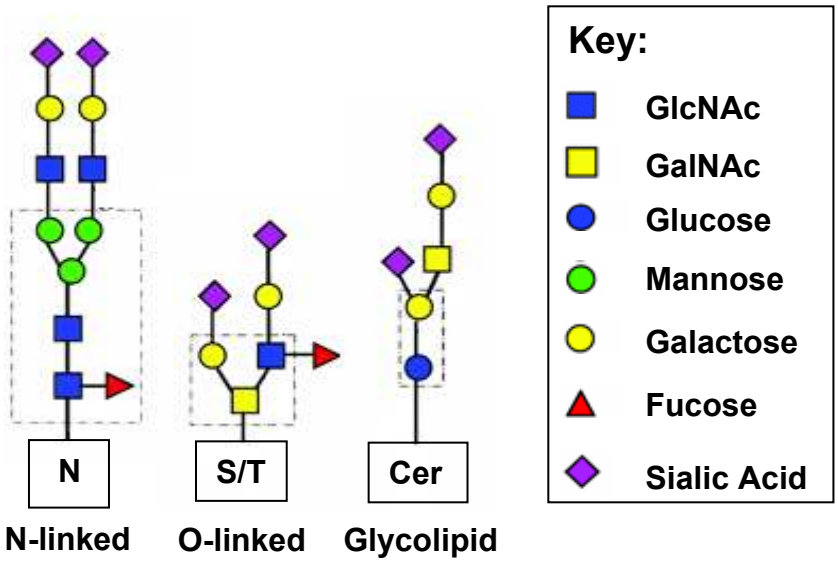

Figure 4.3. Schematic of typical N- and O-linked glycans and glycolipids. Dashed lines indicate core structures for each glycoconjugate.

Table 4.1A mRNA levels encoding proteins involved in core structure synthesis.

Gene Name	NA	NV	AA	AV
N-Glycans				
ALG13	154.6	154.4	153.6	180.8
DPM1	417.1	444.4	407.9	514.4
DPM2	407.9	341.7	308.5	231.0
GPI1(PIGq)	391.6	410.8	436.3	750.0
PIG-a	76.8	70.6	54.5	50.2
Pigb	51.5	47.4	65.6	52.3
PIGF2	66.5	67.2	63.6	80.1
Putative PIG-M	151.6	153.6	159.0	149.8
Defender against cell death protein1	1200.0	1010.9	1246.5	886.4
Oligosaccharyltransferase 48	714.3	490.3	531.6	403.0
RibophorinI	1083.9	1023.0	869.3	722.6
RibophorinII	603.0	436.9	653.2	453.4
GNT1	473.2	517.3	464.0	448.0
GNT2	390.3	366.3	295.0	202.5
a-Mannosidase (Man2B1)	406.6	307.7	366.3	299.4
b-Mannosidase	320.1	332.0	302.6	257.5
MannosidaseII (Man2A1/ManII)	279.4	192.9	298.3	165.2
O-Glycans				
GalNt1(ppGalNAcT1)	623.4	598.7	826.0	1046.5
GalNt2(ppGalNAcT2)	871.3	625.0	614.1	445.5
GalNt3(ppGalNAcT3)	12.2	12.1	12.1	12.8
GalNt4(ppGalNAcT4)	63.2	57.8	68.2	57.5
GalNt6(ppGalNAcT6)	49.2	47.7	56.5	49.9
GalNt7(ppGalNAcT7)	91.3	112.9	87.5	98.9
Glycolipids				
UDP-glucoseceramideglucosyltransferase	188.6	138.2	127.2	100.4
ceramide1--galactosyltransferase	27.2	28.8	23.1	27.8

Table 4.1. Gene expression profiles of glycogenes directly involved in glycan synthesis. Intensity signals were generated with the dChip v1.3 PM-only algorithm and represent the mean of independently prepared samples. (A) Proteins involved in core structure synthesis. (B) Sialyltransferases. (C) Sulfotransferases. (D) Fucosyltransferases. (B,C,D) are considered terminal glycosyltransferases. (E) Glycan degradases; (F) Nucleotide sugar synthesis and transporters. NA, neonatal atria; NV, neonatal ventricle; AA adult atria; AV, adult ventricle.

Table 4.1B. mRNA levels encoding proteins involved in sialylation.

Gene Name	NA	NV	AA	AV
ST3GalI	179.2	142.1	195.6	160.3
ST3GalII	145.1	121.9	122.4	101.7
ST3GalIII	170.2	177.1	205.8	314.8
ST3GalIV	111.3	126.9	132.8	108.0
ST3GalV	319.6	266.6	562.4	1061.3
ST3GalVI	178.1	190.5	409.8	372.6
ST6GalI	257.9	139.1	198.3	82.0
ST6GalII	51.9	54.1	56.2	53.0
ST6GalNAcI	76.8	82.4	81.9	80.4
ST6GalNAcII	77.8	88.1	74.1	76.4
ST6GalNAcIII	40.1	39.9	41.8	49.7
ST6GalNAcIV	107.5	118.3	85.1	94.8
ST6GalNAcV	111.0	111.9	117.7	98.6
ST6GalNAcVI	259.0	304.4	318.2	403.3
ST8SiaI	54.3	61.6	55.3	63.4
ST8SiaII	121.6	48.3	51.2	41.1
ST8SiaIII	61.9	64.3	77.4	107.9
ST8SiaIV	64.3	209.7	112.9	226.7
ST8SiaV	110.2	106.0	120.4	98.5
ST8SiaVI	26.0	65.1	40.2	105.2

Table 4.1C. mRNA levels encoding proteins involved in sulfation.

Gene Name	NA	NV	AA	AV
chondroitin4-O-SulfoT1	178.2	149.5	212.9	144.3
CS4ST-1	68.9	60.7	64.1	46.5
CS4ST-2	146.3	108.2	146.5	103.3
CS6ST-1	66.4	64.8	70.8	71.5
Gal3ST-1	67.8	62.4	64.9	49.3
Gal3ST-2	50.7	53.0	59.3	45.9
Gal3ST-4	15.0	15.8	14.0	18.8
GlcNAc6ST-1	79.3	87.8	85.4	74.5
GlcNAc6ST-2	155.3	136.2	282.6	195.5
GlcNAc6ST-3	34.0	36.4	36.6	35.3
GlcNAc6ST-4	79.8	105.5	83.4	96.6
HS2OST	354.5	295.7	211.2	157.1
HS3OST-1	169.6	107.6	151.2	105.1
HS3OST-3B	66.9	69.6	67.9	61.3
HS6OST-1	186.7	179.1	152.0	155.4
HS6OST-2	53.9	55.9	43.1	45.3
HS6OST-3	58.0	56.3	55.9	58.3
KS6ST-1	284.2	349.9	363.0	528.3
NDST1	112.7	71.3	90.8	54.4
NDST2	131.5	125.2	89.0	93.6
NDST3	34.5	32.3	38.1	40.5
NDST4	43.6	43.4	43.8	43.9

Table 4.1D. mRNA levels encoding proteins involved in fucosylation.

Gene Name	NA	NV	AA	AV
Fut1	128.3	71.9	117.2	56.7
Fut2	57.6	55.8	62.3	62.9
Fut4	34.3	37.5	35.1	33.2
Fut7	79.7	80.9	77.0	72.1
Fut8	218.0	208.0	203.8	198.2
Fut9	11.0	10.7	11.7	13.0
Fut10	70.8	80.5	90.0	99.9
Fut11	216.4	166.7	208.9	130.1
Pofut1	133.8	114.6	122.5	101.3
Pofut2	302.9	240.2	233.6	161.5
Sec1	45.4	48.3	49.2	47.5

Table 4.1E. mRNA levels encoding proteins involved in glycan degradation.

Gene Name	NA	NV	AA	AV
ArylsulfataseA	259.3	197.6	258.3	176.3
ArylsulfataseB	61.4	63.5	61.1	68.2
alpha-GalactosidaseA	177.5	183.5	155.1	172.2
beta-Galactosidase(lactase)	51.5	55.2	51.4	57.2
b-Galactosidase	354.0	271.2	296.5	207.8
b-Glucuronidase(Gus-s)	356.6	344.0	311.1	228.3
hexosaminidaseA	274.1	238.5	328.4	242.5
Hyaluronidase1	63.2	66.4	59.5	47.6
Hyaluronidase2	304.3	267.2	206.5	181.2
a-L-iduronidase	197.0	196.7	212.6	232.2
Acida1_4Glucosidase	481.1	311.0	644.0	515.1
AcidLipase	186.2	165.4	208.5	184.9
AcidSphingomyelinase	754.7	823.6	1308.2	1831.2
alpha-N-Acetylglucosaminidase	151.2	112.6	168.6	135.2
Asah	461.4	431.2	567.2	408.6
Cystinosis	178.3	166.8	170.2	151.6
Galactosylceramidase	37.9	38.6	34.6	40.6
Glucocerebrosidase(gba)	428.1	270.9	385.4	217.3
MPI	456.9	578.7	419.7	773.8
N-Aspartyl-b-Glucosaminidase	591.2	480.7	783.9	391.3
protectiveproteinforbeta-galactosidase	854.5	820.4	1025.1	865.6
SialicAcidTransportProteinLAMP1	2931.2	3159.6	3297.9	3629.8
SialicAcidTransportProteinLAMP2	489.3	303.0	474.3	276.8
a-Mannosidase(Man2B1)	406.6	307.7	366.3	299.4
b-Mannosidase	320.1	332.0	302.6	257.5
MannosidaseII(Man2A1/ManII)	279.4	192.9	298.3	165.2
acylneuraminatelyase	154.9	125.6	123.0	182.4
a-N-Acetyl-Galactosaminidase	245.4	177.5	237.0	143.0
GM2ActivatorProtein	248.5	215.0	269.9	199.6
Neu1	182.1	170.8	183.7	179.3
Neu2	67.6	64.6	73.1	57.7
Neu3	125.0	137.7	157.5	183.5
Galactosamine-6-Sulfatase	109.5	88.7	96.0	74.8
IduronateSulfatase	50.2	59.6	64.9	77.0
SULF1	727.8	389.2	677.6	251.2
SULF2	864.6	939.4	695.5	401.4
N-sulfoglucosaminesulfohydrolase	66.2	68.3	72.5	72.4

Table 4.1F. mRNA levels encoding proteins involved in nucleotide sugar synthesis and transport.

Gene Name	NA	NV	AA	AV
CMP-sialicacid	272.9	238.9	178.5	174.4
UDP-Galactosetransporter	154.6	147.9	173.6	156.1
UDP-galactosetransporterrelated	1157.0	1057.4	791.7	884.7
UDP-GlcNActransporter	107.7	115.9	90.9	81.7
CMP-N-acetylneuraminicacidsynthase	813.5	561.8	714.7	585.7
CMP-Neu5Achydroxylase	66.6	72.1	97.6	94.0
epimerase	213.6	159.3	196.2	116.4
Fucose-1-phosphateguanylyltransferase	87.5	88.6	96.4	82.8
galactokinase(galK)	295.8	293.8	174.0	151.1
Galactose-1-phosphateuridylyltransferase	332.7	514.0	441.0	631.7
GDPfucosesynthetase	155.0	151.1	150.0	222.0
GDP-man4-6dehyd	142.7	107.5	112.4	80.0
GDP-mannosepyrophosphorylaseA	409.6	293.4	628.3	363.7
GlcNAc/ManNAckinase	348.7	372.4	270.9	297.2
GlcNAc2-epimerase	330.1	310.0	381.8	325.9
glucosamine-6-phosphatedeaminase/isomerase	146.5	175.9	160.7	171.3
glucosamine-phosphateN-acetyltransferase	167.2	175.8	114.8	105.0
glucosephosphateisomerase	3481.4	3577.7	3231.8	3325.8
Glutamine-fructose-6-phosphatetransaminase1	227.9	271.7	249.0	380.3
Glutamine-fructose-6-phosphatetransaminase2	65.7	70.0	96.3	137.3
hexokinase1	915.5	963.7	648.3	737.8
ketohexokinase(fructokinase)	134.2	121.8	155.1	171.7
Neu5Ac9-phosphatesynthase	320.7	293.4	188.2	146.7
PAPSsynthetase-1	407.2	395.7	211.2	150.9
PAPSsynthetase-2	75.2	75.6	105.2	75.9
phosphoglucomutase1	821.8	1341.0	741.4	1767.4
phosphomannomutase	156.0	166.4	234.7	305.4
phosphomannomutase1	185.6	151.9	187.4	163.7
pyrophosphorylase	622.6	503.4	589.9	621.1
UDP-Gal-4-Epimerase	86.8	83.3	78.0	65.8
UDP-GlucoseDehydrogenase	565.9	358.3	452.7	165.0
UDP-GlucuronicacidDecarboxylase	144.2	130.2	142.0	153.3
uridinediphosphoglucosepyrophosphorylase2	515.9	543.3	386.1	700.7

five of the seven O-glycan associated enzymes do not change. Of the O-glycan associated enzymes that do change (Galnt1 and Galnt2), Galnt1 is upregulated in the atria compared to the ventricle of both neonatal and adult tissues and Galnt2 is higher in the adult tissues.

Terminal Structures

Core glycan structures are elongated, and often, branches are added contributing to variation of N-glycan structures that differs among cell types (Comelli *et al*.[86] and addressed in chapter 5). Extracellular communication and any modulatory effects of glycans are likely due not only to structural variation, but also, and possibly more importantly, to terminal residues. Not surprisingly, terminal glycosyltransferase expression is highly variable from tissue to tissue. Tables 4.1B, 4.1C and 4.1D illustrate these changes in sialyltransferase, sulfotransferase and fucosyltransferase expression among the four tissues.

Glycan Degradation

Glycan degradation enzymes are intimately involved in glycan biosynthesis as displayed in (Figure 1.4). Removal of glucose and mannose residues allows N-glycosylation to proceed in the endoplasmic reticulum and golgi apparatus after the structure is transferred from dolichol to asparagine of a glycoprotein. Incomplete or improper removal of these glucose and mannose structures leads to improper glycosylation structures and likely a pathological disorder such as

CDG. It should also be noted that degradases included in the GLYCOv2 chip are active at various time points of the glycan lifetime including in the lysosome. As summarized in table 4.1E, the expression of glycan degradases varies among all tissues with no discernible pattern. Each tissue is the highest expresser of at least one gene and the lowest expresser of others.

Nucleotide Sugar Synthesis and Transporters

Enzymes classified under the category of nucleotide sugar synthesis have a role in creating and transporting the sugars that glycosyltransferases add to the glycan structure. These enzymes include transporters that bring the sugars into the proper organelle, epimerases, isomerases, synthases and other enzymes directly involved in nucleotide sugar synthesis. These proteins and their relative expression levels are summarized in table 4.1F which shows varying expression of these genes and that all three expression patterns are present.

Tissue Type Comparison

Chamber and developmental effects can be elucidated using four comparison groups: neonatal atria (NA) vs neonatal ventricle (NV), NA vs adult atria (AA), AA vs adult ventricle (AV), and NV vs AV. The two remaining comparison groups: NA vs AV and AA vs NV are neither chamber specific or developmental comparisons and were excluded from this analysis.

Figure 4.4A. Glycosylatransferases differentially expressed throughout the developing myocardium.

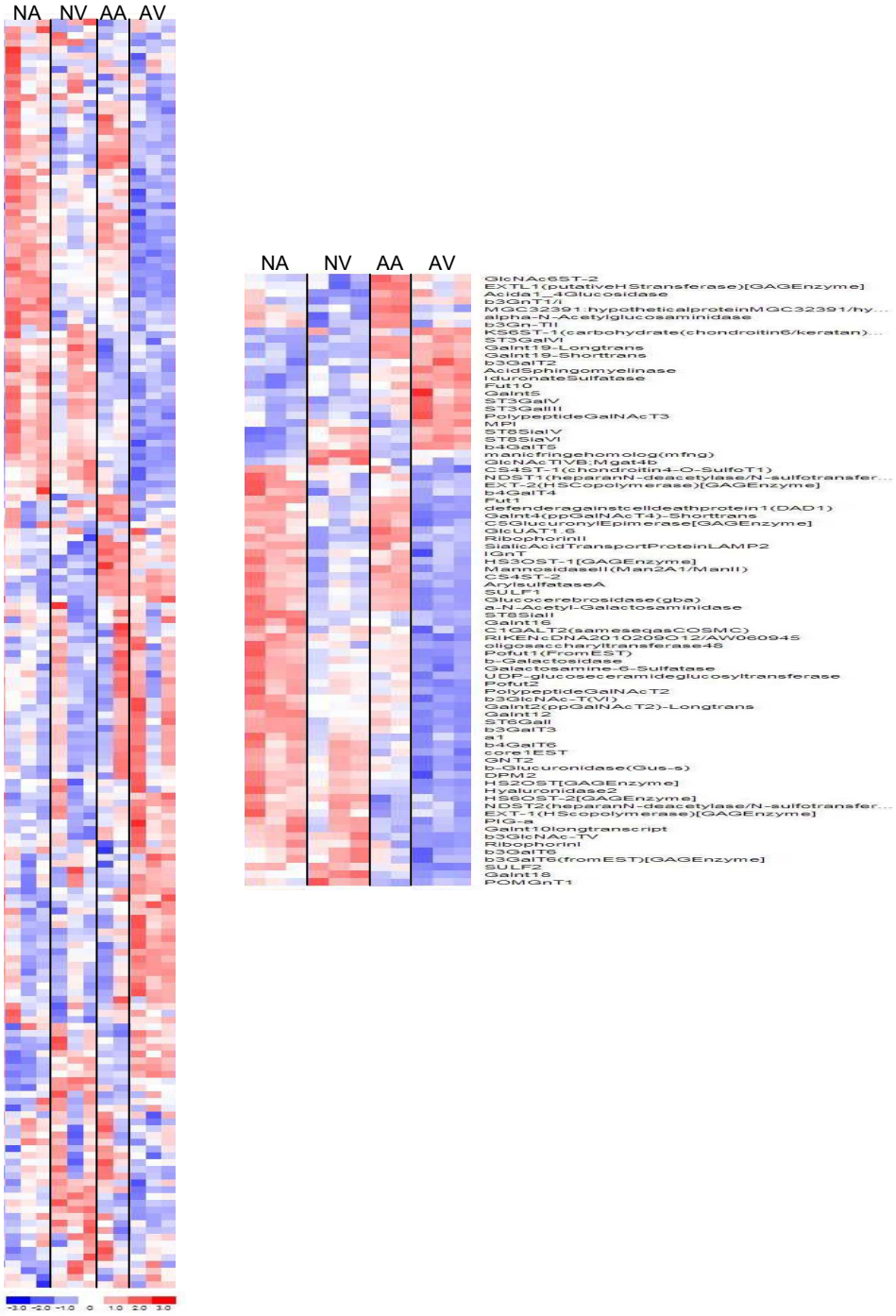

Figure 4.4. Differential expression of glycogenes directly involved in glycan synthesis; (A) glycosyltransferases, (B) glycan degradases, and (C) nucleotide sugar synthesis and transporters. Left panel shows expression relationships of all glycogenes in each category. Right panel shows glycogenes considered to be differentially expressed at $p<0.01$.

Figure 4.4B. Glycan degradses differentially expressed throughout the developing myocardium.

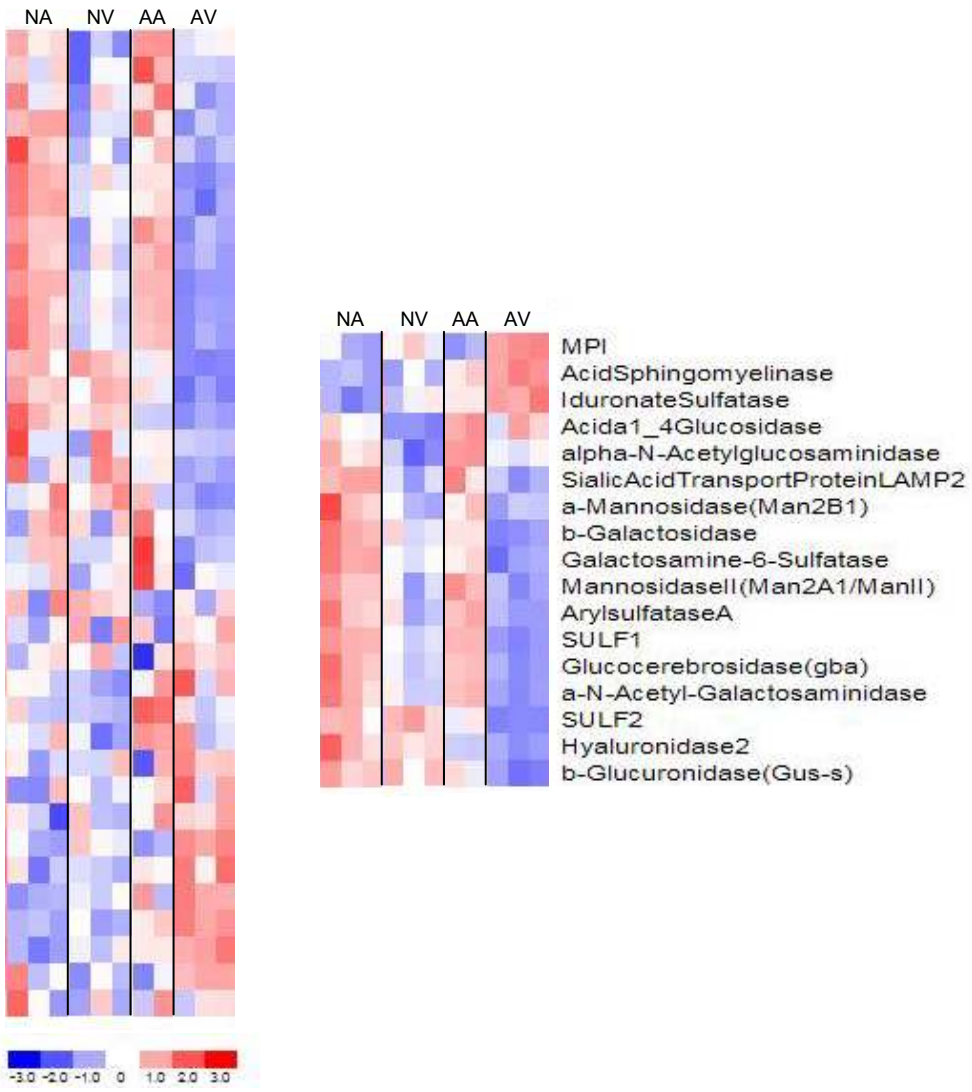

Figure 4.4C. Nucleotide sugar synthesis and transporters differentially expressed throughout the developing myocardium.

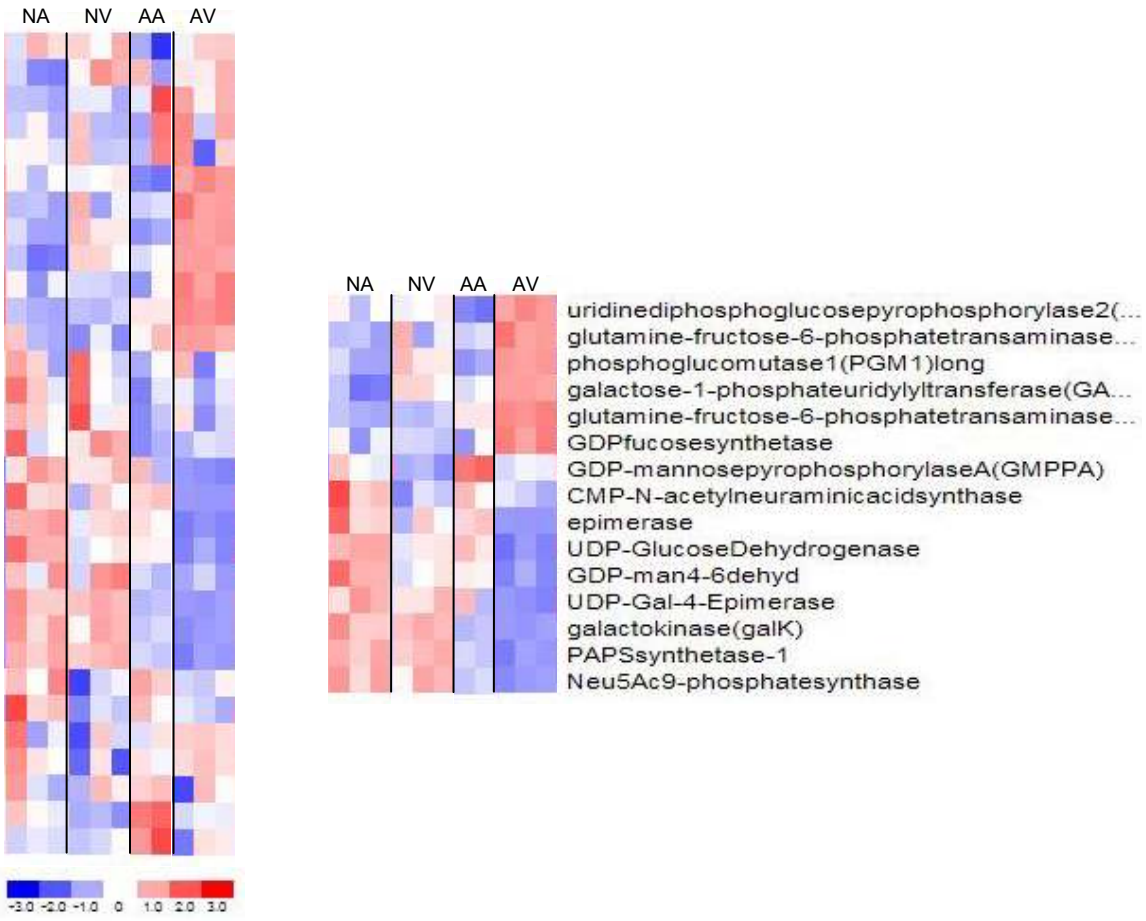

Figure 4.5. Differential expression of glycogenes by category.

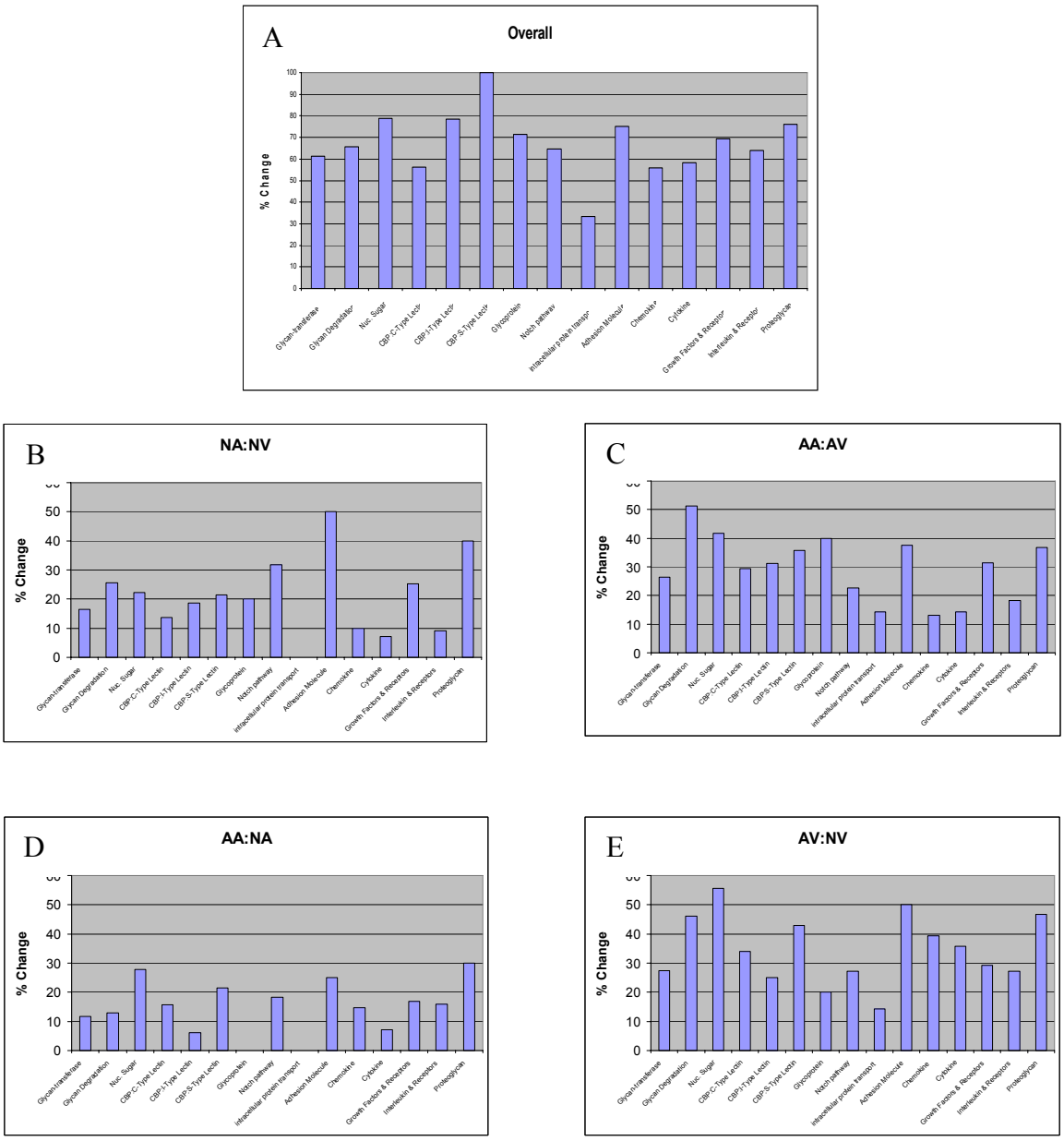

Figure 4.5. Each comparison group shows the % of genes within a type of glycogene that were found to be differentially expressed. (A) Differential expression patterns when all four tissue types are compared. (B) and (C) show the chamber specific differences in neonate and adult respectively. (D) and (E) reveal the developmental changes in glycogene expression by category. Note the patterns of all comparisons are unique.

Glycogene expression is largely different in each of the four comparison groups and is detailed below. Overall, 419 of the 710 genes are differentially expressed in at least one comparison group. These changes are summarized in figures 4.4 and 4.5 which reveals that the proportion of differentially expressed genes is higher than any single comparison group; indicating that one comparison group does not encompass all differentially expressed genes. Surprisingly, the three gene groups directly involved in glycosylation (glycosyltransferases, glycan degradases and those involved in nucleotide sugar synthesis and transport) show that ~46% (110 of 239) of these genes are differentially expressed at $p<0.01$ (Figure 4.4) among the four myocyte types.

Glycogene expression profiles of two tissue types were compared to attempt to identify major developmental and chamber specific changes. Table 4.2 summarizes these changes and shows overall changes between groups and the changes in specific glycogene categories. These data, together with the heatmap data (Figure 4.2 and 4.4), identify a large proportion of overall gene expression changes between tissue types. Specific details of differential expression with each relevant myocyte comparison group is discussed below.

Chamber-Specific Regulation

Neonatal Atria and Ventricle

Expression of glycogene targets in the neonate varies between the atria and ventricle. Specifically, expression of 161 of 710 (22.7%) gene targets are

Table 4.2. Differential glycogene expression profile

	NA:NV		AA:AV		AA:NA		AV:NV		Totals
	n	%	n	%	n	%	n	%	
Glycan-transferase	31	16.4	50	26.5	22	11.6	52	27.5	189
Glycan Degradation	10	25.6	20	51.3	5	12.8	18	46.2	39
Nucleotide Sugar Synthesis and Transport	8	22.2	15	41.7	10	27.8	20	55.6	36
CBP:C-Type Lectin	15	13.8	32	29.4	17	15.6	37	33.9	109
CBP:I-Type Lectin	3	18.8	5	31.3	1	6.3	4	25.0	16
CBP:S-Type Lectin	3	21.4	5	35.7	3	21.4	6	42.9	14
Glycoprotein	2	20.0	4	40.0	0	0.0	2	20.0	10
Notch pathway	7	31.8	5	22.7	4	18.2	6	27.3	22
Intracellular protein transport	0	0.0	1	14.3	0	0.0	1	14.3	7
Adhesion Molecule	4	50.0	3	37.5	2	25.0	4	50.0	8
Chemokine	6	9.8	8	13.1	9	14.8	24	39.3	61
Cytokine	1	7.1	2	14.3	1	7.1	5	35.7	14
Growth Factors & Receptors	45	25.3	56	31.5	30	16.9	52	29.2	178
Interleukin & Receptors	4	9.1	8	18.2	7	15.9	12	27.3	44
Proteoglycan	12	40.0	11	36.7	9	30.0	14	46.7	30

Table 4.2. Summary of the differential expression of glycogenes by category. Both the number and the overall percent of glycogenes differentially expressed are displayed ($p<0.05$).

significantly altered ($p<0.05$). Interestingly, 118 of the 161 (73%) differentially expressed gene targets are expressed at higher levels in the neonatal ventricle. Furthermore, of the genes where expression is considered to be highly different (>1.3-fold change), the proportion remains at approximately 73% (100 gene targets) are in the ventricle. When the p-value is decreased to 0.01, 99 genes are still considered differentially expressed. Differences in glycogene expression between atria and ventricles are evidence of the importance of minor adjustments required for proper cellular function (discussed further in chapter 6).

Adult Atria and Ventricle

The second chamber specific comparison between the adult atria and ventricle shows another large change in glycogene target expression with 253 of the 710 targets (35.6%) altered. Within this comparison, 39.1% of the differentially expressed gene targets are up-regulated in the atria. These figures are modified only slightly when only highly altered (>1.3-fold change) gene targets are analyzed with 36.7% (66 gene targets) of the highly differentially expressed gene targets are in the atria.

Developmental Regulation

Adult and Neonatal Atria

Glycogene expression between neonatal and adult atria indicates that 19.4% ($p<0.05$) (138 of 710 gene targets) of gene targets are significantly differentially expressed. 55.1% of these genes are up-regulation in the adult atria compared

to the neonatal atria. Of the highly differentially expressed genes (>1.3 fold change), these proportions remain approximately the same at 56% and 46% respectively.

Adult and Neonatal Ventricle

The largest change in glycogene target expression is found between neonatal and adult ventricle. 307 of 710 (43.2%) gene targets were significantly differentially expressed with approximately an equal number of gene targets up-regulated in the neonatal (154 gene targets) and adult (153 gene targets) ventricles. Among the highly altered gene targets (>1.3 fold change), neonatal ventricle has higher expression of 115 gene targets compared to 108 for the adult ventricle.

Quantitative PCR verifies microarray data

Gene chip verification is an important process for quality control and duplication of expression levels. Here, we verified each comparison group using three distinct genes for each comparison for a total of twelve. These included sialyltransferases involved in N-glycan synthesis or O-glycan synthesis and growth factors. Tissue type comparisons of the expression of each of the twelve glycogenes are consistent with genechip findings compared to HPRT (Figure 4.6). These data were also analyzed by comparing expression levels to β-actin as the control with similar results (data not shown).

Figure 4.6. qPCR validates the GeneChip microarray data.

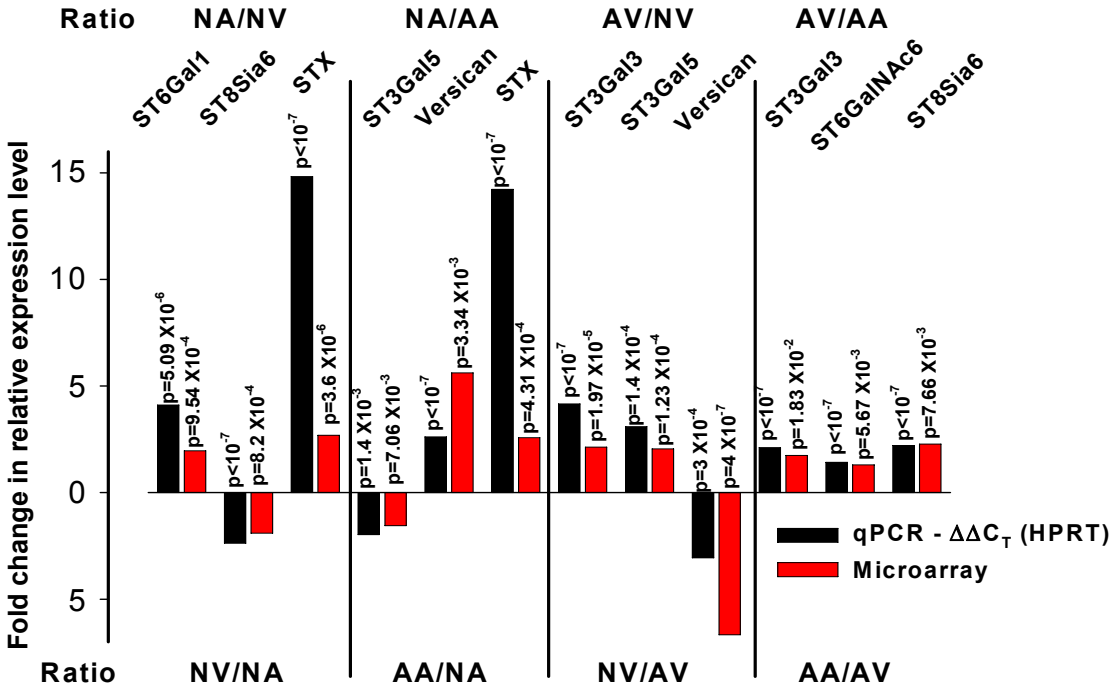

Figure 4.6. Selected genes were investigated by qPCR analysis of RNA to validate GeneChip microarray data. Three glycogenes from each comparison group were studied, revealing that data from both microarray and qPCR were consistent. All genes were normalized to the endogenous control gene, HPRT.

Discussion

Glycogene expression is a developmentally regulated process in the myocardium with large changes in both the developing atria and ventricle. Significant differences are apparent within the developing atria with 19.4% of the genes differentially expressed yet the developing ventricle shows more than twice as many genes differentially expressed at 43.2%.

Not surprisingly, glycogene expression is significantly regulated between cardiac chambers. Differential expression of glycogenes between chambers at the same developmental stage range from 22.7% (neonates) to 35.6% (adults) suggesting that glycan structures are modified between chambers.

Glycogene expression is differently regulated among the four myocyte types indicating that the glycome is remodeled throughout the developing myocardium. The high levels of variation among the four comparison groups provides insight into the possible changes in glycan structure at a cellular level.

CHAPTER 5

THE GLYCOME IS REMODELED THROUGHOUT THE HEART DURING DEVELOPMENT

With such diversity in glycogene expression, one would expect very different populations and relative quantities of glycans synthesized by the cell. Mass spectrometry is a powerful tool for identifying the populations of glycans present in a given sample. The resulting spectra provide insight into changes in N-glycan profiles produced throughout the developing heart. Complete mass spectra are shown in figures 5.1 and 5.2.

High Mannose Structures

The intensity patterns of the first five major high mannose structures (1579, 1783, 1987, 2192 and 2369) are almost identical among all four tissue samples: neonatal atria, neonatal ventricle, adult atria and adult ventricle (blue peaks, Figures 5.1 and 5.3). The high mannose structure at m/z 2369 is the most common structure of the five high mannose structures and is most common overall in three of the four tissues composing over 50% of the total glycan density. The adult atria is the exception with the high mannose structures composing only 23.5% of the total glycan population (Table 5.1). When comparing the pattern of only high mannose structures, m/z 1987 is the least

Figure 5.1A. The population of N-glycans is different among the four myocyte types.

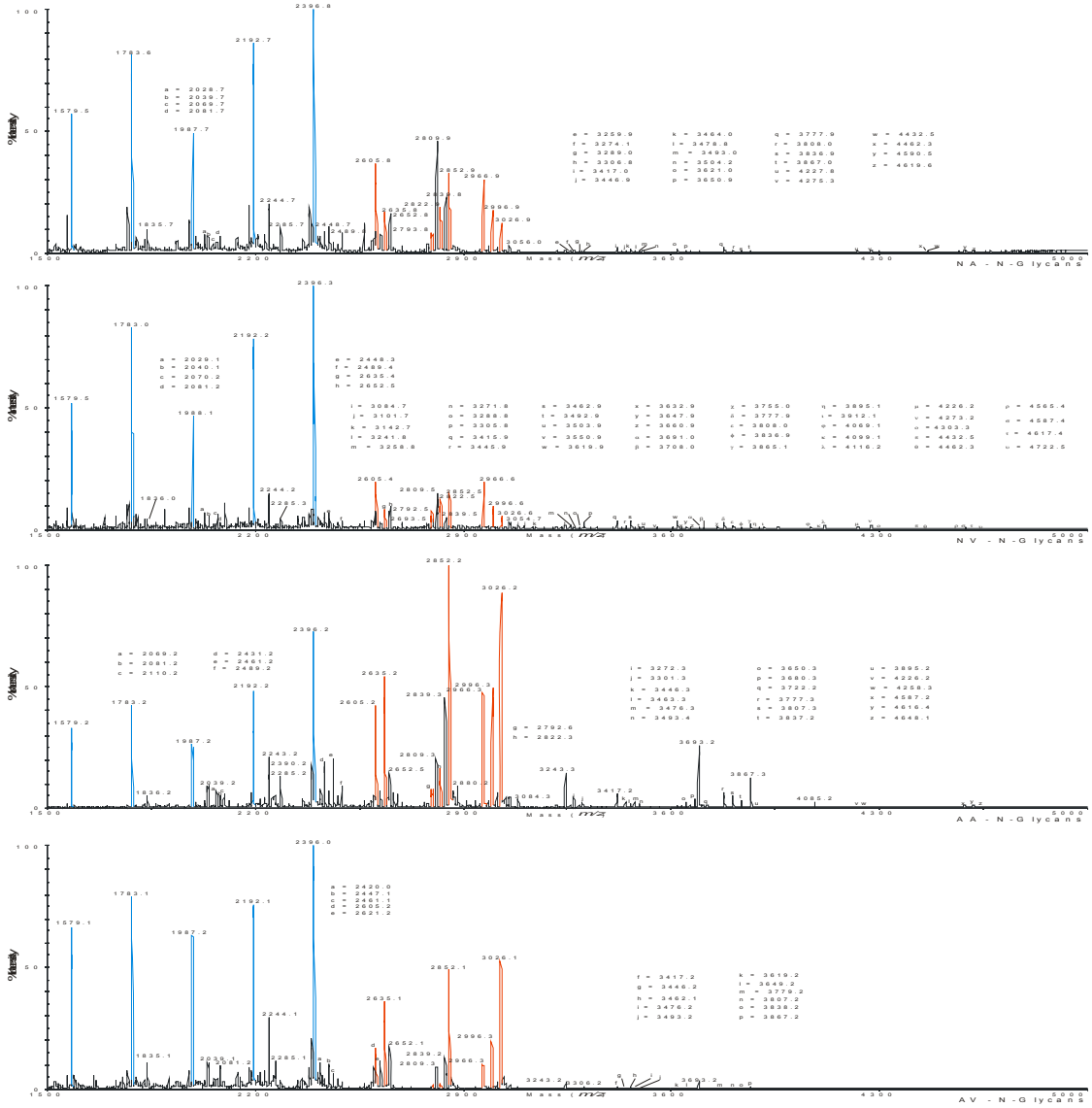

Figure 5.1. (A) Mass Spectrometry profiles of N-glycans in neonatal and adult atria and ventricles utilizing MALDI-TOF MS. . Note that the lower MW structures up to high mannose structures are at relatively high density for each myocyte type (blue peaks). Significant variation in complex glycan structures among myocyte types is readily apparent (red peaks), both in relative levels and types of glycans. Predicted glycan structures for highlighted peaks are shown in neonatal ventricle panel. (B and C) N-glycans associated with masses reported in figure 1A. (B) Glycans with masses between 1500 and 3050 m/z, (C) structures with masses above 3050 m/z. Structures that list the mass in highlighted yellow ovals were determined using MALDI TOF/TOF analyses. Blue square, GlcNAc; green circles, mannoe; yellow circles, glucose; red diamonds, NeuAc; light blue diamonds, NeuGc; red triangles, fucose.

Figure 5.1B. Identified low mass N-glycan structures and their relative mass.

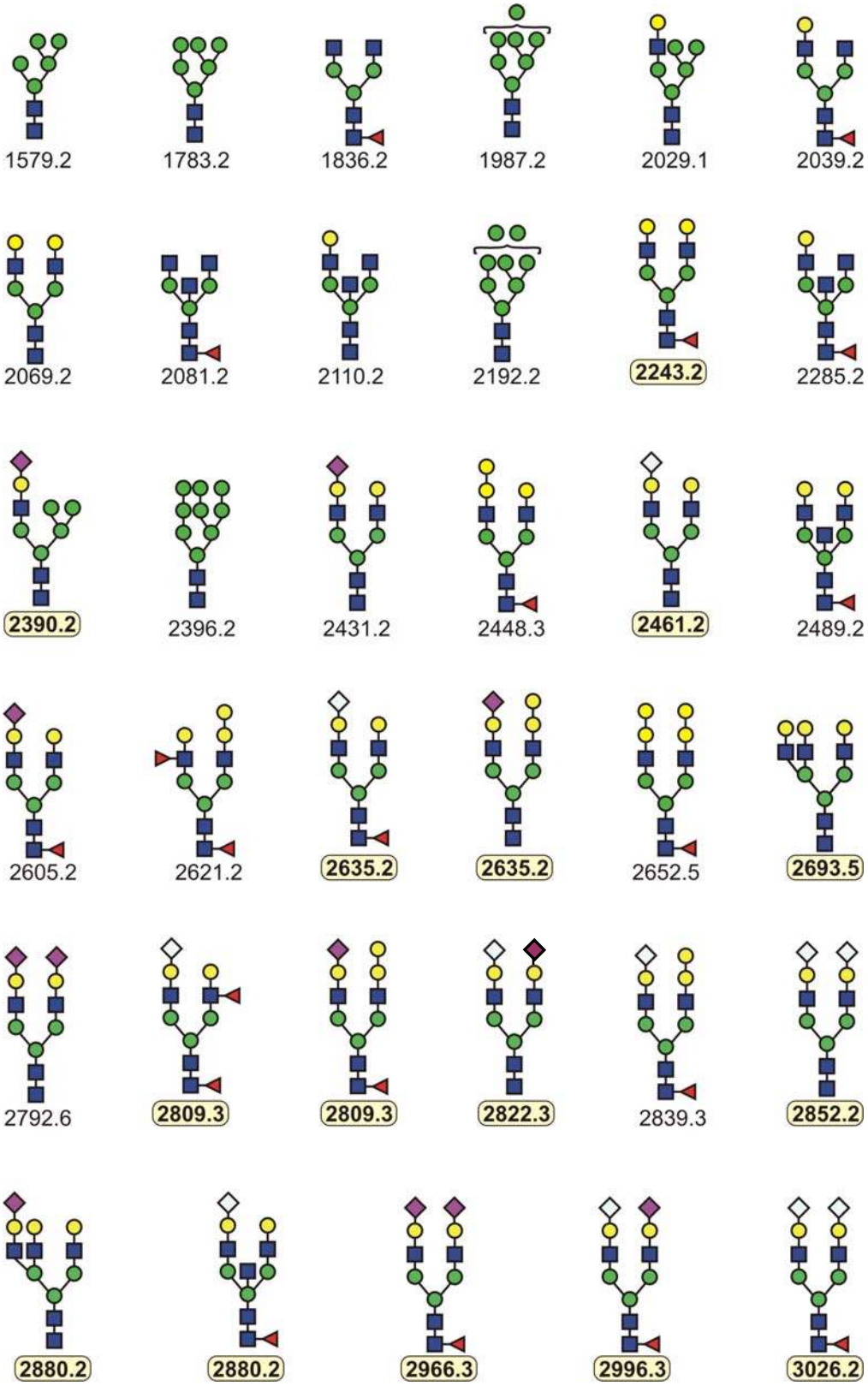

Figure 5.1C. Identified high mass N-glycan structures and their relative mass.

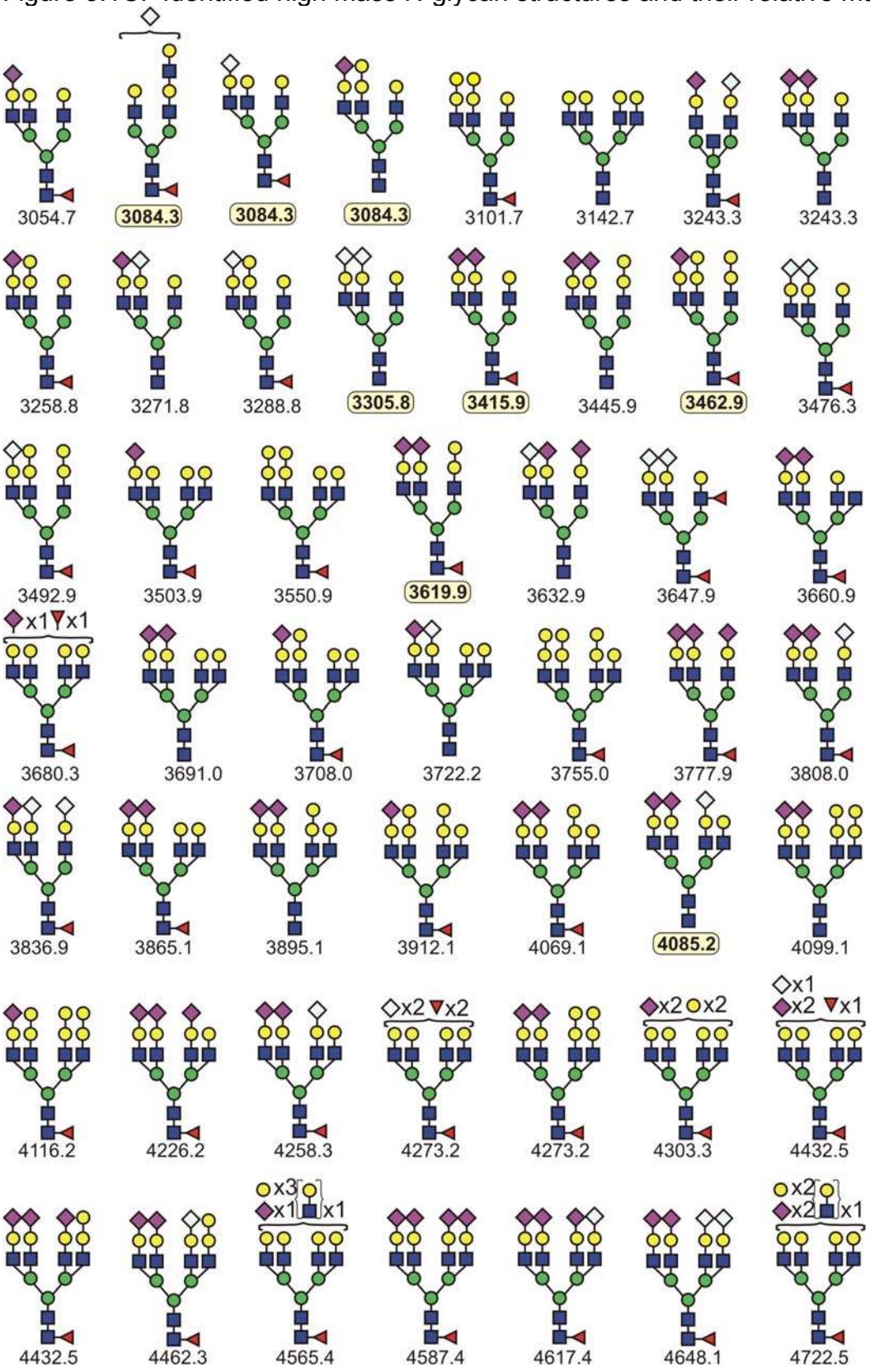

Figure 5.2A. Mass spectra of the neonatal atrial N-glycans.

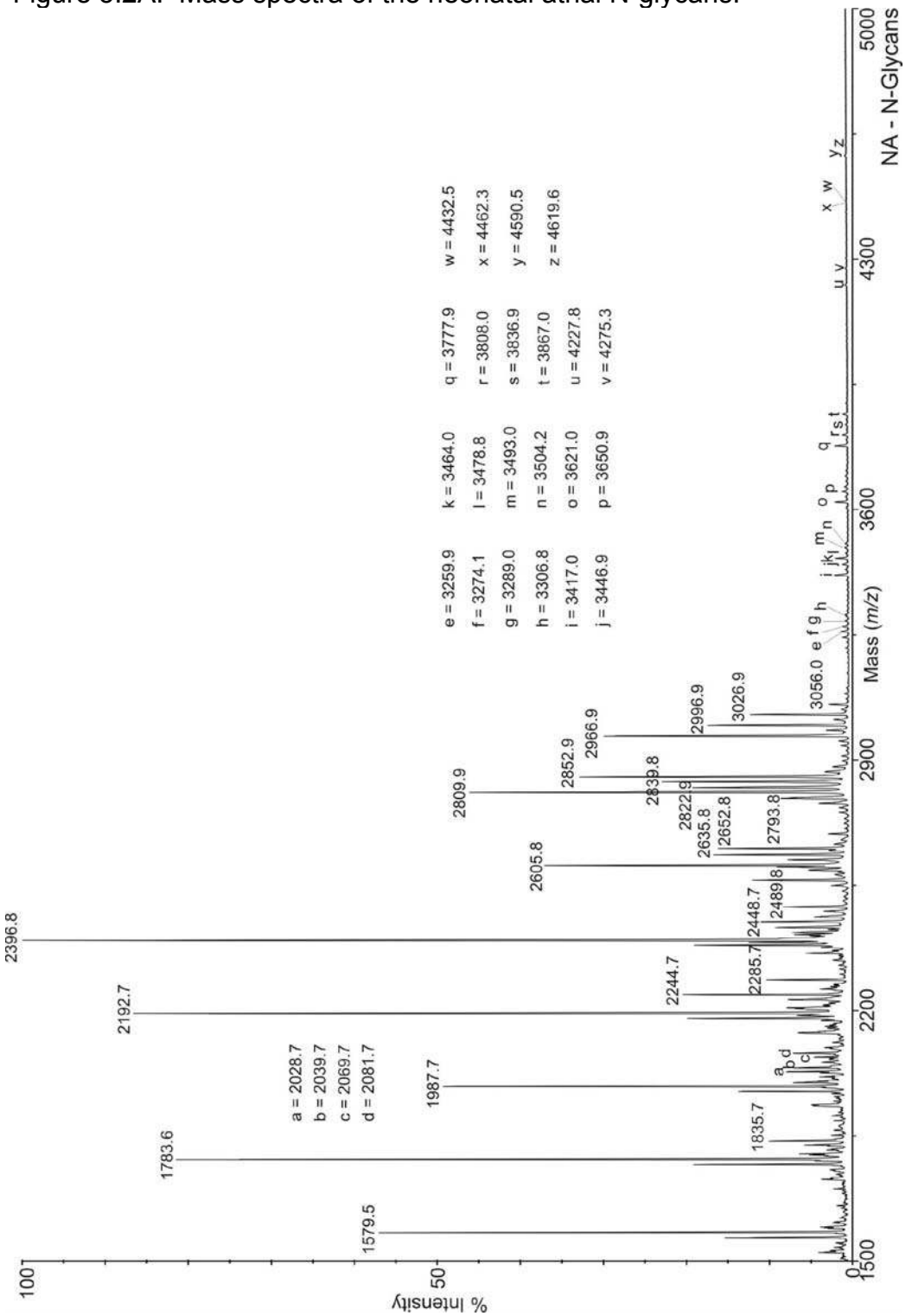

Figure 5.2. MALDI-TOF mass spectra for each tissue type. Each spectrum is an enlarged version of those displayed in figure 5.1 to better show detail. Masses correspond to structures in figure 5.1B and 5.1C.

Figure 5.2B. Mass spectra of the neonatal ventricular N-glycans.

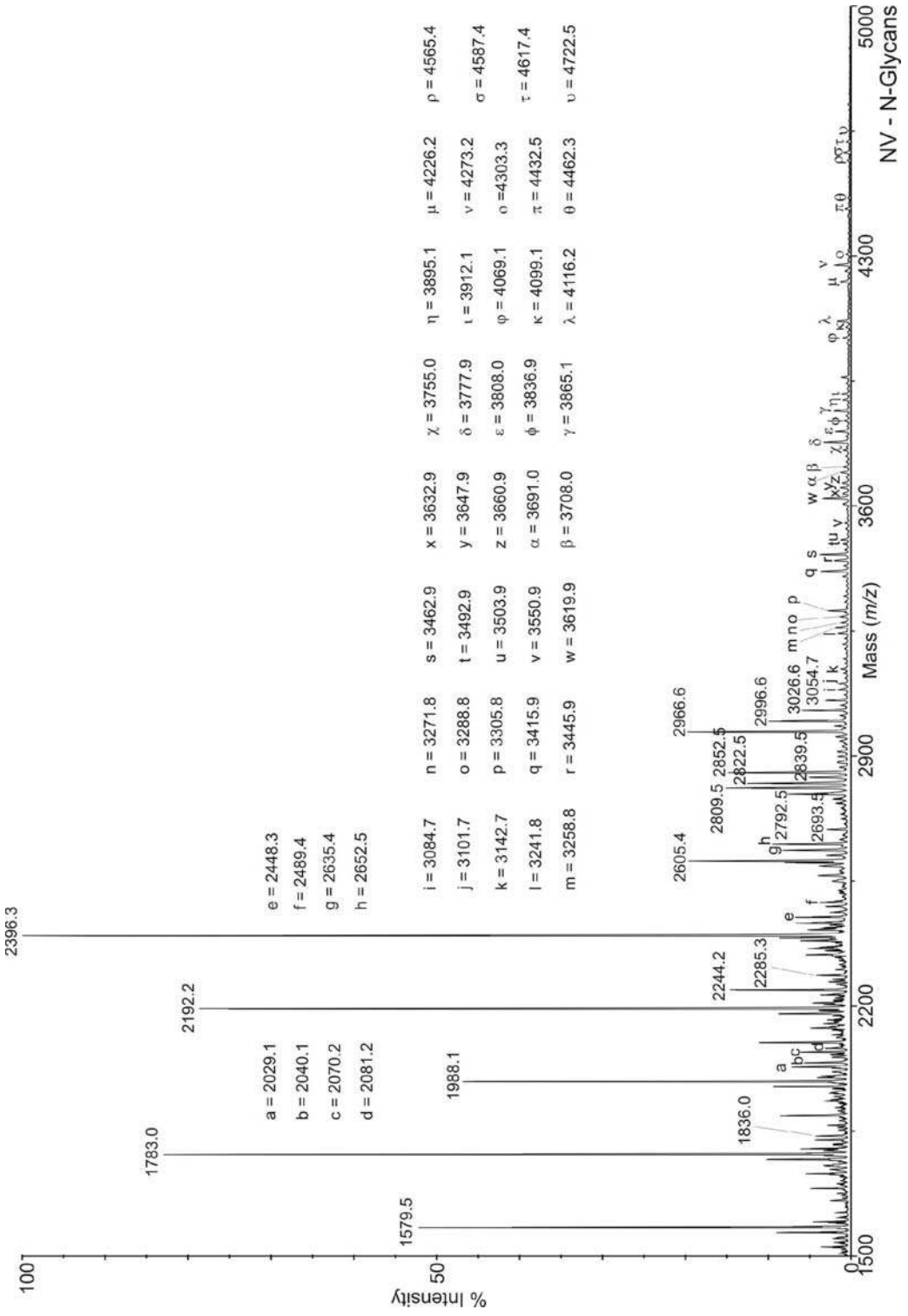

Figure 5.2C. Mass spectra of the adult atrial N-glycans.

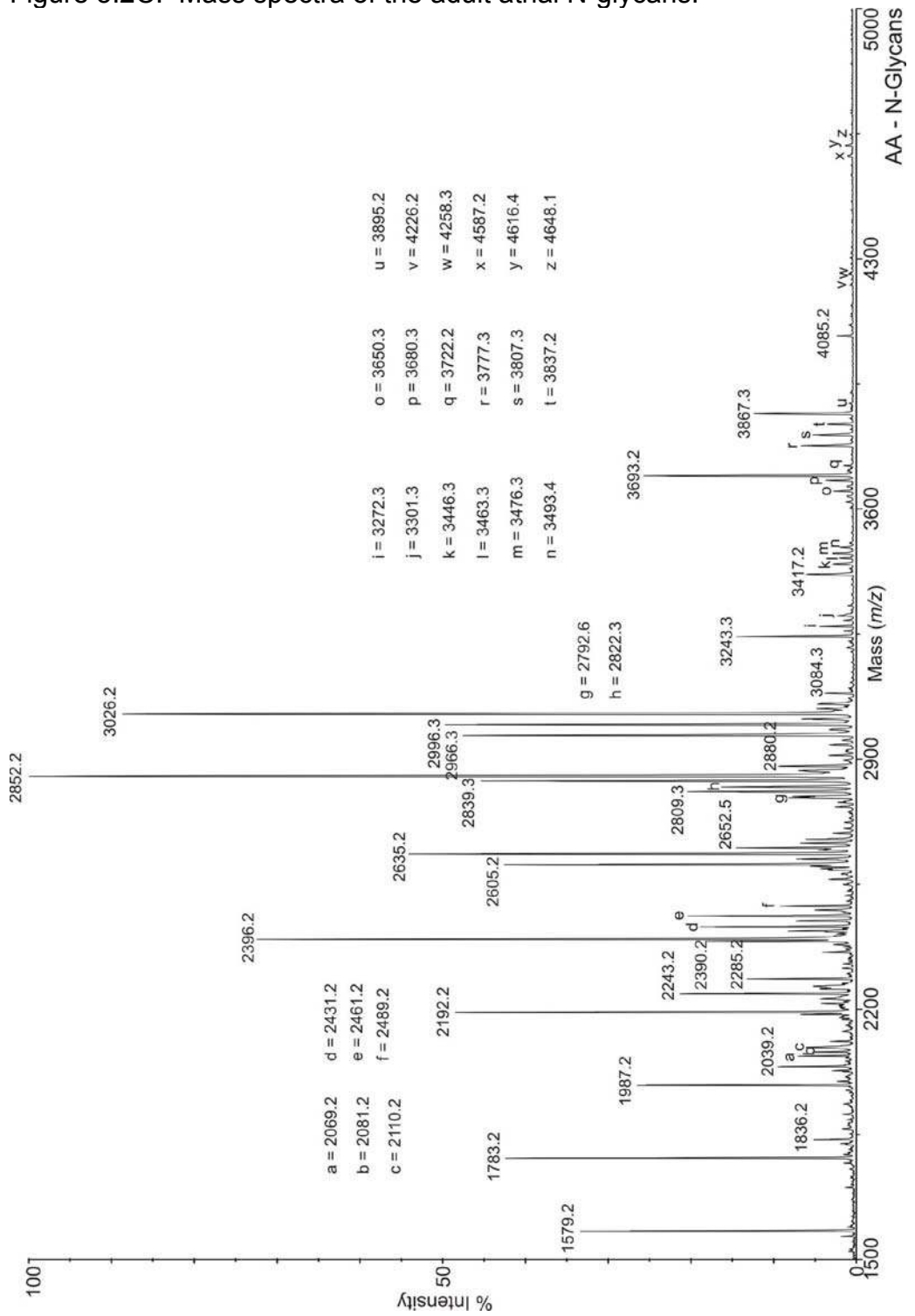

Figure 5.2D. Mass spectra of the adult ventricular N-glycans.

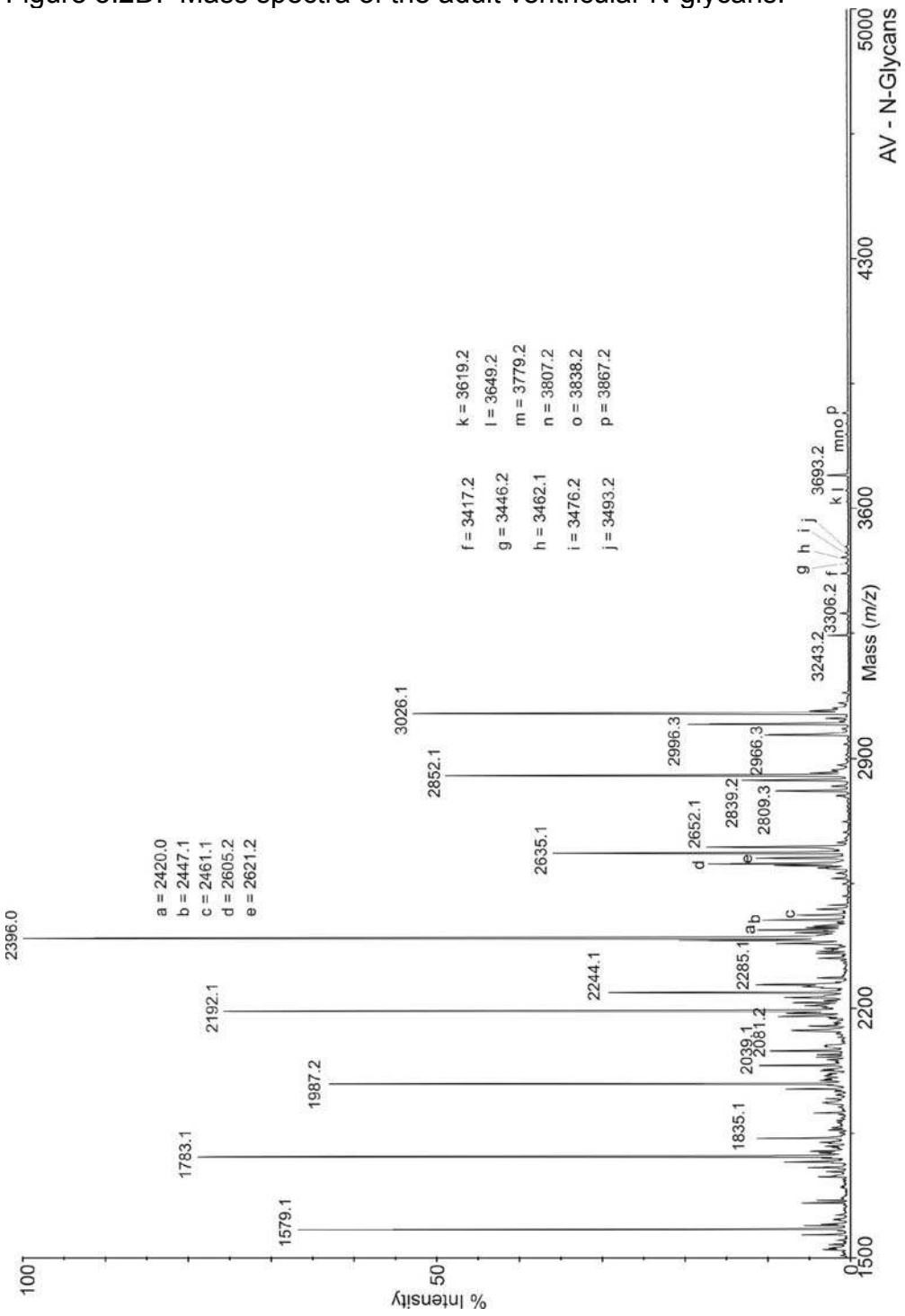

Figure 5.3. Mass spectra of masses between 1500 and 2400 m/z.

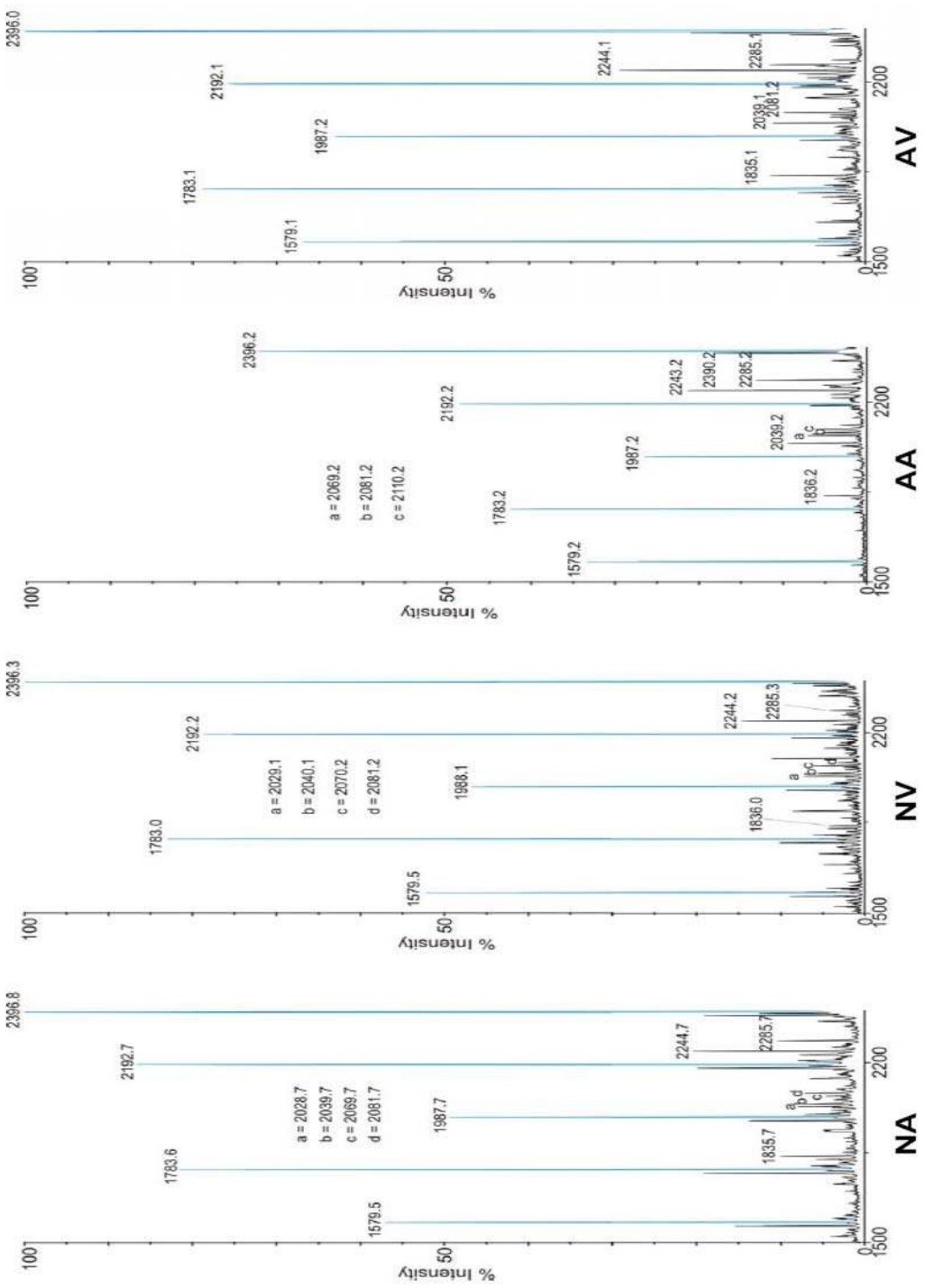

Figure 5.3. Enlarged schematic of spectra between 1500 and 2400 m/z. The blue peaks indicate relative density of high mannose structures.

Figure 5.4. Mass spectra of masses between 2400 and 3050 m/z.

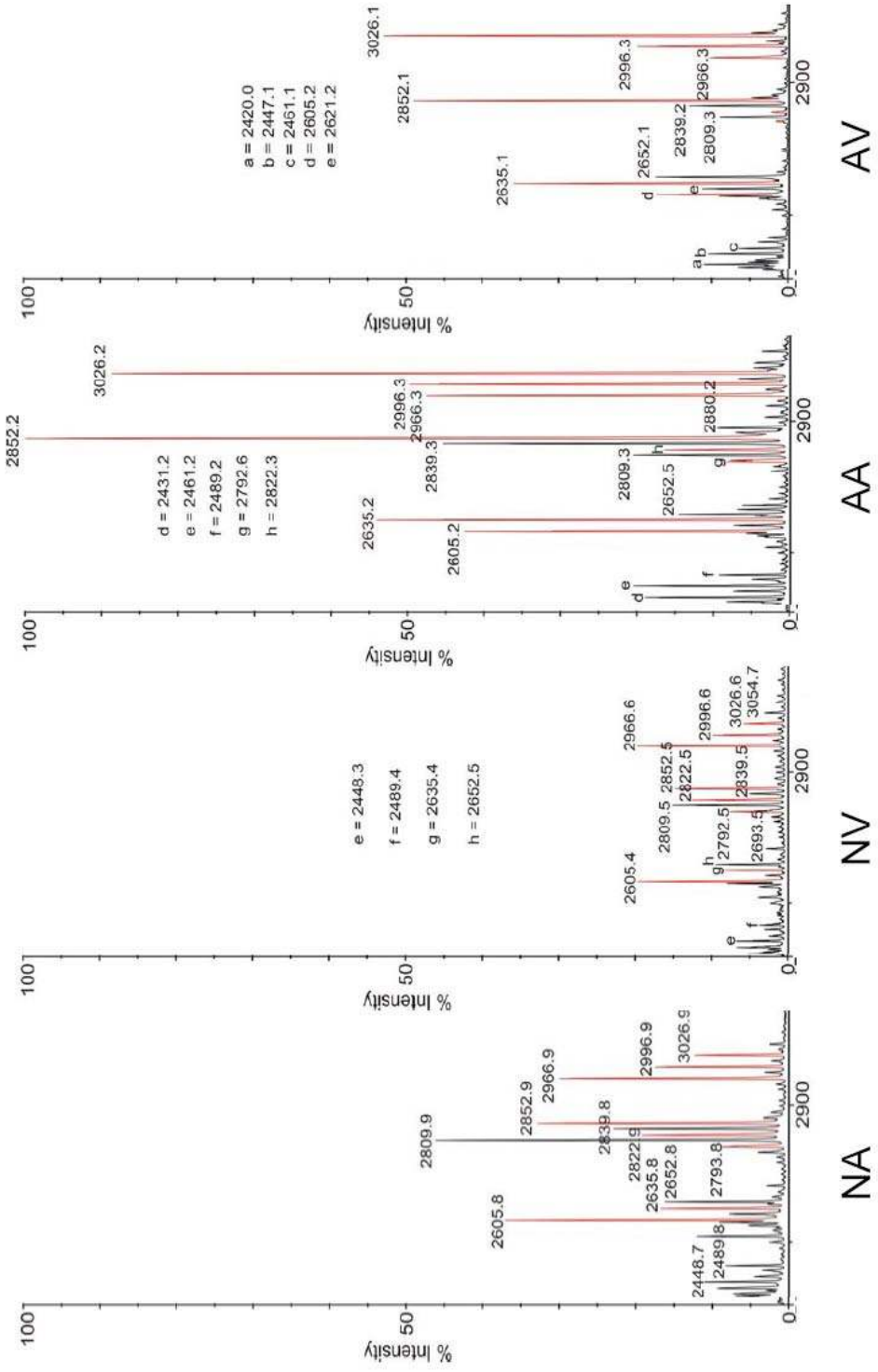

Figure 5.4. Enlarged schematic of spectra between 2400 and 3050 m/z. The red peaks indicate relative density of bi-antennary structures assigned to one of three groups.

Figure 5.5. Spectra of masses above 3050 m/z.

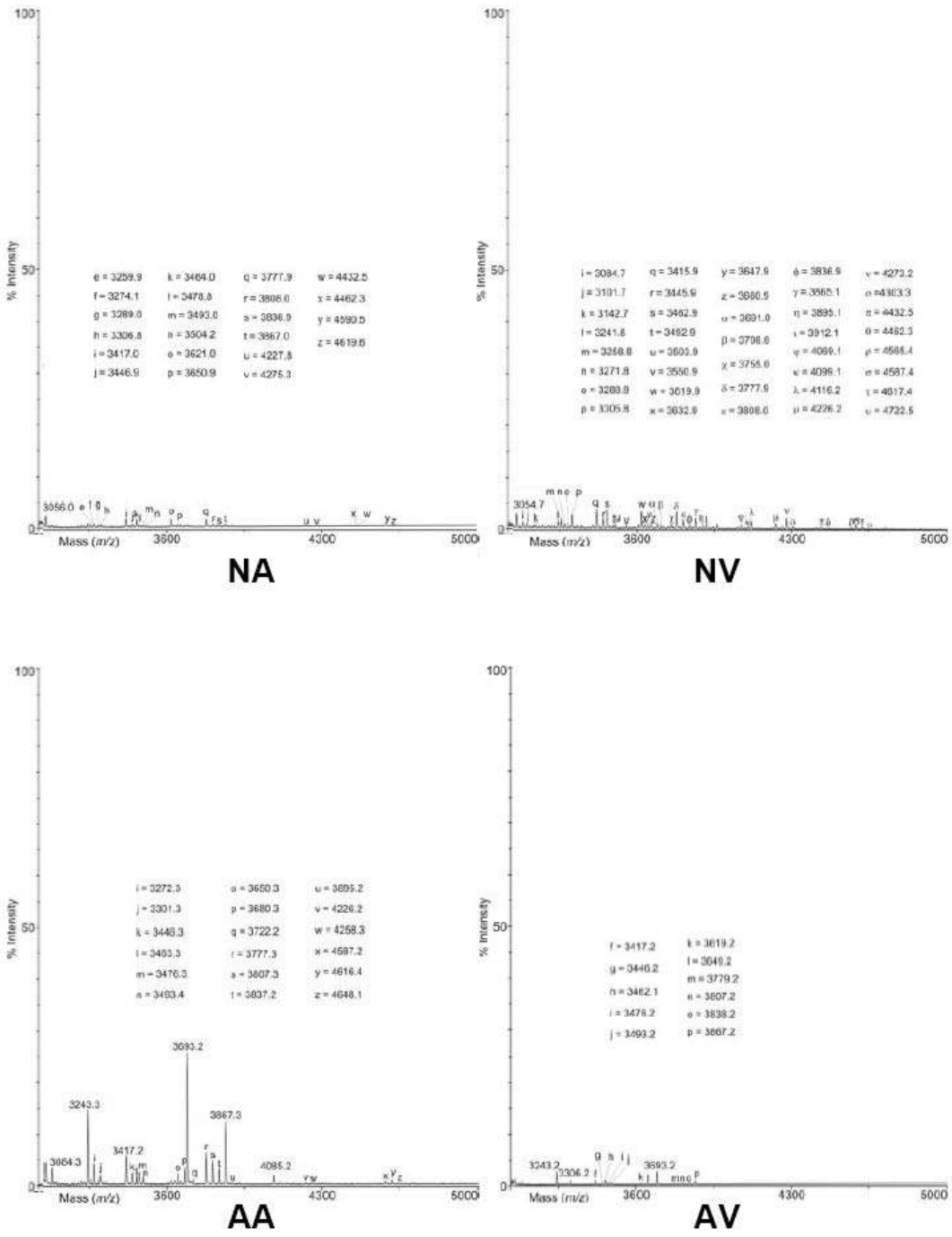

Figure 5.5. Enlarged schematic of spectra above 3050 m/z. These peaks are associated with the most complex and highest mass structures.

Table 5.1. Relative percentage of glycan structures defined by either structure (high mannose) or mass.

	NA	NV	AA	AV
High Mannose	52.06	60.43	23.53	52.95
2400-3050 m/z	37.63	23.24	57.38	35.91
3050-5000 m/z	1.45	8.98	10.44	1.37

Table 5.1. Relative density of glycan structures defined by either structure (high mannose) or mass. Note the low proportion of high mannose glycans and high proportion of higher mass structures in the adult atria (AA) compared to all other groups. Although relative density of glycans in the neonatal atria (NA) and adult ventricle (AV) are similar, the mass spectra are much different as seen in figure 5.1, 5.2A and 5.2D. Neonatal ventricle, NV.

common while 1783 and 2192 are higher and similar in level of expression in all tissue types.

Complex Structures

Complex structures, defined here as those structures that have been processed beyond high mannose stages and have a mass above 2400 m/z, are present in unique relative quantities among all four tissue types. The structures with masses between 2400 and 3050 m/z are bi-antennary complex structures (Figure 5.4) while those with masses above 3050 m/z are mostly tri- and tetra-antennary (Figure 5.5).

Chamber-specific glycan profile changes

Neonatal Atria and Ventricle

The neonatal atria and ventricle spectra are surprisingly similar in terms of glycans present or absent, yet the level of each glycan varies. The neonatal atria have higher relative levels of almost every glycan between 2400 and 3050 m/z accounting for approximately 37.6% of the overall glycan population compared to 23.2% for the neonatal ventricle (Table 5.1). Of particular interest in this region are three sets of sialylated glycans (Figure 5.4):

group 1 consists of glycans at 2605 and 2635 m/z,
group 2 is composed of glycans at 2793, 2822 and 2852 m/z and
group 3 is comprised of glycans at 2966, 2996 and 3026 m/z.

In the neonatal atria and ventricles, groups 1 and 3 decrease in relative level from low m/z to high m/z and group 2 increases in relative glycan level from low m/z to high m/z.

The greater number of unique higher mass (above 3050 m/z) N-glycan structures are present in the neonatal ventricle with several complex structures produced by the ventricle but not the atria (Figure 5.5). In the higher mass region the relative abundance is higher in the ventricle accounting for 8.9% in contrast to 1.4% in the neonatal atria (Table 5.1). Thus, it is likely that the neonatal atria produce the same bi-antennary structures as the ventricle but at a higher relative abundance while the neonatal ventricle produce more tri- and tetra- antennary structures at higher relative levels than the neonatal atria.

Adult Atria and Ventricle

The population of glycans present in the adult atria and ventricle are comparable in some manners and different in others. Note for the adult atria, the data are normalized to the 2852.2 m/z peak whereas the other three tissue types are normalized to the high-mannose structure around 2396 m/z (Figure 5.1). Despite this change, the spectral patterns between 2400 and 3050 m/z for adult atria and ventricle are very similar with adult atria showing higher (57.4% compared to 35.9%) relative levels of each glycan (Table 5.1). Groups 1, 2 and 3 are similar in pattern in that the relative level increases from low to high m/z; although, the

adult ventricle has extremely low relative expression levels of 2793 and 2822 m/z (i.e., barely greater than baseline (Figure 5.4)).

Higher mass structures are present in greater relative abundance and number of species in the adult atria than in the adult ventricle (Figure 5.5). The most complex glycan registers with a minor peak at 3867.2 in the adult ventricle, yet the adult atria had a higher relative level of the glycan at that mass and six glycans register at a higher mass than 3867.2. These high mass structures compose approximately 10.4% of the adult atria overall glycan population compared to 1.4% for the adult ventricle (Table 5.1).

Developmental glycan profile changes

Neonatal and Adult Atria

In contrast to the similarities of age matched comparisons, developmental differences are more apparent. The putative structure of middle mass, bi-antennary glycan structures present are similar throughout atrial development but with much higher relative levels in the adult atria for most structures (Figure 5.4). One major exception is the glycan at 2809 m/z which is the highest peak above 2397 in the neonatal atria whereas this peak is relatively minor in the adult atria. Groups 1 and 3 show opposite patterns with neonatal atria decreasing relative levels from low to high m/z and adult atria increasing relative levels from low to high m/z. Surprisingly, group 2 has an identical pattern in both neonatal and adult atria with increasing relative levels from to low to high m/z.

The higher mass range of both adult and neonatal atria has similar glycan structures, yet each tissue type has some structures that are unique (Figure 5.5). The relative levels of these glycans is higher in the adult atria with over 10% of glycan structures with higher mass than 3050 m/z compared to neonatal atria with higher mass composing only approximately 1.4% of the total glycan structures (Table 5.1).

Neonatal and Adult Ventricle

The developmental changes between adult and neonatal ventricle are prominent in the mass spectra shown in figure 5.1. The portion of glycans in the 2400 to 3050 m/z range is much higher in the adult ventricle (35.9%) compared to the neonatal ventricle (23.2%), but the pattern of expression is also changed (Table 5.1). Groups 1 and 3 have opposite patterns with the neonatal ventricle increasing relative level from low to high m/z and adult decreasing relative level from low to high m/z (Figure 5.4). Group 2 has an identical pattern in both adult and neonatal ventricle.

In contrast, the neonatal ventricles have a much higher proportion (8.9%) of glycans in the higher mass range than the adult ventricle (1.4%) (Table 5.1). The neonatal ventricle also has 37 unique high mass glycan structures compared to the adult ventricle with only 13 (Figure 5.4). This change indicates a shift towards bi-antennary glycans in the adult ventricle.

Discussion

Regulated glycogene expression throughout the heart during development would lead one to expect the glycan profile to also be markedly varied among myocyte types. In fact, each tissue has a unique glycan profile with notable similarities among all tissues. All tissues have an identical pattern of the identified high mannose structures indicating that high mannose structure production is similar in all four tissues. The microarray data correlates quite well that expression levels of enzymes responsible for high mannose synthesis and pruning are comparable across the four tissue types.

There are over 30 different forms of sialic acid produced in nature. In the mouse there are two common sialic acids attached to glycans, N-acetylneuraminic acid (NeuAc) and N-glycolylneuraminic acid (NeuGc). These sialic acids seem to be developmentally regulated in mouse myocardium. Adult tissues seem to produce glycans that add NeuGc preferentially over NeuAc, as shown in groups 1, 2 and 3. Alternatively, this conclusion cannot be made in the neonates since the dominant peak in these groups varies between those with NeuAc (groups 1 and 3) and NeuGc (group 2). These changes are examples of the developmental modifications of glycan structures.

Glycan profiles are markedly different among the four tissue types tested in two of the three glycan mass categories with only the high mannose patterns being similar among the four tissue types. Changes in glycan profiles among the four

tissues are prevalent above 2400 m/z indicating that the modifications in glycan structure are imposed in the latter steps of the glycosylation pathway. Bi-antennary glycans are similar in structure throughout the developing myocardium, yet the relative levels of these glycans change in both in a developmental and chamber-specific manner. Furthermore, the largest variations in the number of glycan structures are at a mass above 3050 m/z where tri- and tetra-antennary structures are located. The glycogene expression data are consistent with these data in that the majority of glycogenes active in the distal golgi apparatus are most commonly differentially expressed.

CHAPTER 6

THE REGULATED EXPRESSION OF A SINGLE POLYSIALYLTRANSFERASE IMPACTS CARDIAC EXCITABILITY

Sialic acid residues are the primary terminal residues and are added to the glycan structure through sialyltransferase activity. Through polysialyltransferase activity, the level of sialylation is greatly increased. Polysialyltransferase enzymes are responsible for addition of sialic acids to sialic acids creating long chains from 5 to 100 residues termed polysialic acid. Expression of the polysialyltransferase, ST8 alpha-N-acetyl-neuraminide alpha-2,8-sialyltransferase 2 (STX), is highly regulated in the developing myocardium. As seen in chapter 4, STX is expressed at much higher levels in the neonatal atria compared to the neonatal ventricle, adult atria and ventricle where STX is essentially not expressed. To ascertain whether a single enzyme whose expression is regulated may affect cardiac excitability, we recorded action potentials from control and STX knockout mice. The results of these studies indicated that Na_v function may be modified by the regulated expression of STX thereby altering atrial action potentials. Here, we also question whether the regulated expression of a single sialyltransferase is sufficient to alter Na_v gating.

The effects of sialic acid residues on the voltage dependence of voltage gated sodium channel (Na_v) gating has been extensively studied [117,118,120,123]. Thus far, it has been determined that sialic acid residues modulate ion channels in an alpha (pore-forming) subunit manner and through the expression of the auxillary subunit, β_1. For Na_v, the mechanism by which sialic acids modulate channel gating is through an apparent electrostatic attraction between the negative surface potential (to which the negatively charged sialic acid residues contribute) and the positively charged amino acids of the channel's voltage sensors [117,118,120,123]. Stocker and Bennett determined that the sodium channel isoform expressed in neonatal ventricles was less-sialylated compared to the same sodium channel isoform in the neonatal atria, adult atria and ventricle indicating another possible mechanism for the cell to manipulate channel gating through changing the glycans attached to the proteins[123]. In this study, we have identified large changes in glycogene expression and glycan structure; consistent with a global mechanism by which cardiac function is altered by a regulated glycome.

The neonatal atrial action potential waveform is altered when STX is absent

To question whether the regulated expression of a single sialyltransferase can alter cardiac excitability, action potential waveforms were recorded from neonatal atria and ventricles of control and STX knockout mice. Proper voltage-gated sodium, potassium and calcium channels are essential to initiate and propagate the action potential in cardiomyocytes. Neonatal atrial action potential recordings reveal a rate of depolarization (dV/dt) that is 65% slower in the knockout atria

Figure 6.1. Expression of STX modifies neonatal atrial, but not ventricular AP waveform.

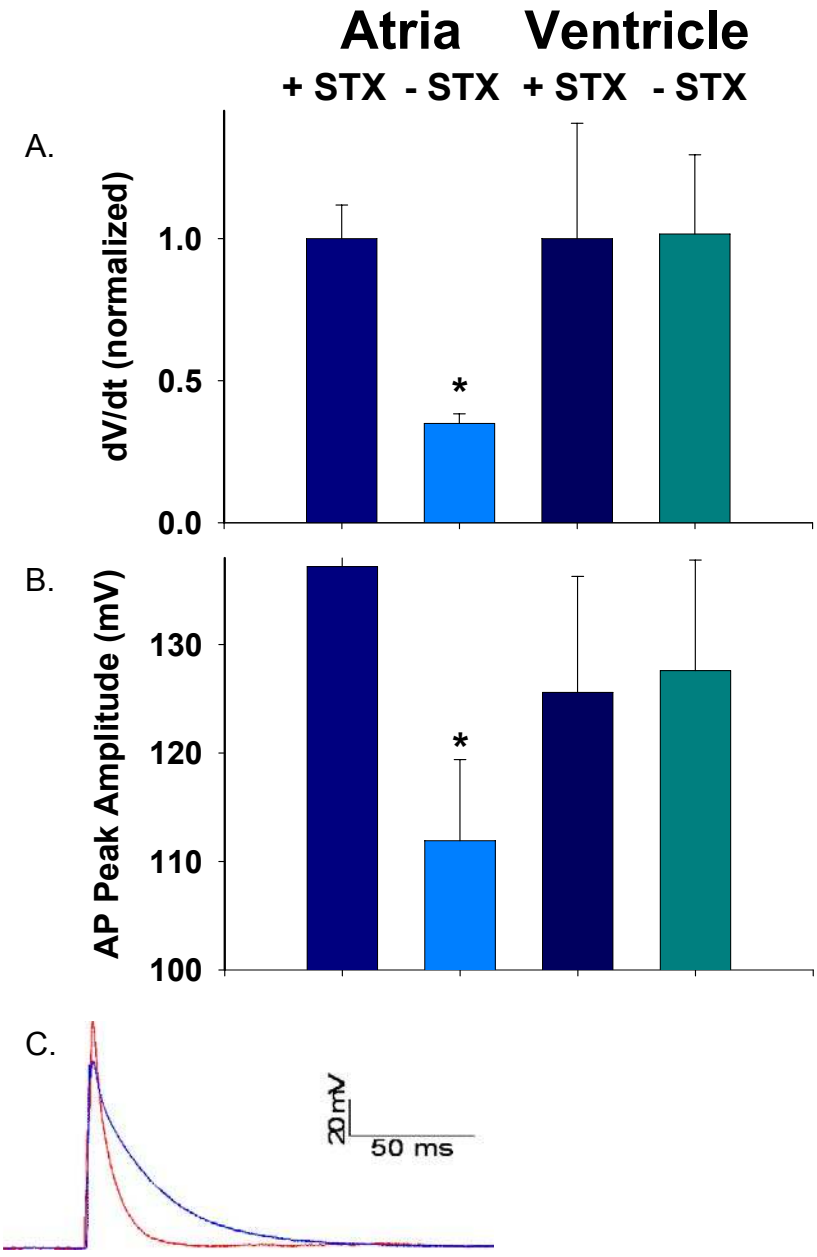

Figure 6.1. Measured parameters of the action potential waveform. Bar graphs of the mean +_ S.E.M. (A) The rate of action potential depolarization. (B) The maximum AP depolarization. (C) Representative action potential traces from STX control (red) and knockout (blue) atria.

compared to the littermate control atria (Figure 6.1). The maximal depolarization of the knockout atria is also 30 mV less than the control atria as determined by peak amplitude (Figure 6.1). These two measurements tend to be associated with the portions of the action potential produced by sodium currents and are consistent with how Na_v dysfunction changes excitability with STX expression. That is, the lack of STX expression in the knockout would cause the channel to gate at more depolarized potentials. These changes lead to a slower action potential depolarization rate. Because the time to reach peak amplitude is increased in the absence of STX, a higher percentage of K_v may be active at the peak of the action potential. Increased K^+ currents during the rising phase of the action potential would offset Na^+ currents and effectively decrease the peak amplitude. No changes in action potential waveform were observed in ventricular myocytes; as expected since STX is not expressed in the ventricle.

The voltage dependence of Na_v gating changes only in the neonatal atria of the STX knockout.

To determine whether the absence of a single sialyltransferase, STX, can modify Na_v gating, Na^+ currents were recorded from atrial and ventricular myocytes isolated from STX knockout mice and compared to littermate controls. Neonatal tissues are ideal to elucidate whether STX can modulate Na_v gating since STX is expressed several times more abundantly in the atria than in the ventricle and both tissues are isolated from the heart of the same animal. The Na_v V_a and V_i measured in the knockout atrial myocyte were 7-9 mV more depolarized and

Figure 6.2. STX causes a change in neonatal atrial Na_v activation voltage, but not in ventricular Na_v activation.

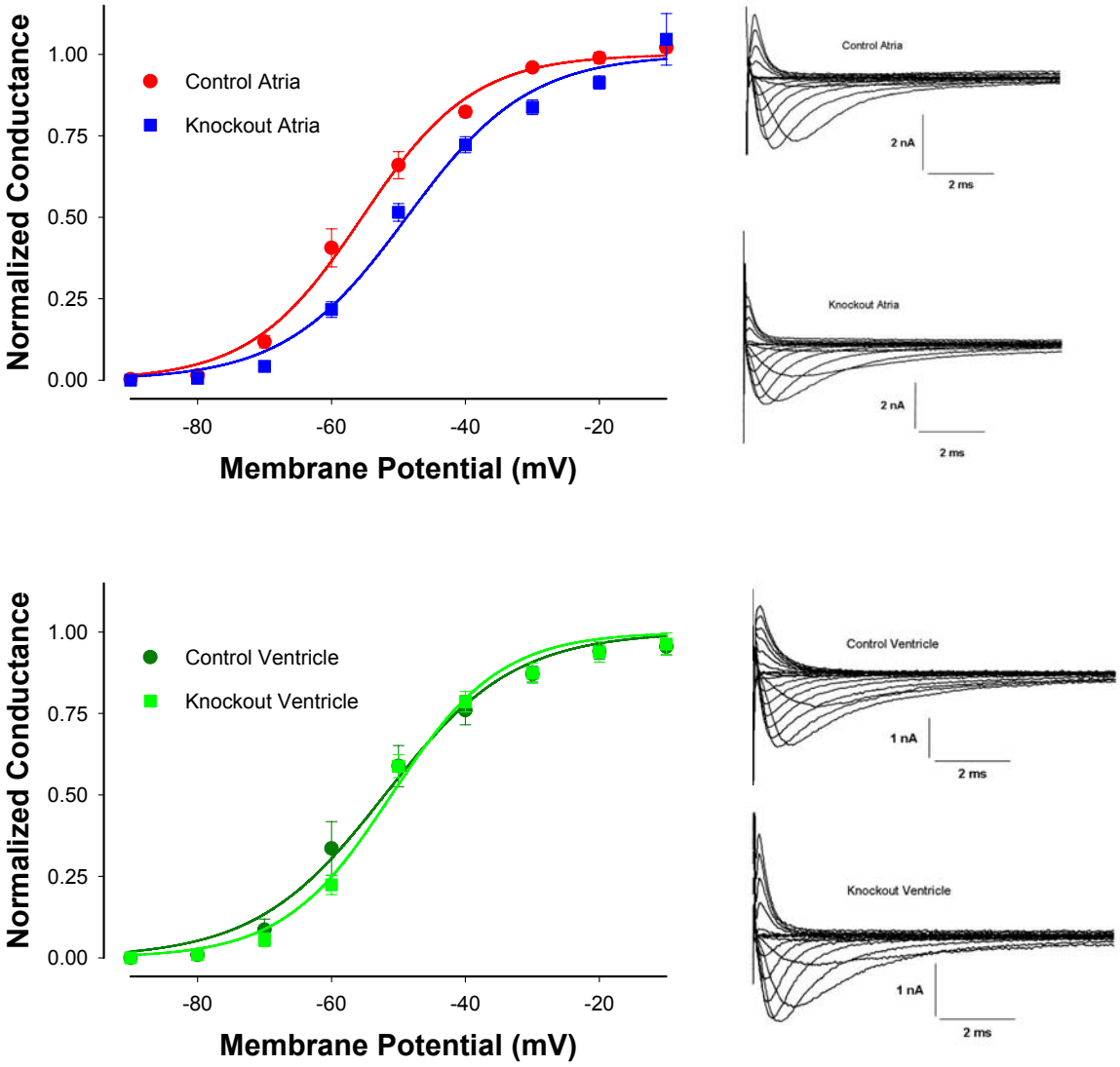

Figure 6.2. Conductance-voltage relationships for control and STX knockout atrial and ventricular Na_v. Data are the mean normalized peak conductance ± S.E.M. Representative current traces are shown to the right.

Figure 6.3. STX causes a change in neonatal atrial Na_v steady state inactivation, but not in ventricular Na_v steady state inactivation.

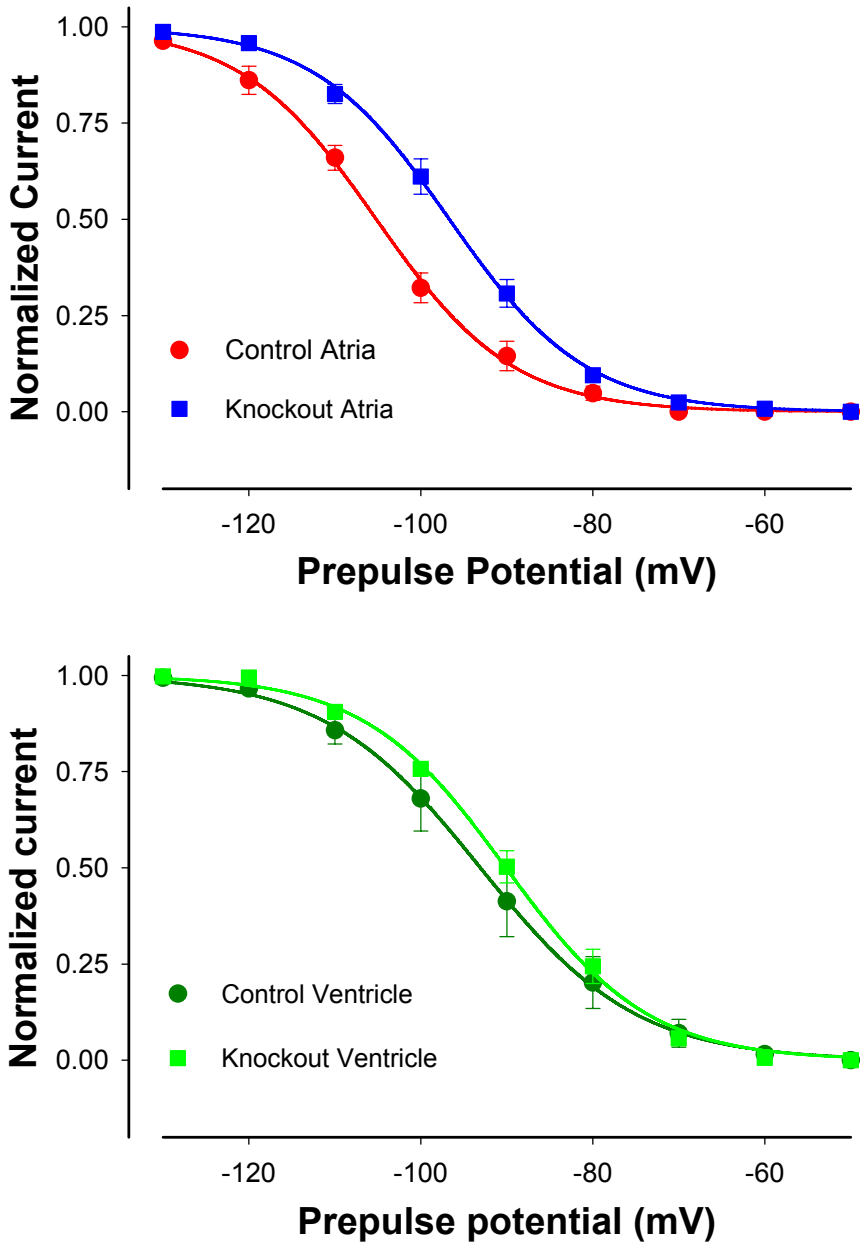

Figure 6.3. Steady-state availability curves for control and STX knockout atrial and ventricular Na_v. Data are the mean normalized current ± S.E.M.

Figure 6.4. Absence of STX causes a slowing of the neonatal atrial Na_v inactivation rate, but has no effect on the kinetics of ventricular Na_v inactivation.

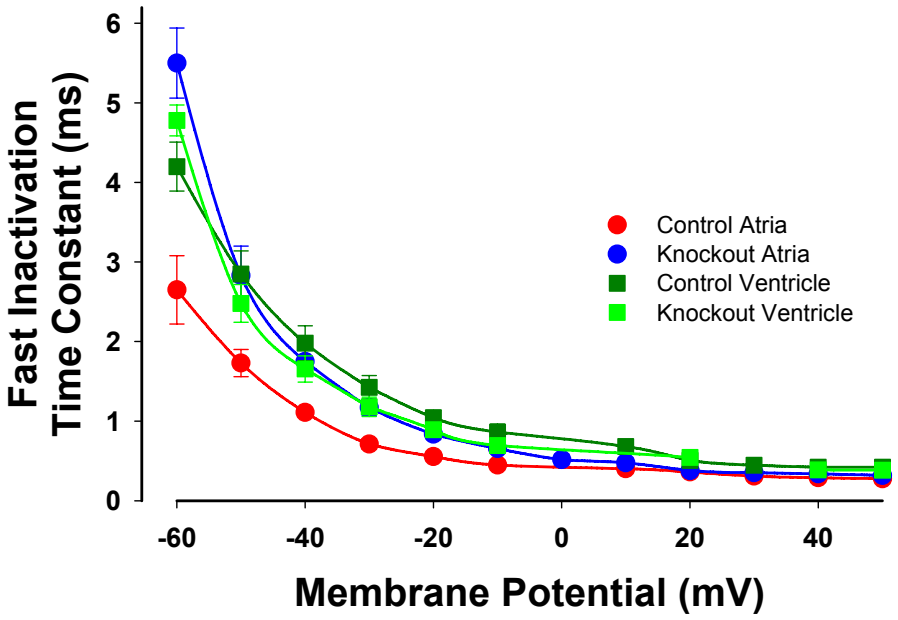

Figure 6.4. Inactivation kinetics for control and STX knockout atrial and ventricular Na_v. Data are the mean time constant of inactivation ± S.E.M.

Figure 6.5. Absence of STX increases the rate of recovery from fast inactivation for neonatal atrial Na_v to rates similar to those measured for control and knockout ventricular Na_v.

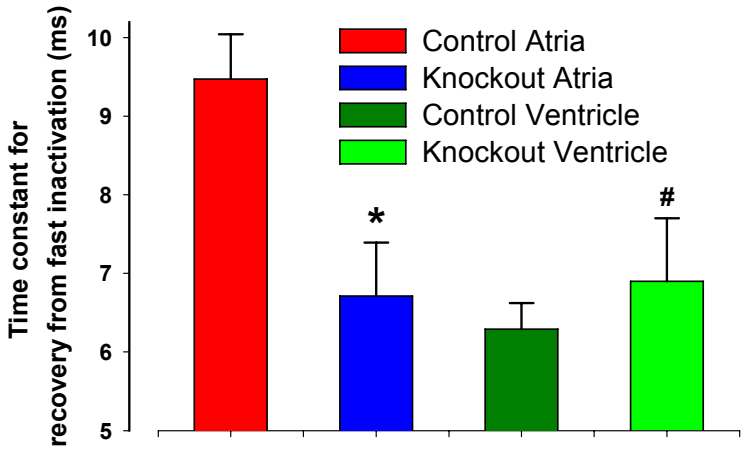

.

Figure 6.5. Recovery from inactivation kinetics of for control and STX knockout atrial and ventricular Na_v. Data are the mean time constant of recovery from inactivation ± S.E.M. Significance ($p < 0.05$) demarcated with an *. Lack of significance demarcated with an #.

Table 6.1. Measured action potential and Na_v parameters.

	Control Atria	Knockout Atria	Control Ventricle	Knockout Ventricle
dV/dt (normalized)	1.00±0.12	0.35±0.03*	1.00±0.41	1.02±0.28#
Maximal Depolarization (mV)	137.2±4.8	111.9±7.5*	125.6±10.7	127.6±10.2#
Na_v V_a (mV)	-55.6±1.7	-48.3±1.1*	-53.8±3.2	-50.7±1.3#
Na_v V_i (mV)	-105.1±1.2	-96.7±1.4*	-92.9±3.5	-90.0±1.2#
Na_v τ_h (ms)	1.73±0.17	2.93±0.37*	2.85±0.29	2.48±0.24#
Na_v τ_{rec} (ms)	9.47±0.57	6.71±0.68*	6.29±0.33	6.90±0.80#

Table 6.1. The measured action potential and Na_v gating parameters measured for control and STX knockout cardiomyocyte Na_v. The data are the mean parameter values ± S.E.M. τ_h data were measured at -50 mV and τ_{rec} data were measured at -120 mV. Significance was determined using a two-tailed Student's t test comparing control atria and ventricles to STX knockout atria and ventricles, respectively. Significance ($p<0.04$) demarcated with an *. Lack of significance demarcated with an #.

control atrial V_a and V_i (figures 6.2 and 6.3). No significant difference in ventricular Na_v steady state gating was observed (figures 6.2 and 6.3). The Na_v kinetic gating properties are again consistent with the steady state parameters. That is, no shift in neonatal ventricular Na_v gating kinetics were observed, but neonatal atrial Na_v kinetics were shifted in the depolarized direction in the absence of STX (Figures 6.4 and 6.5). Collectively, these data reveal the impact of a single glycogene on Na_v function.

Discussion

Alterations of the measured action potential properties are consistent with the changes measured in Na_v gating in the neonatal atria. Shifting the V_a to more depolarized potentials require a greater depolarization to elicit an action potential. Thus, there is a higher proportion of Na_v that are closed as the membrane depolarizes which leads to the slower rate of depolarization (dV/dt) observed. Further, the activation of some K_v channels would cause both a slower rate of depolarization and a smaller maximal depolarization as the outward delayed rectifier K^+ current would counteract membrane depolarization by the inward Na^+ current. Finally, the more depolarized V_i would cause Na_v to inactivate possibly before maximal depolarization; therefore, decreasing Na^+ current and reducing the rate of depolarization and maximal depolarization.

The glycome is remodeled between the neonatal atria and ventricle as shown in the two previous chapters. Here, we showed that the changing glycome may

alter cardiac excitability by modulating action potential waveforms and Na_v function. These data are consistent with our recent study in neonatal rats which revealed a sialic acid dependent shift in Na_v gating parameters in the neonatal atrial myocytes but no shift in ventricular Na_v gating[123]. Na_v of control neonatal atria which expresses STX at relatively high levels, gate at a hyperpolarized potential compared Na_v gating observed in the STX knockout atrial myocytes. Consistent with the Na_v data, AP waveform parameters are altered between the control and knockout STX atrial cardiomyocytes while ventricular myocytes action potentials show no significant change with STX expression.

The slower rates of depolarization and lower peak amplitude seen in the STX knockout atria compared to the control atria are consistent with another study in which cardiomyocyte glycosylation was altered[73]. This study indicated a role for glycosylation in heart failure as studied in a mouse model in which the muscle LIM protein (MLP) is absent. MLP is not associated with glycosylation, yet cardiomyocytes are under-glycosylated compared to control. MLP knockout and neuraminidase-treated myocytes show altered action potential parameters as mentioned above as well as shifts in the voltage-dependence of gating comparable with those currents recorded here.

Together, Na_v and action potential data reveal that changing the expression of a single glycogene can significantly modify cardiac excitability. For this study, we observed the impact of the regulated expression of STX on cardiac excitability,

yet this is only one of the >100 glycogenes that are differentially expressed in the developing heart. If a single enzyme can have this impact on cardiac excitability, the potential of a remodeled glycome on cardiac function is likely substantial.

CHAPTER 7

FINAL DISCUSSION

This study describes two mechanisms by which Na_v function and cardiomyocyte excitability can be modulated through differential glycosylation. The first mechanism, the protein-isoform specific mechanism, indicates that the cell can express combinations of protein isoforms that have similar functions, but are differently glycosylated. This differential glycosylation affects channel function and thereby alters the action potential waveform. The second mechanism, the cell-specific glycosylation mechanism, describes how the change in glycan structure through regulation of glycogene expression in a cell-specific manner.

The first portion of this project focused on Na_v and the manner in which alpha subunit function can be modified by the β_1 isoform. Different combinations of α and β subunits will likely function differently than other combinations giving the cell the ability to slightly alter Na_v function. Ten α and four β Na_v isoforms have been identified and, as shown in chapter 3, β_1 modulated each α subunit function differently.

Na_v alpha subunits show isoform-specific sensitivity to negatively charged sialic acid residues. When expressed in the CHO cell line, no significant shift in the

voltage dependence of $Na_v1.2$ and $Na_v1.7$ gating was observed in this study. Previously, $Na_v1.5$ was shown to be sialic acid insensitive; whereas, $Na_v1.4$ is sensitive to sialic acids attached to the alpha subunit. Interestingly, the β_1 subunit modifies the voltage dependence of Na_v gating in a subunit specific manner. Three of the less-glycosylated Na_v α isoforms tested were modulated by β_1 sialic acids, yet $Na_v1.4$ was insensitive to any effect of β_1 in the CHO cell expression system. Furthermore, when the less-glycosylated $Na_v1.4$ chimera was co-expressed with β_1, it became sensitive to β_1 modulation. Together, these data indicate that alpha and/or β_1 sialylation modulates Na_v gating in a saturating manner.

The modulation of Na_v gating by β_1 was abolished when co-expressed in the non-sialylating Lec2 cell line; likewise, β_1 was unable to modulate gating of any alpha subunit isoform when the β_1 N-glycosylation sites were mutated. Thus, the effect of β_1 can be attributed entirely to the glycans attached. We conclude that β_1 modulated Na_v gating in a sialic acid dependent, saturating manner.

With each alpha subunit having a unique glycosylation signature, changing which alpha subunit is expressed could result in a sialic acid dependent shift in channel voltage dependence. Four beta subunits likely modulate alpha subunit gating through various mechanisms - as we have shown here, β_1 modulates gating through glycosylation, but the three remaining beta isoforms may alter channel gating through other, glycosylation dependent or independent mechanisms. A

recent report described this exact effect with the β_2 subunit. Johnson and Bennett reported that β_2 caused a sialic acid dependent hyperpolarizing shift in $Na_v1.5$ gating while β_2 caused a sialic acid independent depolarizing shift in the voltage dependence of $Na_v1.2$ gating[121]. Co-expression of both β_1 and β_2 with each α subunit revealed an additive effect. $Na_v1.5{\cdot}\beta_1{\cdot}\beta_2$ produced a larger hyperpolarizing shift in gating; whereas, $Na_v1.2{\cdot}\beta_1{\cdot}\beta_2$ gated like $Na_v1.2$ alone. These differences in the manner in which β_1 and β_2 impact α subunit gating indicates that expression of various combinations of alpha and beta subunits would create an array of voltages at which the channel gates.

In vivo, Na_v alpha and beta isoform expression may be up- or down-regulated in response to development or pathologies, and this could result in a sialic acid dependent change in the voltage dependence of Na_v gating. Theoretically, Na_v gating can be modulated in hundreds of ways through unique combinations of differently glycosylated alpha and beta subunits. $Na_v1.5$ is the primary Na_v isoform expressed in both chambers of the developing heart. However, in the developing skeletal muscle, the Na_v α isoform changes from $Na_v1.5$ in the neonate to Na_v 1.4 in the adult[183-185]. The adult skeletal muscle isoform is heavily glycosylated compared to the neonatal isoform [117,118]. As previously reported, the $Na_v1.4$ gating is sialic acid sensitive while $Na_v1.5$ is insensitive to sialic acid modulation when expressed in CHO cells[118]. β_1 is developmentally regulated in the rodent heart where it is highly expressed in the adult ventricle, but expressed at much lower levels in the neonatal atria and ventricle and adult atria[123].

Expression of various combinations of α and auxillary subunits may create a spectrum of channel gating parameters that are glycosylation dependent; thus, supporting the relevance of the protein-specific mechanism by which Na_v function is modulated.

As described, the second mechanism studied here questioned whether cell specific change in glycogene expression and the corresponding changes in glycan structure are relevant to Na_v gating. Glycogene expression varies widely between cardiac chambers and through development with over 46% of glycosylation-associated genes differentially expressed. Comparison of neonatal and adult ventricular myocyte glycogene expression showed the highest proportion of differential expression at 43.2% while the neonatal and adult atria showed the lowest at 19.4%. Corresponding to these changes in glycogene expression, we report large changes in N-glycan structures throughout the developing myocardium.

Mass spectrometry of the cardiomyocyte glycans throughout development showed major differences in glycan structure between each myocyte comparison group. All groups had similar ratios of high mannose structures. However, there was marked variation throughout the developing myocardium in the more complex structures above 2400 m/z. The adult atria had the highest proportion of complex N-glycans of any myocyte type (mass ranges of 2400-3050 and 3050-5000 m/z). Neonatal atria and adult ventricle had comparable levels of N-

glycans in the 3050-5000 m/z and were the lowest relative levels of the four tissues studied. In addition, the structures of these glycans varied among myocyte types, with each tissue having at least one unique glycan. Observations derived from these data support a second mechanism by which glycosylation might impact cardiac function, through cell-specific regulation of glycosylation. That is, the GeneChip and glycan screening data indicate that the glycome is remodeled throughout the myocardium and during development.

These studies have led to a proposed model that predicts that gating of Na_v is modulated by glycans through two mechanisms (Figure 7.1). The left panel describes the "protein isoform-mediated" mechanism which is controlled at the transcriptional level where alpha and beta subunit isoforms are expressed. Each alpha subunit has a unique glycosylation signature creating currents unique to the combination of alpha and beta isoforms.

The right panel shows the model for the "cell-specific glycosylation" mechanism of modulation. Here, the glycogene profile determines the glycan structures present and how sodium currents are modulated by the remodeled glycome. The neonatal and adult atria and ventricles express the same Na_v α subunit isoform yet apparently have unique glycan structures which cause the channels to gate differently. Tight control of glycogene expression is essential for cells to consistently produce appropriate glycans for that cell's particular function. Minor changes in glycogene expression may alter glycan structure and therefore

Figure 1. Model proposing glycosylation-dependent control and modulation of Na_v gating.

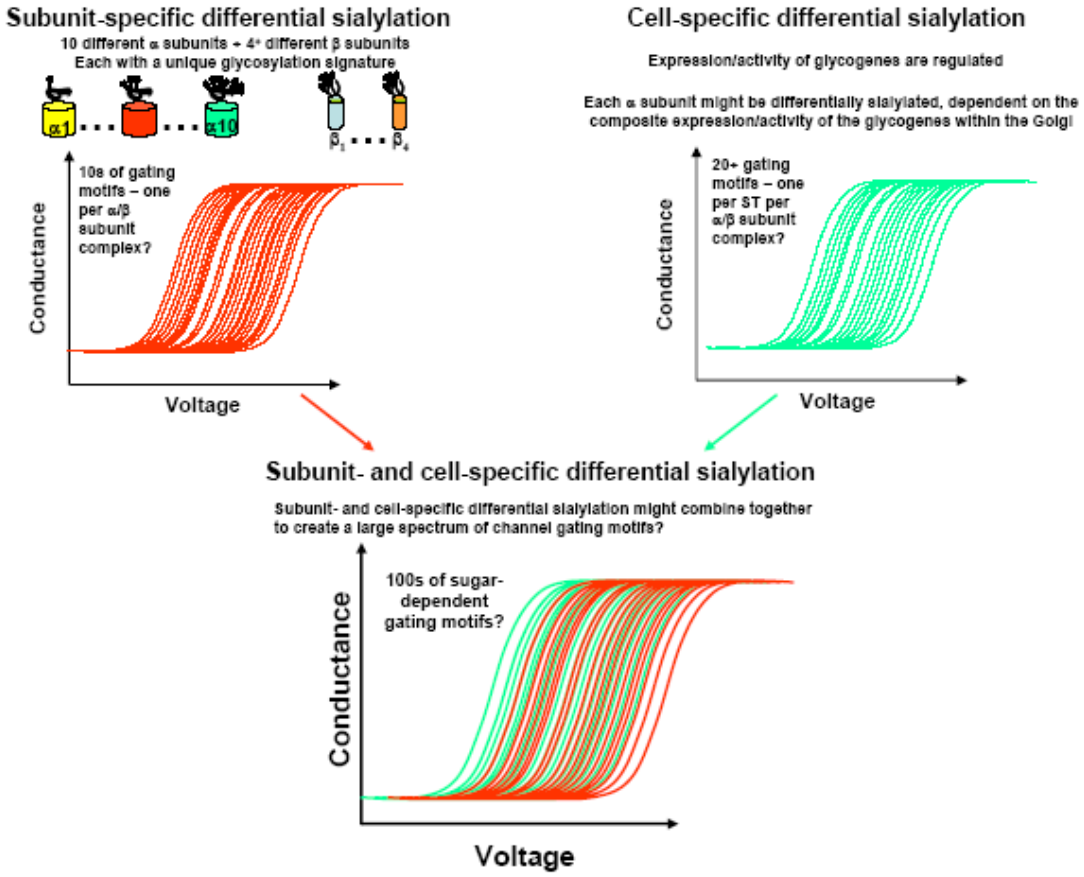

Figure 1. This model describes two mechanisms by which a cell can modulate Na_v gating. The protein-specific (left panel) and the cell-specific glycosylation (right panel) mechanisms together create a spectrum of possible channel gating motifs (bottom panel).

change the manner in which glycans mediate cell adhesion, self vs. non-self recognition, molecular trafficking, receptor activation and even modulate cellular excitability. We find here that slight changes in glycan structure, specifically changing sialic acid levels, could alter sodium channel function (as characterized by the G-V curves shown in figure 6.1). Hundreds of possible sodium channel G-V curves would result following these slight changes in glycan composition. Combination of these two mechanisms would create a spectrum of Na_v that gate at various voltages.

Although both mechanisms describe means by which sodium channel function may be modified, there may be examples in which one of the two mechanisms is dominant. In the dorsal root ganglion (DRG), there is an apparent change in the level of glycosylation of Na_v 1.9 through development[186]. The DRG expression of Na_v1.9 does not change, yet the level of glycosylation is greater in the neonate compared to adult. This study also showed a functional impact of glycosylation on Na_v gating with approximately a 7 mV depolarizing shift in V_i in the adult compared to neonate. When treated with neuraminidase (an enzyme that removes sialic acid residues), this voltage shift was abolished. Unlike other studies, no effects on activation were identified, indicating that glycosylation may impact gating of Na_v in an isoform dependent manner.

In this study we showed that a single polysialyltransferase, STX, is expressed essentially only in the neonatal atria. In the absence of STX, both Na_v function

and action potential parameters were altered in neonatal atrial myocytes. No modulation of Na_v gating or action potential waveform was observed in neonatal ventricular myocytes; consistent with the fact that STX is not expressed in the ventricle. In wild type atrial myocytes, STX must be important for proper excitability and other possible processes not studied here. This further supports the model presented above that slight alterations in glycosylation may alter channel function in a cell-specific manner since the same Na_v α subunit is expressed in the neonatal atria and ventricles.

Changing the expression of a single glycogene can have dramatic effects upon cellular excitability as shown with STX in the neonatal atria. Therefore, if one of more than 100 regulated glycogenes can alter cardiac excitability, the potential impact of the remodeled glycome on cardiac function is considerable; not only on cardiac excitability, but on a range of cardiac processes.

Significance of this study

The broad role of glycans in normal and pathophysiological processes demands tight control of glycans present on cell surfaces that may differ from cell to cell and from tissue to tissue. Glycans are essential to regulate protein folding, cell adhesion, molecular trafficking and clearance, receptor activation, endocytosis and signal transduction. Furthermore, glycans determine blood type and immunity.

Through understanding differential glycosylation of cells and tissues, we better understand normal function and the dysfunction associated with pathophysiological conditions. Drug side effects are a result of the drug disrupting the normal physiological process in a system not associated with the target system[88,89]. Improving the effectiveness of a drug and preventing side effects is a main goal in therapeutic research. Targeting glycans may allow researchers to obtain this goal. Because each tissue expresses a unique population of glycans, therapeutics can be developed that use glycans to target specific tissues for drug delivery.

Altered glycans are a hallmark of the tumor phenotype. Cancer cells over- and under- express naturally occurring glycans and expression of glycans restricted to embryonic tissues [88]. Furthermore, if the embryonic glycan forms could be modified to elicit an immune response to the tumor, a side-effect free, effective cancer therapeutic would be developed.

Cardiac arrhythmias are associated with various ion channel maladies. Several reports indicate point mutations of $Na_v1.5$ cause aberrant inactivation leading to a persistent sodium current which can lead to LQTS by creating inward sodium current in phase 2 of the cardiac action potential [129,171]. Persistent sodium current would counteract the outward rectifying K+ current, extending the phase 2 of the cardiac action potential and the QT segment of ECG. By shifting the V_a to more hyperpolarized potentials, Na_v will open following lesser depolarizations,

thus limiting extension of phase 2 and LQTS. Although new methods of modifying glycans are currently under investigation, several methods may be used to modify sodium channel function including gene therapy which may involve either mechanism explained above. First, glycosyltransferase DNA could be delivered to the cell which could directly increase sialylation (via STX for example) or increase glycan branching and overall sialylation. Second, auxiliary subunits may be expressed to modify Na_v function.

The goal of this work was to identify and explain a model by which glycans can modulate activity of proteins (specifically Na_v) and how this may influence cardiac excitability. Furthermore, we explained the vast changes in glycogene expression and glycan structures that occur throughout the developing myocardium and how the regulated expression of a single polysialyltransferase modulates cardiac excitability. Pathological and stressor mediated (i.e. cigarette smoke) studies in all organ systems might be studied in a similar manner to better understand the changes in the glycome and excitability that these conditions induce. Through further research and development of glycan focused and glycan mediated therapeutics, maladies caused by or marked by changes in glycan structures may be treated.

REFERENCES

(1) Minino AM, Heron MP, Murphy SL, Kochanek KD. Deaths: final data for 2004. *Natl Vital Stat Rep.* 2007;55:1-119.

(2) Gosiewska A, Yi CF, Brown LJ, Cullen B, Silcock D, Geesin JC. Differential expression and regulation of extracellular matrix-associated genes in fetal and neonatal fibroblasts. *Wound Repair Regen.* 2001;9:213-222.

(3) Harrell MD, Harbi S, Hoffman JF, Zavadil J, Coetzee WA. Large-scale analysis of ion channel gene expression in the mouse heart during perinatal development. *Physiol Genomics.* 2007;28:273-283.

(4) Ishii A, Ikeda T, Hitoshi S et al. Developmental changes in the expression of glycogenes and the content of N-glycans in the mouse cerebral cortex. *Glycobiology.* 2007;17:261-276.

(5) Zhou J, Law HK, Cheung CY, Ng IH, Peiris JS, Lau YL. Differential expression of chemokines and their receptors in adult and neonatal macrophages infected with human or avian influenza viruses. *J Infect Dis.* 2006;194:61-70.

(6) Kistler PM, Sanders P, Fynn SP et al. Electrophysiologic and electroanatomic changes in the human atrium associated with age. *J Am Coll Cardiol.* 2004;44:109-116.

(7) Kondo RP, Anderson RH, Kupershmidt S, Roden DM, Evans SM. Development of the cardiac conduction system as delineated by minK-lacZ. *J Cardiovasc Electrophysiol.* 2003;14:383-391.

(8) Zhang JF, Robinson RB, Siegelbaum SA. Sympathetic neurons mediate developmental change in cardiac sodium channel gating through long-term neurotransmitter action. *Neuron.* 1992;9:97-103.

(9) Plotnikov AN, Sosunov EA, Patberg KW et al. Cardiac memory evolves with age in association with development of the transient outward current. *Circulation.* 2004;110:489-495.

(10) Kaplan P, Jurkovicova D, Babusikova E et al. Effect of aging on the expression of intracellular Ca(2+) transport proteins in a rat heart. *Mol Cell Biochem.* 2007;301:219-226.

(11) Brunelli E, Perrotta I, Bonacci A, Tripepi S. Differential expression of aquaporin 3 in Triturus italicus from larval to adult epidermal conversion. *Eur J Histochem.* 2007;51:25-32.

(12) Wu C, Hayama E, Imamura S, Matsuoka R, Nakanishi T. Developmental changes in the expression of voltage-gated potassium channels in the ductus arteriosus of the fetal rat. *Heart Vessels.* 2007;22:34-40.

(13) Schug N, Braig C, Zimmermann U et al. Differential expression of otoferlin in brain, vestibular system, immature and mature cochlea of the rat. *Eur J Neurosci.* 2006;24:3372-3380.

(14) Navarro-Tableros V, Fiordelisio T, Hernandez-Cruz A, Hiriart M. Physiological development of insulin secretion, calcium channels, and GLUT2 expression of pancreatic rat beta-cells. *Am J Physiol Endocrinol Metab.* 2007;292:E1018-E1029.

(15) Fry M. Developmental expression of Na+ currents in mouse Purkinje neurons. *Eur J Neurosci.* 2006;24:2557-2566.

(16) Holtje M, Brunk I, Grosse J et al. Differential distribution of voltage-gated potassium channels Kv 1.1-Kv1.6 in the rat retina during development. *J Neurosci Res.* 2007;85:19-33.

(17) Wada A. Roles of voltage-dependent sodium channels in neuronal development, pain, and neurodegeneration. *J Pharmacol Sci.* 2006;102:253-268.

(18) Wooltorton JR, Gaboyard S, Hurley KM et al. Developmental changes in two voltage-dependent sodium currents in utricular hair cells. *J Neurophysiol.* 2007;97:1684-1704.

(19) Surges R, Brewster AL, Bender RA, Beck H, Feuerstein TJ, Baram TZ. Regulated expression of HCN channels and cAMP levels shape the properties of the h current in developing rat hippocampus. *Eur J Neurosci.* 2006;24:94-104.

(20) MacDonald SH, Ruth P, Knaus HG, Shipston MJ. Increased large conductance calcium-activated potassium (BK) channel expression accompanied by STREX variant downregulation in the developing mouse CNS. *BMC Dev Biol.* 2006;6:37.:37.

(21) Bacharova L. The structural and electrical remodeling of myocardium in LVH and its impact on the QRS voltage. *Anadolu Kardiyol Derg.* 2007;7 Suppl 1:37-42.

(22) Benitah JP, Gomez AM, Bailly P et al. Heterogeneity of the early outward current in ventricular cells isolated from normal and hypertrophied rat hearts. *J Physiol.* 1993;469:111-138.

(23) Bodi I, Muth JN, Hahn HS et al. Electrical remodeling in hearts from a calcium-dependent mouse model of hypertrophy and failure: complex nature of K+ current changes and action potential duration. *J Am Coll Cardiol.* 2003;41:1611-1622.

(24) Brundel BJ, Van G, I, Henning RH et al. Alterations in potassium channel gene expression in atria of patients with persistent and paroxysmal atrial fibrillation: differential regulation of protein and mRNA levels for K+ channels. *J Am Coll Cardiol.* 2001;37:926-932.

(25) Brundel BJ, Van G, I, Henning RH et al. Ion channel remodeling is related to intraoperative atrial effective refractory periods in patients with paroxysmal and persistent atrial fibrillation. *Circulation.* 2001;103:684-690.

(26) Brundel BJ, Henning RH, Kampinga HH, Van G, I, Crijns HJ. Molecular mechanisms of remodeling in human atrial fibrillation. *Cardiovasc Res.* 2002;54:315-324.

(27) Cerbai E, Barbieri M, Mugelli A. Occurrence and properties of the hyperpolarization-activated current If in ventricular myocytes from normotensive and hypertensive rats during aging. *Circulation.* 1996;94:1674-1681.

(28) Desplats PA, Denny CA, Kass KE et al. Glycolipid and ganglioside metabolism imbalances in Huntington's disease. *Neurobiol Dis.* 2007;27:265-277.

(29) Diskin S, Kumar J, Cao Z et al. Detection of differentially expressed glycogenes in trabecular meshwork of eyes with primary open-angle glaucoma. *Invest Ophthalmol Vis Sci.* 2006;47:1491-1499.

(30) Hill JA. Electrical remodeling in cardiac hypertrophy. *Trends Cardiovasc Med.* 2003;13:316-322.

(31) Huang B, Qin D, El-Sherif N. Early down-regulation of K+ channel genes and currents in the postinfarction heart. *J Cardiovasc Electrophysiol.* 2000;11:1252-1261.

(32) Huang B, Qin D, Deng L, Boutjdir M, Sherif N. Reexpression of T-type Ca2+ channel gene and current in post-infarction remodeled rat left ventricle. *Cardiovasc Res.* 2000;46:442-449.

(33) Huang B, El-Sherif T, Gidh-Jain M, Qin D, El-Sherif N. Alterations of sodium channel kinetics and gene expression in the postinfarction remodeled myocardium. *J Cardiovasc Electrophysiol.* 2001;12:218-225.

(34) Jiang M, Zhang M, Tang DG et al. KCNE2 protein is expressed in ventricles of different species, and changes in its expression contribute to electrical remodeling in diseased hearts. *Circulation.* 2004;109:1783-1788.

(35) Kaprielian R, Wickenden AD, Kassiri Z, Parker TG, Liu PP, Backx PH. Relationship between K+ channel down-regulation and [Ca2+]i in rat ventricular myocytes following myocardial infarction. *J Physiol.* 1999;517 (Pt 1):229-245.

(36) Keung EC. Calcium current is increased in isolated adult myocytes from hypertrophied rat myocardium. *Circ Res.* 1989;64:753-763.

(37) Le BS, Demolombe S, Chambellan A et al. Microarray analysis reveals complex remodeling of cardiac ion channel expression with altered thyroid status: relation to cellular and integrated electrophysiology. *Circ Res.* 2003;92:234-242.

(38) Li GR, Lau CP, Ducharme A, Tardif JC, Nattel S. Transmural action potential and ionic current remodeling in ventricles of failing canine hearts. *Am J Physiol Heart Circ Physiol.* 2002;283:H1031-H1041.

(39) Lockstone HE, Harris LW, Swatton JE, Wayland MT, Holland AJ, Bahn S. Gene expression profiling in the adult Down syndrome brain. *Genomics.* 2007;90:647-660.

(40) Martinez ML, Heredia MP, Delgado C. Expression of T-type Ca(2+) channels in ventricular cells from hypertrophied rat hearts. *J Mol Cell Cardiol.* 1999;31:1617-1625.

(41) McIntosh MA, Cobbe SM, Kane KA, Rankin AC. Action potential prolongation and potassium currents in left-ventricular myocytes isolated from hypertrophied rabbit hearts. *J Mol Cell Cardiol.* 1998;30:43-53.

(42) Mukherjee R, Spinale FG. L-type calcium channel abundance and function with cardiac hypertrophy and failure: a review. *J Mol Cell Cardiol.* 1998;30:1899-1916.

(43) Mukherjee R, Hewett KW, Walker JD, Basler CG, Spinale FG. Changes in L-type calcium channel abundance and function during the transition to pacing-induced congestive heart failure. *Cardiovasc Res.* 1998;37:432-444.

(44) Rozanski GJ, Xu Z, Zhang K, Patel KP. Altered K+ current of ventricular myocytes in rats with chronic myocardial infarction. *Am J Physiol.* 1998;274:H259-H265.

(45) Schoonderwoerd BA, Van G, I, Van Veldhuisen DJ, Van den Berg MP, Crijns HJ. Electrical and structural remodeling: role in the genesis and maintenance of atrial fibrillation. *Prog Cardiovasc Dis.* 2005;48:153-168.

(46) Tomaselli GF, Marban E. Electrophysiological remodeling in hypertrophy and heart failure. *Cardiovasc Res.* 1999;42:270-283.

(47) Tomaselli GF, Rose J. Molecular aspects of arrhythmias associated with cardiomyopathies. *Curr Opin Cardiol.* 2000;15:202-208.

(48) Tomita F, Bassett AL, Myerburg RJ, Kimura S. Diminished transient outward currents in rat hypertrophied ventricular myocytes. *Circ Res.* 1994;75:296-303.

(49) Van Wagoner DR, Pond AL, McCarthy PM, Trimmer JS, Nerbonne JM. Outward K+ current densities and Kv1.5 expression are reduced in chronic human atrial fibrillation. *Circ Res.* 1997;80:772-781.

(50) Van Wagoner DR, Pond AL, Lamorgese M, Rossie SS, McCarthy PM, Nerbonne JM. Atrial L-type Ca2+ currents and human atrial fibrillation. *Circ Res.* 1999;85:428-436.

(51) Van Wagoner DR, Nerbonne JM. Molecular basis of electrical remodeling in atrial fibrillation. *J Mol Cell Cardiol.* 2000;32:1101-1117.

(52) Yao JA, Jiang M, Fan JS, Zhou YY, Tseng GN. Heterogeneous changes in K currents in rat ventricles three days after myocardial infarction. *Cardiovasc Res.* 1999;44:132-145.

(53) Charpentier F, Liu QY, Rosen MR, Robinson RB. Age-related differences in beta-adrenergic regulation of repolarization in canine epicardial myocytes. *Am J Physiol.* 1996;271:H1174-H1181.

(54) Hewett KW, Rosen MR. Developmental changes in the rabbit sinus node action potential and its response to adrenergic agonists. *J Pharmacol Exp Ther.* 1985;235:308-312.

(55) Huynh TV, Chen F, Wetzel GT, Friedman WF, Klitzner TS. Developmental changes in membrane Ca2+ and K+ currents in fetal, neonatal, and adult rabbit ventricular myocytes. *Circ Res.* 1992;70:508-515.

(56) Osaka T, Joyner RW. Developmental changes in calcium currents of rabbit ventricular cells. *Circ Res.* 1991;68:788-796.

(57) Osaka T, Joyner RW. Developmental changes in the beta-adrenergic modulation of calcium currents in rabbit ventricular cells. *Circ Res.* 1992;70:104-115.

(58) Pond AL, Nerbonne JM. ERG proteins and functional cardiac I(Kr) channels in rat, mouse, and human heart. *Trends Cardiovasc Med.* 2001;11:286-294.

(59) Nerbonne JM. Molecular basis of functional voltage-gated K+ channel diversity in the mammalian myocardium. *J Physiol.* 2000;525 Pt 2:285-298.

(60) Yue L, Melnyk P, Gaspo R, Wang Z, Nattel S. Molecular mechanisms underlying ionic remodeling in a dog model of atrial fibrillation. *Circ Res.* 1999;84:776-784.

(61) Ausma J, Wijffels M, Thone F, Wouters L, Allessie M, Borgers M. Structural changes of atrial myocardium due to sustained atrial fibrillation in the goat. *Circulation.* 1997;96:3157-3163.

(62) Ausma J, Wijffels M, van EG et al. Dedifferentiation of atrial cardiomyocytes as a result of chronic atrial fibrillation. *Am J Pathol.* 1997;151:985-997.

(63) Wijffels MC, Kirchhof CJ, Dorland R, Allessie MA. Atrial fibrillation begets atrial fibrillation. A study in awake chronically instrumented goats. *Circulation.* 1995;92:1954-1968.

(64) Santana LF, Nunez-Duran H, Dilly KW, Lederer WJ. Sodium current and arrhythmogenesis in heart failure. *Heart Fail Clin.* 2005;1:193-205.

(65) Kass RS, Tsien RW, Weingart R. Ionic basis of transient inward current induced by strophanthidin in cardiac Purkinje fibres. *J Physiol.* 1978;281:209-226.

(66) Koumi S, Backer CL, Arentzen CE. Characterization of inwardly rectifying K+ channel in human cardiac myocytes. Alterations in channel behavior in myocytes isolated from patients with idiopathic dilated cardiomyopathy. *Circulation.* 1995;92:164-174.

(67) Nuss HB, Kaab S, Kass DA, Tomaselli GF, Marban E. Cellular basis of ventricular arrhythmias and abnormal automaticity in heart failure. *Am J Physiol.* 1999;277:H80-H91.

(68) Rossow CF, Minami E, Chase EG, Murry CE, Santana LF. NFATc3-induced reductions in voltage-gated K+ currents after myocardial infarction. *Circ Res.* 2004;94:1340-1350.

(69) Thuringer D, Deroubaix E, Coulombe A, Coraboeuf E, Mercadier JJ. Ionic basis of the action potential prolongation in ventricular myocytes from Syrian hamsters with dilated cardiomyopathy. *Cardiovasc Res.* 1996;31:747-757.

(70) Knollmann BC, Knollmann-Ritschel BE, Weissman NJ, Jones LR, Morad M. Remodelling of ionic currents in hypertrophied and failing hearts of transgenic mice overexpressing calsequestrin. *J Physiol.* 2000;525 Pt 2:483-498.

(71) Lederer WJ, Tsien RW. Transient inward current underlying arrhythmogenic effects of cardiotonic steroids in Purkinje fibres. *J Physiol.* 1976;263:73-100.

(72) Pogwizd SM, Schlotthauer K, Li L, Yuan W, Bers DM. Arrhythmogenesis and contractile dysfunction in heart failure: Roles of sodium-calcium exchange, inward rectifier potassium current, and residual beta-adrenergic responsiveness. *Circ Res.* 2001;88:1159-1167.

(73) Ufret-Vincenty CA, Baro DJ, Lederer WJ, Rockman HA, Quinones LE, Santana LF. Role of sodium channel deglycosylation in the genesis of cardiac arrhythmias in heart failure. *J Biol Chem.* 2001;276:28197-28203.

(74) Ma TS, Baker JC, Bailey LE. Excitation-contraction coupling in normal and myopathic hamster hearts III: functional deficiencies in interstitial glycoproteins. *Cardiovasc Res.* 1979;13:568-577.

(75) Ohtsubo K, Marth JD. Glycosylation in cellular mechanisms of health and disease. *Cell.* 2006;126:855-867.

(76) Ramamurthy T, Yamasaki S, Takeda Y, Nair GB. Vibrio cholerae O139 Bengal: odyssey of a fortuitous variant. *Microbes Infect.* 2003;5:329-344.

(77) Gong F, Lu QS, You Y et al. [Preparation of transfusable human universal red blood cell with recombinant alpha-galactosidase.]. *Zhongguo Shi Yan Xue Ye Xue Za Zhi.* 2005;13:313-316.

(78) Taylor ME, Drickamer K. *Introduction to Glycobiology*. 2nd ed. New York, NY: Oxford University Press; 2006.

(79) Varki A, Cummings RD, Esko JD, Freeze HH, Hart GW, Marth JD. *Essentials of Glycobiology*. 1st ed. New York, NY: Cold Spring Harbor Laboratory Press; 1999.

(80) Kornfeld R, Kornfeld S. Assembly of asparagine-linked oligosaccharides. *Annu Rev Biochem.* 1985;54:631-664.

(81) Lehle L, Strahl S, Tanner W. Protein glycosylation, conserved from yeast to man: a model organism helps elucidate congenital human diseases. *Angew Chem Int Ed Engl.* 2006;45:6802-6818.

(82) Marquardt T, Denecke J. Congenital disorders of glycosylation: review of their molecular bases, clinical presentations and specific therapies. *Eur J Pediatr.* 2003;162:359-379.

(83) Kojima N, Yoshida Y, Kurosawa N, Lee YC, Tsuji S. Enzymatic activity of a developmentally regulated member of the sialyltransferase family (STX): evidence for alpha 2,8-sialyltransferase activity toward N-linked oligosaccharides. *FEBS Lett.* 1995;360:1-4.

(84) Turnbull JE, Field RA. Emerging glycomics technologies. *Nat Chem Biol.* 2007;3:74-77.

(85) Freeze HH. Genetic defects in the human glycome. *Nat Rev Genet.* 2006;7:537-551.

(86) Comelli EM, Head SR, Gilmartin T et al. A focused microarray approach to functional glycomics: transcriptional regulation of the glycome. *Glycobiology.* 2006;16:117-131.

(87) Haliloglu G, Topaloglu H. Glycosylation defects in muscular dystrophies. *Curr Opin Neurol.* 2004;17:521-527.

(88) Dube DH, Bertozzi CR. Glycans in cancer and inflammation--potential for therapeutics and diagnostics. *Nat Rev Drug Discov.* 2005;4:477-488.

(89) Fuster MM, Esko JD. The sweet and sour of cancer: glycans as novel therapeutic targets. *Nat Rev Cancer.* 2005;5:526-542.

(90) Jaeken J, Matthijs G. Congenital disorders of glycosylation: a rapidly expanding disease family. *Annu Rev Genomics Hum Genet.* 2007;8:261-278.

(91) Teixeira AR, Nitz N, Guimaro MC, Gomes C, Santos-Buch CA. Chagas disease. *Postgrad Med J.* 2006;82:788-798.

(92) Bern C, Montgomery SP, Herwaldt BL et al. Evaluation and treatment of chagas disease in the United States: a systematic review. *JAMA.* 2007;298:2171-2181.

(93) Colli W. Trans-sialidase: a unique enzyme activity discovered in the protozoan Trypanosoma cruzi. *FASEB J.* 1993;7:1257-1264.

(94) Keating MT, Sanguinetti MC. Molecular and cellular mechanisms of cardiac arrhythmias. *Cell.* 2001;104:569-580.

(95) Hille B. *Ion channels of excitable membranes*. 3rd ed. Sunderland, MA: Sinauer Associates; 2001.

(96) Yu FH, Catterall WA. Overview of the voltage-gated sodium channel family. *Genome Biol.* 2003;4:207.

(97) Jiang Y, Lee A, Chen J et al. X-ray structure of a voltage-dependent K+ channel. *Nature.* 2003;423:33-41.

(98) Long SB, Campbell EB, MacKinnon R. Crystal structure of a mammalian voltage-dependent Shaker family K+ channel. *Science.* 2005;309:897-903.

(99) Long SB, Campbell EB, MacKinnon R. Voltage sensor of Kv1.2: structural basis of electromechanical coupling. *Science.* 2005;309:903-908.

(100) Long SB, Tao X, Campbell EB, MacKinnon R. Atomic structure of a voltage-dependent K+ channel in a lipid membrane-like environment. *Nature.* 2007;450:376-382.

(101) Ahern CA, Horn R. Specificity of charge-carrying residues in the voltage sensor of potassium channels. *J Gen Physiol.* 2004;123:205-216.

(102) Ahern CA, Horn R. Focused electric field across the voltage sensor of potassium channels. *Neuron.* 2005;48:25-29.

(103) Campos FV, Chanda B, Roux B, Bezanilla F. Two atomic constraints unambiguously position the S4 segment relative to S1 and S2 segments in the closed state of Shaker K channel. *Proc Natl Acad Sci U S A.* 2007;104:7904-7909.

(104) Chanda B, Asamoah OK, Blunck R, Roux B, Bezanilla F. Gating charge displacement in voltage-gated ion channels involves limited transmembrane movement. *Nature.* 2005;436:852-856.

(105) Cohen BE, Grabe M, Jan LY. Answers and questions from the KvAP structures. *Neuron.* 2003;39:395-400.

(106) Posson DJ, Ge P, Miller C, Bezanilla F, Selvin PR. Small vertical movement of a K+ channel voltage sensor measured with luminescence energy transfer. *Nature.* 2005;436:848-851.

(107) Richardson J, Blunck R, Ge P et al. Distance measurements reveal a common topology of prokaryotic voltage-gated ion channels in the lipid bilayer. *Proc Natl Acad Sci U S A.* 2006;103:15865-15870.

(108) Swartz KJ. Towards a structural view of gating in potassium channels. *Nat Rev Neurosci.* 2004;5:905-916.

(109) Bendahhou S, O'Reilly AO, Duclohier H. Role of hydrophobic residues in the voltage sensors of the voltage-gated sodium channel. *Biochim Biophys Acta.* 2007;1768:1440-1447.

(110) Blanchet J, Chahine M. Accessibility of four arginine residues on the S4 segment of the Bacillus halodurans sodium channel. *J Membr Biol.* 2007;215:169-180.

(111) Elinder F, Arhem P, Larsson HP. Localization of the extracellular end of the voltage sensor S4 in a potassium channel. *Biophys J.* 2001;80:1802-1809.

(112) Elinder F, Nilsson J, Arhem P. On the opening of voltage-gated ion channels. *Physiol Behav.* 2007;92:1-7.

(113) Lu Z, Klem AM, Ramu Y. Ion conduction pore is conserved among potassium channels. *Nature.* 2001;413:809-813.

(114) Isom LL. Sodium channel beta subunits: anything but auxiliary. *Neuroscientist.* 2001;7:42-54.

(115) Miller JA, Agnew WS, Levinson SR. Principal glycopeptide of the tetrodotoxin/saxitoxin binding protein from Electrophorus electricus: isolation and partial chemical and physical characterization. *Biochemistry.* 1983;22:462-470.

(116) Schmidt JW, Catterall WA. Palmitylation, sulfation, and glycosylation of the alpha subunit of the sodium channel. Role of post-translational modifications in channel assembly. *J Biol Chem.* 1987;262:13713-13723.

(117) Bennett E, Urcan MS, Tinkle SS, Koszowski AG, Levinson SR. Contribution of sialic acid to the voltage dependence of sodium channel gating. A possible electrostatic mechanism. *J Gen Physiol.* 1997;109:327-343.

(118) Bennett ES. Isoform-specific effects of sialic acid on voltage-dependent Na+ channel gating: functional sialic acids are localized to the S5-S6 loop of domain I. *J Physiol.* 2002;538:675-690.

(119) Hagen BM, Sanders KM. Deglycosylation of the beta1-subunit of the BK channel changes its biophysical properties. *Am J Physiol Cell Physiol.* 2006;291:C750-C756.

(120) Johnson D, Montpetit ML, Stocker PJ, Bennett ES. The sialic acid component of the beta1 subunit modulates voltage-gated sodium channel function. *J Biol Chem.* 2004;279:44303-44310.

(121) Johnson D, Bennett ES. Isoform-specific effects of the beta2 subunit on voltage-gated sodium channel gating. *J Biol Chem.* 2006;281:25875-25881.

(122) Johnson D, Bennett ES. Gating of the shaker potassium channel is modulated differentially by N-glycosylation and sialic acids. *Pflugers Arch.* 2007.

(123) Stocker PJ, Bennett ES. Differential sialylation modulates voltage-gated Na+ channel gating throughout the developing myocardium. *J Gen Physiol.* 2006;127:253-265.

(124) Thornhill WB, Wu MB, Jiang X, Wu X, Morgan PT, Margiotta JF. Expression of Kv1.1 delayed rectifier potassium channels in Lec mutant Chinese hamster ovary cell lines reveals a role for sialidation in channel function. *J Biol Chem.* 1996;271:19093-19098.

(125) Ufret-Vincenty CA, Baro DJ, Santana LF. Differential contribution of sialic acid to the function of repolarizing K(+) currents in ventricular myocytes. *Am J Physiol Cell Physiol.* 2001;281:C464-C474.

(126) Watanabe I, Wang HG, Sutachan JJ, Zhu J, Recio-Pinto E, Thornhill WB. Glycosylation affects rat Kv1.1 potassium channel gating by a combined surface potential and cooperative subunit interaction mechanism. *J Physiol.* 2003;550:51-66.

(127) Watanabe I, Zhu J, Sutachan JJ, Gottschalk A, Recio-Pinto E, Thornhill WB. The glycosylation state of Kv1.2 potassium channels affects trafficking, gating, and simulated action potentials. *Brain Res.* 2007;1144:1-18. Epub;%2007 Jan 31.:1-18.

(128) Zhang Y, Hartmann HA, Satin J. Glycosylation influences voltage-dependent gating of cardiac and skeletal muscle sodium channels. *J Membr Biol.* 1999;171:195-207.

(129) Abriel H, Cabo C, Wehrens XH et al. Novel arrhythmogenic mechanism revealed by a long-QT syndrome mutation in the cardiac Na(+) channel. *Circ Res.* 2001;88:740-745.

(130) Bennett ES. Effects of channel cytoplasmic regions on the activation mechanisms of cardiac versus skeletal muscle Na(+) channels. *Biophys J.* 1999;77:2999-3009.

(131) Hamill OP, Marty A, Neher E, Sakmann B, Sigworth FJ. Improved patch-clamp techniques for high-resolution current recording from cells and cell-free membrane patches. *Pflugers Arch.* 1981;391:85-100.

(132) Jang-Lee J, North SJ, Sutton-Smith M et al. Glycomic profiling of cells and tissues by mass spectrometry: fingerprinting and sequencing methodologies. *Methods Enzymol.* 2006;415:59-86.

(133) Dell A, Reason AJ. Carbohydrate analysis. *Curr Opin Biotechnol.* 1993;4:52-56.

(134) Isenberg G, Klockner U. Calcium tolerant ventricular myocytes prepared by preincubation in a "KB medium". *Pflugers Arch.* 1982;395:6-18.

(135) Goldin AL, Barchi RL, Caldwell JH et al. Nomenclature of voltage-gated sodium channels. *Neuron.* 2000;28:365-368.

(136) Chen C, Westenbroek RE, Xu X et al. Mice lacking sodium channel beta1 subunits display defects in neuronal excitability, sodium channel expression, and nodal architecture. *J Neurosci.* 2004;24:4030-4042.

(137) Isom LL, De Jongh KS, Patton DE et al. Primary structure and functional expression of the beta 1 subunit of the rat brain sodium channel. *Science.* 1992;256:839-842.

(138) Chen C, Cannon SC. Modulation of Na+ channel inactivation by the beta 1 subunit: a deletion analysis. *Pflugers Arch.* 1995;431:186-195.

(139) Isom LL, Scheuer T, Brownstein AB, Ragsdale DS, Murphy BJ, Catterall WA. Functional co-expression of the beta 1 and type IIA alpha subunits of sodium channels in a mammalian cell line. *J Biol Chem.* 1995;270:3306-3312.

(140) McClatchey AI, Cannon SC, Slaugenhaupt SA, Gusella JF. The cloning and expression of a sodium channel beta 1-subunit cDNA from human brain. *Hum Mol Genet.* 1993;2:745-749.

(141) McCormick KA, Isom LL, Ragsdale D, Smith D, Scheuer T, Catterall WA. Molecular determinants of Na+ channel function in the extracellular domain of the beta1 subunit. *J Biol Chem.* 1998;273:3954-3962.

(142) McCormick KA, Srinivasan J, White K, Scheuer T, Catterall WA. The extracellular domain of the beta1 subunit is both necessary and sufficient for beta1-like modulation of sodium channel gating. *J Biol Chem.* 1999;274:32638-32646.

(143) Meadows L, Malhotra JD, Stetzer A, Isom LL, Ragsdale DS. The intracellular segment of the sodium channel beta 1 subunit is required for its efficient association with the channel alpha subunit. *J Neurochem.* 2001;76:1871-1878.

(144) Meadows LS, Malhotra J, Loukas A et al. Functional and biochemical analysis of a sodium channel beta1 subunit mutation responsible for generalized epilepsy with febrile seizures plus type 1. *J Neurosci.* 2002;22:10699-10709.

(145) Meadows LS, Chen YH, Powell AJ, Clare JJ, Ragsdale DS. Functional modulation of human brain Nav1.3 sodium channels, expressed in mammalian cells, by auxiliary beta 1, beta 2 and beta 3 subunits. *Neuroscience.* 2002;114:745-753.

(146) Smith MR, Smith RD, Plummer NW, Meisler MH, Goldin AL. Functional analysis of the mouse Scn8a sodium channel. *J Neurosci.* 1998;18:6093-6102.

(147) Smith RD, Goldin AL. Functional analysis of the rat I sodium channel in xenopus oocytes. *J Neurosci.* 1998;18:811-820.

(148) Spampanato J, Escayg A, Meisler MH, Goldin AL. Generalized epilepsy with febrile seizures plus type 2 mutation W1204R alters voltage-dependent gating of Na(v)1.1 sodium channels. *Neuroscience.* 2003;116:37-48.

(149) Vijayaragavan K, O'Leary ME, Chahine M. Gating properties of Na(v)1.7 and Na(v)1.8 peripheral nerve sodium channels. *J Neurosci.* 2001;21:7909-7918.

(150) Zimmer T, Benndorf K. The human heart and rat brain IIA Na+ channels interact with different molecular regions of the beta1 subunit. *J Gen Physiol.* 2002;120:887-895.

(151) Amir R, Argoff CE, Bennett GJ et al. The role of sodium channels in chronic inflammatory and neuropathic pain. *J Pain.* 2006;7:S1-29.

(152) Craner MJ, Klein JP, Renganathan M, Black JA, Waxman SG. Changes of sodium channel expression in experimental painful diabetic neuropathy. *Ann Neurol.* 2002;52:786-792.

(153) Guo F, Yu N, Cai JQ et al. Voltage-gated sodium channel Na(v)1.1, Na(v)1.3 and beta(1) subunit were up-regulated in the hippocampus of spontaneously epileptic rat. *Brain Res Bull.* 2008;75:179-187.

(154) Van WA, Matthews G. Expression of sodium channels Nav1.2 and Nav1.6 during postnatal development of the retina. *Neurosci Lett.* 2006;403:315-317.

(155) Waxman SG, Craner MJ, Black JA. Na+ channel expression along axons in multiple sclerosis and its models. *Trends Pharmacol Sci.* 2004;25:584-591.

(156) Sashihara S, Oh Y, Black JA, Waxman SG. Na+ channel beta 1 subunit mRNA expression in developing rat central nervous system. *Brain Res Mol Brain Res.* 1995;34:239-250.

(157) Sashihara S, Greer CA, Oh Y, Waxman SG. Cell-specific differential expression of Na(+)-channel beta 1-subunit mRNA in the olfactory system during postnatal development and after denervation. *J Neurosci.* 1996;16:702-713.

(158) Sutkowski EM, Catterall WA. Beta 1 subunits of sodium channels. Studies with subunit-specific antibodies. *J Biol Chem.* 1990;265:12393-12399.

(159) Yang JS, Bennett PB, Makita N, George AL, Barchi RL. Expression of the sodium channel beta 1 subunit in rat skeletal muscle is selectively associated with the tetrodotoxin-sensitive alpha subunit isoform. *Neuron.* 1993;11:915-922.

(160) Abriel H, Wehrens XH, Benhorin J, Kerem B, Kass RS. Molecular pharmacology of the sodium channel mutation D1790G linked to the long-QT syndrome. *Circulation.* 2000;102:921-925.

(161) Akai J, Makita N, Sakurada H et al. A novel SCN5A mutation associated with idiopathic ventricular fibrillation without typical ECG findings of Brugada syndrome. *FEBS Lett.* 2000;479:29-34.

(162) Bendahhou S, Cummins TR, Kwiecinski H, Waxman SG, Ptacek LJ. Characterization of a new sodium channel mutation at arginine 1448 associated with moderate Paramyotonia congenita in humans. *J Physiol.* 1999;518 (Pt 2):337-344.

(163) Bendahhou S, Cummins TR, Tawil R, Waxman SG, Ptacek LJ. Activation and inactivation of the voltage-gated sodium channel: role of segment S5 revealed by a novel hyperkalaemic periodic paralysis mutation. *J Neurosci.* 1999;19:4762-4771.

(164) Bendahhou S, Cummins TR, Hahn AF, Langlois S, Waxman SG, Ptacek LJ. A double mutation in families with periodic paralysis defines new aspects of sodium channel slow inactivation. *J Clin Invest.* 2000;106:431-438.

(165) Bennett PB, Yazawa K, Makita N, George AL, Jr. Molecular mechanism for an inherited cardiac arrhythmia. *Nature.* 1995;376:683-685.

(166) Green DS, Hayward LJ, George AL, Jr., Cannon SC. A proposed mutation, Val781Ile, associated with hyperkalemic periodic paralysis and cardiac dysrhythmia is a benign polymorphism. *Ann Neurol.* 1997;42:253-256.

(167) Green DS, George AL, Jr., Cannon SC. Human sodium channel gating defects caused by missense mutations in S6 segments associated with myotonia: S804F and V1293I. *J Physiol.* 1998;510 (Pt 3):685-694.

(168) Makita N, Shirai N, Wang DW et al. Cardiac Na(+) channel dysfunction in Brugada syndrome is aggravated by beta(1)-subunit. *Circulation.* 2000;101:54-60.

(169) Scheffer IE, Harkin LA, Grinton BE et al. Temporal lobe epilepsy and GEFS+ phenotypes associated with SCN1B mutations. *Brain.* 2007;130:100-109.

(170) Spampanato J, Escayg A, Meisler MH, Goldin AL. Functional effects of two voltage-gated sodium channel mutations that cause generalized epilepsy with febrile seizures plus type 2. *J Neurosci.* 2001;21:7481-7490.

(171) Splawski I, Timothy KW, Tateyama M et al. Variant of SCN5A sodium channel implicated in risk of cardiac arrhythmia. *Science.* 2002;297:1333-1336.

(172) Wallace RH, Scheffer IE, Barnett S et al. Neuronal sodium-channel alpha1-subunit mutations in generalized epilepsy with febrile seizures plus. *Am J Hum Genet.* 2001;68:859-865.

(173) Wallace RH, Scheffer IE, Parasivam G et al. Generalized epilepsy with febrile seizures plus: mutation of the sodium channel subunit SCN1B. *Neurology.* 2002;58:1426-1429.

(174) Wallace RH, Hodgson BL, Grinton BE et al. Sodium channel alpha1-subunit mutations in severe myoclonic epilepsy of infancy and infantile spasms. *Neurology.* 2003;61:765-769.

(175) Wang DW, Yazawa K, George AL, Jr., Bennett PB. Characterization of human cardiac Na+ channel mutations in the congenital long QT syndrome. *Proc Natl Acad Sci U S A.* 1996;93:13200-13205.

(176) Wang Q, Shen J, Li Z et al. Cardiac sodium channel mutations in patients with long QT syndrome, an inherited cardiac arrhythmia. *Hum Mol Genet.* 1995;4:1603-1607.

(177) Wang Q, Shen J, Splawski I et al. SCN5A mutations associated with an inherited cardiac arrhythmia, long QT syndrome. *Cell.* 1995;80:805-811.

(178) Wehrens XH, Abriel H, Cabo C, Benhorin J, Kass RS. Arrhythmogenic mechanism of an LQT-3 mutation of the human heart Na(+) channel alpha-subunit: A computational analysis. *Circulation.* 2000;102:584-590.

(179) Wehrens XH, Rossenbacker T, Jongbloed RJ et al. A novel mutation L619F in the cardiac Na+ channel SCN5A associated with long-QT syndrome (LQT3): a role for the I-II linker in inactivation gating. *Hum Mutat.* 2003;21:552.

(180) Xu R, Thomas EA, Gazina EV et al. Generalized epilepsy with febrile seizures plus-associated sodium channel beta1 subunit mutations severely reduce beta subunit-mediated modulation of sodium channel function. *Neuroscience.* 2007;148:164-174.

(181) Kitagawa H, Paulson JC. Differential expression of five sialyltransferase genes in human tissues. *J Biol Chem.* 1994;269:17872-17878.

(182) Livingston BD, Paulson JC. Polymerase chain reaction cloning of a developmentally regulated member of the sialyltransferase gene family. *J Biol Chem.* 1993;268:11504-11507.

(183) Goldin AL. Resurgence of sodium channel research. *Annu Rev Physiol.* 2001;63:871-894.

(184) Trimmer JS, Cooperman SS, Agnew WS, Mandel G. Regulation of muscle sodium channel transcripts during development and in response to denervation. *Dev Biol.* 1990;142:360-367.

(185) Yang JS, Sladky JT, Kallen RG, Barchi RL. TTX-sensitive and TTX-insensitive sodium channel mRNA transcripts are independently regulated in adult skeletal muscle after denervation. *Neuron.* 1991;7:421-427.

(186) Tyrrell L, Renganathan M, Dib-Hajj SD, Waxman SG. Glycosylation alters steady-state inactivation of sodium channel Nav1.9/NaN in dorsal root ganglion neurons and is developmentally regulated. *J Neurosci.* 2001;21:9629-9637.

ABOUT THE AUTHOR

Marty Louis Montpetit was born September 10, 1978 in Tecumseh, Michigan. Marty graduated from Tecumseh High School in 1996 and enrolled at Grand Valley State University where he received his B.S. degree in Health Sciences. While attending Grand Valley, he joined Alpha Sigma Phi Fraternity where he held many leadership positions and received several scholarship commendations. Marty served as a Teaching Assistant and, after graduation, Instructor of the Physiology Laboratory Course at Grand Valley. In 2001, he enrolled in the graduate program at the University of South Florida College of Medicine and joined the laboratory of Eric S. Bennett, Ph.D. He earned his Masters of Science in Medical Sciences in 2001 and was accepted as a candidate for Ph.D. study. Finally, he successfully completed the requirements necessary to be awarded his Ph.D. in Medical Sciences from the University of South Florida College of Medicine in early 2008.